UNIVERSIDADE D
COIMBRA

Ana Luísa Abrantes de Matos

ELUCIDATING THE FUNCTION OF THE RETROPEPSIN APRC AS A MOONLIGHTING IMMUNE EVASION OF *RICKETTSIA*

Dissertação realizada no Centro de Neurociências e Biologia Celular da Universidade de Coimbra no âmbito do Mestrado em Biologia Celular e Molecular, orientada pela Doutora Isaura Simões e Doutora Ana Luísa Carvalho e apresentada ao Departamento de Ciências da Vida da Faculdade de Ciências e Tecnologia da Universidade de Coimbra

Julho de 2022

UNIVERSIDADE D
COIMBRA

Ana Luísa Abrantes de Matos

ELUCIDATING THE FUNCTION OF THE RETROPEPSIN APRC AS A MOONLIGHTING IMMUNE EVASION OF *RICKETTSIA*

Dissertação realizada no Centro de Neurociências e Biologia Celular da Universidade de Coimbra no âmbito do Mestrado em Biologia Celular e Molecular, orientada pela Doutora Isaura Simões e Doutora Ana Luísa Carvalho e apresentada ao Departamento de Ciências da Vida da Faculdade de Ciências e Tecnologia da Universidade de Coimbra

Julho de 2022

This worked was concluded at the Center for Neuroscience and Cell Biology (CNC) of the University of Coimbra, under the scientific supervision of Professor Isaura Simões and Professor Ana Luísa Carvalho, with the support of the Faculty of Science and Technology of the University of Coimbra

This work was financed by the European Regional Development Fund (ERDF), through the COMPETE 2020 - Operational Programme for Competitiveness and Internationalisation and Portuguese national funds via FCT – Fundação para a Ciência e a Tecnologia, under project[s] POCI-01-0145-FEDER-029592 (PTDC/SAU-INF/29592/2017), and UIDB/04539/2020, UIDP/04539/2020 and LA/P/0058/2020.

Part of the introduction is published in the review article Matos, A. L., Curto, P., & Simões, I. (2022). Moonlighting in Rickettsiales: Expanding Virulence Landscape. Tropical Medicine and Infectious Disease, 7(2), 32. DOI: 10.3390/tropicalmed7020032

Acknowledgments

To begin with, I would like to express my deepest gratitude to my supervisor, Doctor Isaura Simões, for the unconditional support, dedication, guidance, availability, motivation, and contagious enthusiasm for science, which was essential for the development of this dissertation. I am also grateful towards Doctor Isaura Simões and assistant researcher Pedro Curto for their patience and transmitted knowledge.

I would also like to express my gratitude to Dr. Ana Luísa Carvalho, academic tutor at DCV, for her prompt availability.

I am thankful towards the amazing people I met at UC-Biotech, for their company, sympathy, support, and advice.

A special thanks to my dear friends for all the great moments and memories, encouragement, advice and friendship.

Lastly, I deeply appreciate my family, especially my mother and grandmother, for all the support, love and encouragement they have given me throughout my life.

Resumo

As proteínas “moonlight” exercem múltiplas funções e estão presentes em diferentes organismos. Estas proteínas estão presentes em bactérias comensais e patogénicas, potencialmente contribuindo para a virulência das últimas. O sistema do complemento é fundamental para impedir a infeção e disseminação bacteriana, porém há bactérias que apresentam mecanismos de evasão ao sistema imunitário, escapando aos efeitos bactericidas do soro. *Rickettsia* é um género de bactérias intracelulares obrigatórias transmitidas por vetores artrópodes, causando doenças ligeiras a potencialmente fatais. Atualmente há uma preocupação crescente com as rickettsioses e o seu impacto na saúde mundial devido à emergência e reemergência destes patógenos, aumento da distribuição geográfica dos seus vetores e ao aumento exponencial da resistência a antibióticos. Deste modo, é crucial encontrar outros alvos para tratar as rickettsioses. Um potencial alvo é a protease aspártica APRc, um homólogo das retropepsinas altamente conservado em *Rickettsia*. A APRc modula fatores de virulência da superfície de *Rickettsia*, liga imunoglobulinas do soro, medeia a evasão ao sistema imunitário e resultados preliminares demonstram que a APRc apresenta substratos no soro humano, sugerindo que esta protease possui atividade “moonlight”. Ao longo deste trabalho demonstrámos que a APRc liga a diferentes isoformas de IgG dependente da concentração, ligando preferencialmente a IgG1 e IgG3. Também foi demonstrado que a APRc liga às cadeias leves de anticorpos, ligando preferencialmente à cadeia leve κ e formando complexos APRc-κ. Mais ainda, mostramos que a APRc liga a C3, C4 e C4BP e origina produtos proteolíticos destas proteínas. A presença de IgG aumenta ligeiramente a interação com C4. A degradação proteolítica do C3 não altera a produção da anafilotoxina C3a. Porém, observa-se um grande impacto da APRc na inibição das vias do complemento. Concluindo, com este estudo caracterizámos interações APRc-IgG e confirmámos que a APRc apresenta substratos no soro, contribuindo para o reconhecimento desta protease como uma proteína “moonlight” e como um potencial alvo terapêutico para tratar rickettsioses.

Palavras-chave: Atividade “moonlight”, sistema do complemento, evasão do sistema imunitário, *Rickettsia*, APRc, retropepsina, factores de virulência

Abstract

Moonlighting proteins exert more than one function and are present in different organisms, including bacteria. These proteins are present in commensal and in pathogenic bacteria, potentially contributing to the virulence of the latter. The complement system is crucial to stop bacterial infection and spreading, however bacteria display mechanisms of immune evasion, escaping to the bactericidal effects of the serum. *Rickettsia* is a genus of obligate intracellular bacteria transmitted through arthropod vectors, causing mild to life-threatening diseases such as Mediterranean Spotted Fever and Epidemic Typhus. Currently, there is an increased concern about rickettsioses and their impact on global health because of the emerging and re-emerging of these pathogens, increasing geographical distribution of its vectors, and the exponential increase of antibiotic resistance. Therefore, it is crucial to find other therapeutic targets to treat rickettsial diseases. One potential target is the Aspartic Protease from *Rickettsia conorii* (APRc), a highly conserved membrane embedded retropepsin-like homologue. APRc modulates *Rickettsia* surface virulence factors, binds immunoglobulins from the serum, mediates immune evasion and preliminary data indicates that APRc presents substrates in human serum, suggesting that this protease has moonlighting activity. With this work, we demonstrated that APRc binds to different IgG isoforms in a concentration-dependent manner, binding preferentially to IgG1 and IgG3. It was also demonstrated that APRc binds to the antibody light chains, binding preferentially κ light chain and forming APRc-κ complexes. We also validated that APRc binds to and cleaves C3, C4, and C4BP. Moreover, our data suggests that IgG increases APRc-C4 interaction. The proteolytic degradation of C3 does not change the production of the anaphylatoxin C3a. However, it is observed a decrease in the activation of all three complement pathways upon incubation with APRc, confirming a role in immune evasion. In conclusion, with this study we further characterized APRc-IgG interactions and confirmed that APRc targets other serum proteins, contributing to acknowledging this protease as a moonlighting protein and as a potential target to treat rickettsioses.

Keywords: Moonlight activity, complement system, immune evasion, *Rickettsia*, APRc, retropepsin, virulence factor

Table of contents

List of abbreviations

ABM	Actin based motility
AG	Ancestral Group
AMPs	Antimicrobial peptides
APRc	Aspartic protease from *Rickettsia conorii*
BSA	Bovine serum albumin
C4BP	C4-binding protein
CD40	Cluster of differentiation 40
CFI	Complement factor I
DTT	Dithiothreitol
Ecb	Extracellular complement-binding
ECM	Extracellular matrix
EF	Elongation factor
Efb	Extracellular fibrinogen-binding
ELISA	Enzyme-linked immunosorbent assay
ER	Endoplasmic reticulum
PARP	Poly (ADP-ribose) polymerase
GAPDH	Glyceraldehyde 3-phosphate dehydrogenase
HBSS	Hanks' Balanced Salt Solution
HIV-1 PR	Human immunodeficiency virus-1 protease
HPLC	High-pressure liquid chromatography
HRP	Horseradish peroxidase
Hsp	Heat shock protein

Ig	Immunoglobulins
IMAC	Immobilized metal affinity chromatography
IPTG	Isopropyl-β-D-thiogalactopyranoside
LAP	Listeria adhesion protein
LPS	Lipopolysaccharide
MAC	Membrane attack complex
MBL	Mannose-binding lectin
MprF	Multiple peptide resistance factor protein
NHS	Normal Human Serum
NHSΔIgG/IgM	NHS depleted in IgG and IgM
PAMPs	Pathogen-associated molecular pattern
PBS	Phosphate-buffered saline
PBS-T	PBS containing 0,05% Tween
PFA	Paraformaldehyde
PI3	Phosphoinositide 3
PRRs	Pattern recognition receptors
RMSF	Rocky Mountain spotted fever
PrsA	Parvulin-like peptidyl-prolylcis-transisomerase
OmpB	Outer membrane protein B
rpoB	RNA polymerase β-subunit-encoding gene
Sca	Surface cell antigen
SDS-PAGE	SDS-polyacrylamide gel electrophoresis
SEC	Size-exclusion chromatography

SFG	Spotted fever group
SpA	Staphylococcal protein A
TBS	Tris-buffer saline
TG	Typhus group
TLR4	Toll-like receptor 4
TRG	Transitional group
TRP120	Tandem repeat protein 120
UCS	Umbilical cord serum

List of Figures

Chapter I – Introduction

1.1 Bacterial moonlight proteins

Moonlight proteins comprise a subset of proteins that present more than one physiologically relevant function that is not due to gene fusion, multiple RNA splice variants, or pleiotropic effects (C. J. Jeffery, 1999). Another characteristic of these proteins is that the functions exerted are independent of each other, meaning that the inactivation of one function must not affect the others. According to MoonProt 3.0 (Chen et al., 2021) (http://moonlightingproteins.org) and MultitaskProtDB-II (Franco-Serrano et al., 2018) (http://wallace.uab.es/multitaskII), two repositories where these activities are being compiled, there are over 500 annotated moonlight/multitasking proteins, being extraordinarily diverse and involved in a large array of biological functions. Since many of the proteins evolved to exert various functions, there is not a shared sequence or structural feature that can be used to foresee the moonlighting activity, being mainly discovered by serendipity, proteomics, and yeast two-hybrid assays (Huberts & van der Klei, 2010). Additionally, if a protein is homologous to a moonlighting/multitasking protein, it does not imply that it presents the same functions since it can exert one, both, or none of the moonlighting protein functions (C. J. Jeffery, 2015). Another complication is identifying all the functions of a moonlight protein based on their structure/polypeptide (C. J. Jeffery, 2015). Due to this, it is difficult to identify and predict if a protein presents moonlight activity. However, bioinformatics approaches have been in development to aid in this process (Hernández et al., 2015; Khan et al., 2017; Shirafkan et al., 2021).

Moonlight proteins are present in several organisms, including animals, plants, yeasts, bacteria, and viruses (C. J. Jeffery, 2015; Ribeiro et al., 2019). These proteins have been gaining attention by playing important roles in autoimmune diseases, diabetes, and cancer (C. J. Jeffery, 2018). In bacteria, moonlighting proteins are present in both pathogenic and commensal bacteria, and many of these proteins are highly conserved in these organisms (G. Wang et al., 2014). Importantly, 25% of moonlight proteins are classified as virulence factors and may contribute to bacterial pathogenesis and

virulence (Espinosa-Cantú et al., 2020; C. Jeffery, 2018). Virulence factors are expressed and secreted by the pathogen, allowing it to colonize the host, establish infection, and evade the immune system, and can be classified into different groups, depending on their function (A. K. Sharma et al., 2017). Cytosolic factors allow bacteria to adapt to the host environment by undergoing quick adaptative metabolic, physiological, and morphological shifts. Membrane-associated factors facilitate bacteria adhesion and invasion of host cells, and secretory factors allow them to evade the host's innate and adaptive immune system as well as cause tissue damage (A. K. Sharma et al., 2017). Due to this, moonlight proteins are good targets to treat bacteria-caused diseases because they can be involved in many steps of infection. Major groups of bacterial moonlight proteins implicated in virulence include metabolic enzymes of the glycolytic and other metabolic pathways, molecular chaperones, and protein-folding catalysts (Henderson & Martin, 2011). Among these, most moonlighting virulence factors mediate adhesion and modulation of leukocyte activity.

Proteins with moonlight activity often exert their canonical function in a different cell compartment of their moonlight function **(Figure 1).** One example is the glycolytic enzyme Glyceraldehyde 3-phosphate dehydrogenase (GAPDH), the first identified bacterial moonlight protein (Kainulainen & Korhonen, 2014). GAPDH catalyzes the conversion of D-glyceraldehyde 3-phosphate to 3-phosphoD-glyceroyl phosphate in glycolysis when present inside the cell, and on the cell surface of group A streptococci can present adhesive functions *in vitro* (Pancholi & Fischetti, 1992). Besides presenting more than one function in group A streptococci, GAPDH moonlighting activity is also present in other species. In *Bacillus anthracis*, *Lactobacillus crispatus*, *Staphylococcus aureus,* and *Staphylococcus pneumoniae* GAPDH also binds to plasmin. Furthermore, GAPDH can bind fibronectin, an extracellular matrix component (ECM), and bind complement protein C5a, mediating immune evasion, among other described functions (Kainulainen & Korhonen, 2014).

Bacterial adherence factors are cell surface proteins that form and maintain physical interactions with host cells and tissues **(Figure 1).** This feature is crucial in pathogenic bacteria because it promotes infection but is also important in commensal

bacteria to maintain a symbiotic relationship with the host (C. Jeffery, 2018). Enolase is a well-characterized moonlight protein that converts 2-phosphoglycerate to phosphoenolpyruvate in glycolysis and can exert other functions on the surface of pathogens (C. Jeffery, 2018). Enolase can bind to the host's ECM or airway mucins and can bind to the coagulation cascade protease plasminogen in *Borrelia burgdorferi*, *Candida albicans*, *Streptococcus pneumoniae*, among others, contributing to bacterial virulence (Amblee & Jeffery, 2015).

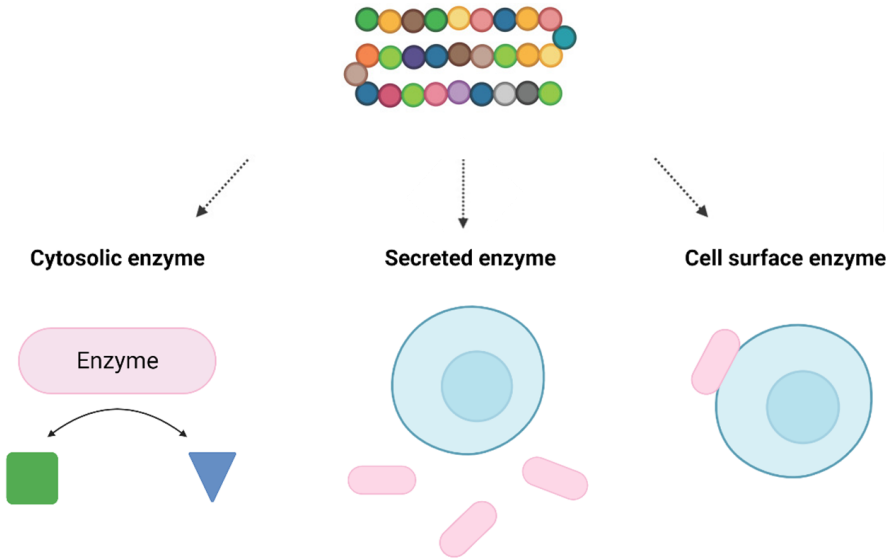

Figure 1: Schematic representation of a moonlight protein. Moonlight proteins comprise a variety of proteins where one polypeptide chain performs more than one function. Proteins with moonlight activity present different functions inside and outside of the cell. For example, a protein can convert a substrate (square) to a product (triangle) in the cytosol and exert a second function when is present at the cell surface. Cytosolic moonlight proteins can be secreted as signaling molecules, regulating various cell types in an organism or modulating host responses in the case of a pathogen. Surface moonlight proteins can act as adhesins, promoting the binding of the bacteria to the surface of host cells or the extracellular matrix. Furthermore, they can bind proteases, like plasminogen, promoting the degradation and invasion of the host tissue when the protease is active. Image adapted from (Liu & Jeffery, 2020).

Moonlight cytosolic proteins can be secreted as signaling molecules, regulating various cell types in an organism or modulating host responses in the case of a pathogen **(Figure 1).** In the cytosol, chaperones are proteins that bind and assist the folding or unfolding of macromolecular structures in order to prevent misfolding and promote reassembly and correct assembly of protein complexes (C. Jeffery, 2018). In mammals, heat shock protein 60 (Hsp60), GroEL, is a chaperone that mediates mitochondrial

protein import in the cell (C. Jeffery, 2018). However, it has been demonstrated that bacterial Hsp60/GroEL can mediate adhesion in several species, including *Clostridium difficile*, *Helicobacter pylori*, *Chlamydia pneumoniae*, contributing to their virulence (C. Jeffery, 2018). Elongation factor (EF)-tu is another example. It is a cytoplasmic protein important in protein synthesis that transports and catalyzes the binding of aminoacyl-tRNA to the ribosome. However, besides its canonical function, EF-tu can act as an adhesin at the surface of several pathogens such as *Mycobacterium pneumoniae* and *Pseudomonas aeruginosa* by binding fibronectin and plasminogen, respectively (Dallo et al., 2002; Kunert et al., 2007).

Among these multitasking proteins are also proteolytic enzymes mainly located in the membrane or secreted and recognized as virulence factors in various pathogenic bacteria (Culp & Wright, 2017). These molecules cleave specific peptide bonds of target proteins, resulting in activation, inactivation, generation of new proteins, and even changing protein function, being important in colonization and evasion of the host immune defenses, acquisition of nutrients for growth and proliferation, and facilitation of dissemination or tissue damage during infection (Lebrun et al., 2009; Rogers & Overall, 2013). For example, streptococcal C5a peptidase is a surface serine protease that cleaves and inactivates complement protein C5a. Furthermore, this protease can mediate fibronectin binding, acting as an adhesin. This moonlight function is important for streptococci virulence, helping in the attachment and invasion of eukaryotic cells (Beckmann et al., 2002). Additionally, *Escherichia coli* presents the protease OmpT, which acts as an adhesin to human cells (Torres et al., 2020; Wan et al., 2014).

1.2 Intracellular bacterial moonlight proteins

Moonlight activity is not exclusive of extracellular bacteria, being present in various intracellular pathogens such as *Listeria monocytogenes*, *Shigella flexneri, Legionella pneumophila,* and *Mycobacterium tuberculosis*. These organisms are responsible for causing diseases of global importance, as is the case of Legionnaire's disease or tuberculosis, resulting in significant morbidity and mortality (Leon-Sicairos et

al., 2015). Intracellular bacteria need the host cells to efficiently replicate and proliferate during infection, escaping the hosts' immune system (Bourdonnay & Henry, 2016). Most species enter the host through disruptions in the mucosae and the skin; however, others can enter directly into the bloodstream via bites of vectors such as mosquitoes and ticks (Mak & Saunders, 2006). Furthermore, intracellular pathogens can multiply into several cell types, such as epithelial cells, fibroblasts, monocytes/macrophages, and dendritic cells (Eisenreich et al., 2019).

Intracellular bacteria can form actin tails inside the host cells in order to spread from cell to cell. This structure is important in bacterial virulence and helps to spread the infection. Actin-based motility (ABM) requires actin polymerization and is mediated by the expression of bacterial factors that hijack host cell actin nucleation machinery or exhibit intrinsic actin nucleation properties (Köseoğlu & Agaisse, 2019). Besides ABM factor's canonical function, they can also display adhesion functions, such as bacterial aggregation, biofilm formation, and host cell adhesion/invasion. Some ABM factors that exert this moonlight function are *L. monocytogenes* ActA and *S. flexneri* IcsA (Köseoğlu & Agaisse, 2019)**.**

As previously described, Hsp60 chaperone mediates adhesion in several species (C. Jeffery, 2018). In *S. typhimurium,* Hsp60 also mediates bacterium aggregation to intestinal mucus (Ensgraber & Loos, 1992). Moreover, it was also observed that Hsp65 inhibition decreases bacterial binding in the intestine suggesting its role in this early step of infection (Ensgraber & Loos, 1992). Listeria adhesion protein (LAP) is an alcohol acetaldehyde dehydrogenase that acts as an adhesin in *L. monocytogenes*, being also a moonlighting protein (Jagadeesan et al., 2010). Hsp60 from *L. monocytogenes* interacts with LAP and promotes bacterial adhesion in enterocyte-like cells (Wampler et al., 2004). Furthermore, *L. pneumophila* Hsp60 presence on the cells' surface can also mediate invasion into non-phagocytic cells (Garduño et al., 1998). Bacterial Hsp70, DnaK, is the most conserved and ubiquitous heat shock protein (D. Sharma & Masison, 2009). Hsp70 can bind to plasminogen and cause its subsequent conversion to plasmin, the active form of the protease. This promotes the host ECM and basement membrane degradation, aiding host tissue invasion (Amblee & Jeffery, 2015; Henderson & Martin,

2011). Furthermore, *M. tuberculosis* DnaK can bind to the cluster of differentiation 40 (CD40), contributing to the synthesis of monocyte chemokines and the maturation of dendritic cells (Liu & Jeffery, 2020).

GAPDH also presents moonlight activity in intracellular bacteria. Besides its canonical function in glycolysis, GAPDH can be present on the surface of *L. monocytogenes* and *S. aureus* and bind plasmin, being important in the invasion and proliferation of these pathogens (Kainulainen & Korhonen, 2014). Moreover, enolase can bind ECM components plasminogen and laminin in *S. aureus*, contributing to the invasion of host tissues (Amblee & Jeffery, 2015). Other metabolic enzymes such as malate synthase from *M. tuberculosis* can act as an adhesin by binding fibronectin and laminin (Kinhikar et al., 2006). Moreover, *M. tuberculosis* glutamine synthetase can bind fibronectin and plasminogen (Xolalpa et al., 2007). Bacterial autolysins are peptidoglycan hydrolases that break down peptidoglycan components of cells, being important in cell division, separation, and cell wall turnover (Heilmann et al., 2003). Aaa autolysin present in *S. aureus* presents adhesive properties by binding fibronectin (Heilmann et al., 2005). Furthermore, Ami autolysin from *L. monocytogenes* can also mediate adherence to eukaryotic cells (Milohanic et al., 2000).

1.3 Complement system

Mammalian immune systems are very complex and provide defense against pathogens and host processes that cause disease (Dunkelberger & Song, 2009). The immune system is divided into two subsystems that are interconnected: innate and adaptive immunity. The adaptive immune system comprises T and B lymphocytes which recognize a variety of specific antigens, enabling the elimination of pathogens. Additionally, this subsystem gives rise to immunological memory and tailored immune responses (Dunkelberger & Song, 2009). The innate immune system presents immunological effectors that provide, robust, immediate, and nonspecific immune responses. In contrast, this subsystem does not provide immunological memory (Dunkelberger & Song, 2009).

The complement system is a crucial component of innate immunity, being one of the major effector mechanisms of this immune system. It consists in soluble proteins, membrane expressed receptors and regulators that are normally inactive, but in response to the recognition of molecular components they become sequentially activated causing a proteolytic cascade (Merle et al., 2015). This activation leads to the generation of proinflammatory mediators (anaphylatoxins), opsonization of pathogens surface mediated by opsonins and targeted lysis of the pathogen through the formation of a membrane attack complex (MAC) (Dunkelberger & Song, 2009). The complement system can be activated by the classical, alternative, and lectin pathways **(Figure 2)**.

The classical pathway initiates when C1q in complex with C1r and C1s serine proteases (C1 complex) bind to the Fc region of complement antibodies bound to pathogenic surfaces. The C1 complex cleaves C4 and C2 forming C4a, C4b, C2a and C2b. The larger fragments C4b and C2b associate and form the C3 convertase that has the ability to cleave C3 (Schartz & Tenner, 2020). The formation of the C3 convertase is the point at which all complement activation cascades converge. The cleavage of C3 generates anaphylatoxin C3a and opsonin C3b. C3b can bind covalently to hydroxyl groups of carbohydrates and proteins, binding to the microorganism. Finally, this binding leads to the further activation of the complement, forming anaphylatoxins and the assembly of MAC (Dunkelberger & Song, 2009). This pathway is also important in opsonophagocytosis. In the presence or absence of antibodies, C3b can bind to the pathogen, occurring opsonization (Mak et al., 2014). Opsonization facilitates the binding and entry into phagocytic cells due to the presence of complement receptors on the surface of the phagocytic cells such as macrophages (Mak et al., 2014). After the bacteria bind and are phagocytosed, they are degraded by lysosomes.

The lectin pathway initiates with the recognition of pattern recognition receptors (PRRs) such as mannose-binding lectin (MBL) and ficolins, being recognized as nonself (Dunkelberger & Song, 2009). The binding of MBL to the pathogen activates MBL-associated serine proteases, cleavage of C2 and C4 and subsequent generation of the C3 convertase.

Finally, the alternative pathway is initiated by spontaneous hydrolysis of C3 to C3b, which binds to the pathogen surface and binds Factor B. Factor B is cleaved into Ba and

Bb by Factor D, forming the alternative pathway C3 convertase C3bBb. This convertase transforms C3 into C3a and C3b, forming an amplification loop (Dunkelberger & Song, 2009). Properdin stabilizes the C3 and C5 convertase through extending the half-lives of the C3 and C5 converting enzymes, being important in the enhancing activity of this pathway (Frank & Sullivan, 2014).

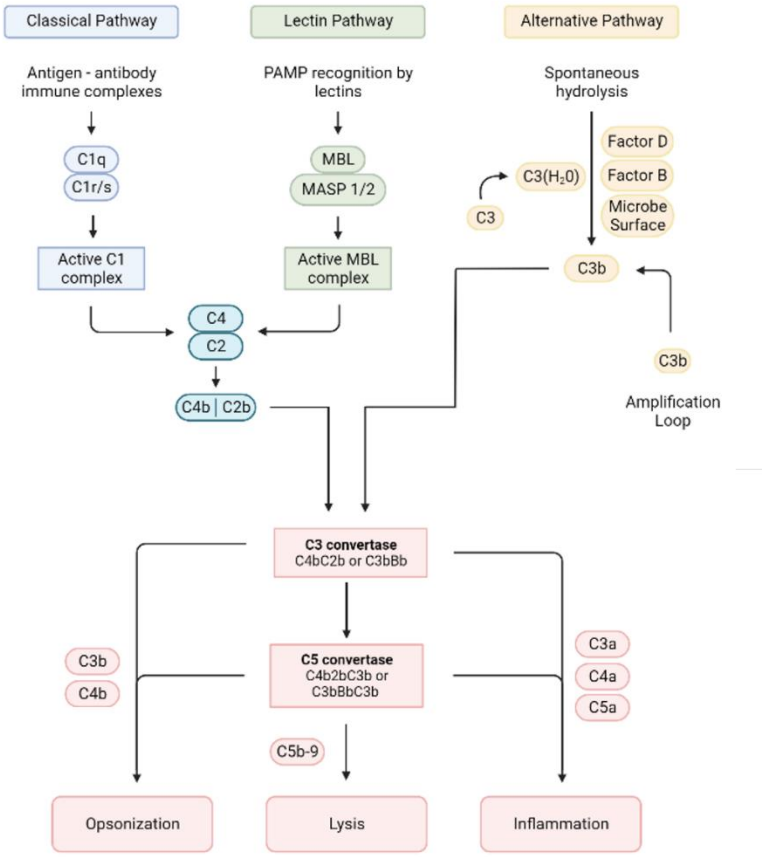

Figure 2: Schematic representation of the complement system cascade. The complement system can be activated by three pathways: classical, lectin, and alternative pathway. Classical pathway starts with the binding of C1q to antibodies present on the pathogen surface, recruiting C1r and C1s, resulting in the formation of C1 complex. C1 complex cleaves C4 and C2. C4b binds to the target cell surface and C2b binds to C4b forming the C3 convertase. Lectin pathway is activated by binding pattern recognizing mannose-binding lectins (MBLs) to carbohydrates on the surface of the pathogens. Activated MBL-associated serine protease (MASP) in the MBL-MASP complex cleaves C4 and C2, causing the subsequent formation of C3 convertase. The alternative pathway is activated by the spontaneous hydrolysis of C3, resulting in the formation of C3b. C3b binds to Factor B, and Factor D cleaves Factor B to Ba and Bb, resulting in the C3 convertase C3bBb. These pathways converge in the formation of the C3 convertase. C3b associates with C3 convertase, cleaving C5. C5b can bind to C6, C7, C8 and C9 to form the membrane attack complex on the surface of the pathogen, causing its lysis. Furthermore, these pathways can cause inflammation and opsonization. Image created in Biorender.

There are several proteins that can inhibit the complement, diminishing its activation to prevent errant activation and damages in the healthy host. The regulation occurs mainly at the level of the convertases, both in their assembly and enzymatic activity, and assembly of the MAC. Complement factor I (CFI) is a regulator of the classical and alternative pathway by cleaving C4b and C3b, respectively (Du Clos & Mold, 2013). Another modulator of the classical pathway is Factor H. Factor H presents cofactor activity with CFI-mediated C3 proteolytic activation, competes with factor Bb to bind to C3b and accelerates the decay of C3 convertase (Dunkelberger & Song, 2009; Riley et al., 2012). Furthermore, C4-binding protein (C4BP) regulates the activation of the classical and MBL pathways. C4BP accelerates the decay of unstable C3 and C5 convertases of the mentioned pathways by binding to C4b and displaying C2b. This protein is also a cofactor of CFI mediating the cleavage and inactivation of C4b (Ferreira & Cortes, 2022; Schartz & Tenner, 2020).

1.4 Immune evasion

The complement system is crucial to protect the host against invading pathogens. However, pathogens have adapted to the host environment by evolving evasion mechanisms that avoid, inactivate or manipulate the human complement system (Reddick & Alto, 2014; Rosbjerg et al., 2017). Bacteria present multiple tactics including modulation of their cell surface, release of proteins that inhibit or degrade host immune factors or mimic host molecules. These mechanisms can target the three complement activation pathways and consequently the final part of the cascade. Due to this, there is an increasing difficulty to develop new vaccines and new treatments.

The first described mechanism of complement evasion is the mimicking of complement regulatory proteins (Hovingh et al., 2016). *B. burgdorferi*, the only bacteria that uses this mechanism, expresses CD59-like protein on the membrane that binds C8b and C9, inhibiting the formation of MAC (Pausa et al., 2003). Bacteria can also express proteases that cleave complement components. *Pseudomonas aeruginosa* secretes two proteases, mainly *Pseudomonas* elastase and *Pseudomonas* alkaline protease, that degrade C1q and C3, inhibiting complement activation on the bacterial surface (Hovingh et al., 2016). Moreover, *Streptococcus pyogenes* can produce Streptococcal pyrogenic

exotoxin B that can cleave several substrates, including C3, immunoglobulins (Ig) and properdin. The degradation of C3 impairs the formation of C3 convertase and opsonization of bacteria. Additionally, cleavage of Ig prevents the IgG-mediated phagocytosis and cleavage of properdin impairs the alternative pathway by unstabilizing the C3 convertase (Hovingh et al., 2016).

Besides mimicking or cleaving complement proteins, bacteria can express molecules that inhibit the complement system, mainly targeting C3 (Hovingh et al., 2016). *S. aureus* expresses staphylococcal superantigen like 7 that binds C5, preventing the formation of C5a and subsequent decrease of neutrophil migration to the infection site (Hovingh et al., 2016). Additionally, *S.aureus* expresses extracellular fibrinogen-binding (Efb) protein and its homologue extracellular complement-binding (Ecb) protein that bind the C3d domain of C3b, inhibiting the formation of C3 convertase C3bBb and C5 convertase (Jongerius et al., 2007). Secreted factors Efb and Ecb can also form a complex with factor H and C3b on the cell surface of the pathogen, enhancing C3b degradation (Amdahl et al., 2010). Bacteria may present additional strategies such as binding to host proteins, avoiding the recognition by complement components. *Haemophilus influenzae* recruitment of C4BP to the bacterial membrane interferes with the classical pathway since it decreases C3b deposition and increases serum resistance, preventing cell lysis (Hallström et al., 2007). Other examples of C4BP-binding bacteria are *E. coli* (Tseng et al., 2012), *Neisseria gonorrhoeae* (Ram et al., 2001), *Streptococcus pyogenes* (Jenkins et al., 2006) and *S. aureus* (Hair et al., 2013), among others. *S. aureus* surface protein A (spA) interacts with the Fc region of IgG, forming a coating around the bacteria and avoiding neutrophil receptor recognition (A. Cruz et al., 2022; Foster, 2005). Moreover, it has been recently demonstrated that spA interaction with Fc region inhibits IgG hexamerization, interfering in the initiation of the classical pathway and downstream complement activation (A. R. Cruz et al., 2021).

Antimicrobial peptides (AMPs) protect the host against bacterial infection. These molecules are secreted by host cells such as epithelial cells of the skin and act as a tissue protective mechanism by presenting bactericidal and immunomodulatory properties (Thomassin et al., 2012). Moreover, neutrophils also secrete AMPs at the infection site (Reddick & Alto, 2014). AMPs bind to the anionic cell membrane of bacteria and disrupt

the membrane integrity, occurring efflux of essential molecules and ions. *S. aureus* presents the multiple peptide resistance factor protein (MprF) that protects the bacteria against defensin-like cationic peptides, a type of AMPs (Ernst et al., 2009). The hydrophilic C-terminal domain of MprF adds an L-Lysine to the anionic phospholipid phosphatidylglycerol when present in the inner leaflet of the bacterial membrane and the membrane-bound N-terminal portion of MprF flips the lipid to the outer leaflet. Finally, the positively charged lysine residue acts as an electrostatic buffer, diminishing bacterial affinity for cationic AMPs (Ernst et al., 2009). *E. coli* presents a different mechanism to be protected from AMPs. *E. coli* protease OmpT contributes to the degradation of α-helical AMPs, promoting bacterial survival (Thomassin et al., 2012).

Most host organisms recognize pathogen-associated molecular pattern (PAMPs) through PRRs with subsequent production of cell immune mechanisms or/and recruitment of immune cells in order to diminish infection (Matsuura, 2013). Various bacteria can modify the molecular structure of their PAMPs and consequently avoid their recognition by the immune system. Lipopolysaccharide (LPS) is present in the cell wall of Gram-negative bacteria, being composed by several O-antigen side chains that are anchored in the outer leaflet by Lipid A. Lipid A is recognized by host proteins PRR complex, occurring the activation of innate immune signaling pathways (Maldonado et al., 2016). *Yersinia pestis* has the ability to reduce the acetylation state of Lipid A when there is an increase of temperature from 21^{o}C to 37^{o}C. The hypoacetylation of Lipid A diminishes the recognition by the LPS receptor toll-like receptor 4 (TLR4), facilitating bacterial evasion and enhancing pathogenicity (Matsuura, 2013). Moreover, when *Shigella* is internalized by the host cells, hypoacetylated Lipid A is used to escape the activation of the innate immune system, allowing them to spread and disseminate (Reddick & Alto, 2014).

1.5 *Rickettsia*

Rickettsia is a genus of obligate intracellular bacteria that presents a small and conserved genome (Andersson et al., 1998; McLeod et al., 2004). These organisms are globally widespread, and their geographical distribution is mostly defined by both vector and natural host constraints. Based on molecular analysis, *Rickettsia* can be divided into

four groups: Spotted fever group (SFG), Ancestral Group (AG), Typhus group (TG) and Transitional group (TRG) (Thu et al., 2019). Many rickettsial species belonging to the TG and SFG are pathogenic to humans. The developed disease in the host depends on the pathogens specie, ranging from mild illness to rapidly fatal disease (Dumler, 2012; Sahni et al., 2019). For example, *R. conorii* causes Mediterranean spotted fever and is associated with high morbidity and mortality (Curto, Riley, et al., 2019a; Rovery & Raoult, 2008), and *R. prowazekii* causes epidemic typhus and is responsible for epidemics, being associated with high fatality rates if the infected person does not receive antibiotic treatment (Akram et al., 2021). Furthermore, *R. prowazekii* is present in category B of potential bioterrorism by the United States Centers for Disease Control and Prevention (Walker & Ismail, 2008), demonstrating its pathogenicity.

There is a growing concern about the globally increasing incidence of SFG rickettsioses; not only the most severe forms of these diseases but, particularly, milder forms caused by new species of rickettsiae (European Centre for Disease Prevention and Control., 2013; Parola et al., 2013). For example, the incidence of SFG rickettsioses in the U.S. has significantly increased over the last two decades, from 1.7 to 19.2 cases per million persons from 2000 to 2017 (Binder & Armstrong, 2019; Drexler et al., 2016, pp. 2008–2012). Rocky Mountain spotted fever (RMSF), caused by *R. rickettsii* is still the most severe and fatal of the SFR. Recent outbreaks of RMSF in Mexico (2004-2016) resulted in case fatality rates of ~29%-30% (higher in children <10), representing an expanding public health problem (Álvarez-Hernández et al., 2017). Mediterranean spotted fever, caused by *R. conorii* is endemic to the Mediterranean basin and considered the most prevalent rickettsial disease in Europe (Spernovasilis et al., 2021). There is also a growing concern in Europe about the increasing incidence of milder rickettsioses, such as tick (*Dermacentor*)-borne lymphadenopathy/Dermacentor-borne necrotic erythema and lymphade-nopathy (TIBOLA/DEBONEL) syndrome (Buczek et al., 2020), and the epidemiological importance of SFG rickettsioses in Africa is increasingly recognized (Heinrich et al., 2015). Importantly, rickettsial diseases caused by *R. typhi* and *R. felis* occur worldwide, and emergence patterns for both are evident in many regions of the globe (Brown & Macaluso, 2016; Caravedo Martinez et al., 2021).

Rickettsia can be transmitted to various mammalian hosts, including humans and animals, through arthropod vectors such as ticks, lice, and fleas (Walker & Ismail, 2008). When the vector is infected, *Rickettsia* can grow and multiply in several organs including the ovaries that will originate the oocytes, occurring transovarial transmission, as well as trans-stadial passage since the infection prevails from egg to adult (Walker & Ismail, 2008). Vectors' salivary glands are also infected by *Rickettsia*, allowing the passage of the bacteria to animals or humans when they are bitten by the infected vector. Furthermore, *Rickettsia* can also be passed from an infected animal to an uninfected vector resulting in horizontal acquisition (Walker & Ismail, 2008).

In the host, *Rickettsia* infects mainly endothelial cells, although it has been shown that *Rickettsia* can also infect other types of cells, such as macrophages. In fact, it is suggested that the ability for *Rickettsia* to enter in macrophages depends on the degree of pathogenicity, which may help to explain why certain species cause disease (Curto et al., 2016; Curto, Riley, et al., 2019b; Curto, Santa, et al., 2019). Curto and colleagues have demonstrated that pathogenic *R. conorii* can survive and proliferate in THP-1 macrophages, but non-pathogenic *R. montanensis* proliferation is compromised and bacteria are rapidly destroyed (Curto et al., 2016). Additionally, both species trigger different proteomic signatures in macrophage-like cells during infection. *R. conorii* causes a metabolic rewriting of macrophages transforming into anti-inflammatory M2-like macrophages, augments several enzymes of metabolic pathways such as tricarboxylic acid cycle, and induces the accumulation of proteins involved in protein processing and quality control in endoplasmic reticulum (ER). Additionally, various proteasome and immunoproteasome subunits are less abundant in *R. conorii* and *R. montanensis* that might contribute to escape immune surveillance (Curto, Santa, et al., 2019). Recent evidence by Engström and colleagues have shown that *R. parkeri* mutant lacking outer membrane protein B (OmpB) was unable to grow in macrophages, and the dissemination of *Rickettsia* through the different mouse organs was severely impaired (Engström et al., 2019). These results support a role of macrophages in the dissemination of *Rickettsia*.

Rickettsia can enter the non-phagocytic cells by adhering to the host membrane, being phagocytosed. After, there is the formation of phagosomes that bacteria can

evade and start to multiply in the cell. *Rickettsia* can manipulate the cell cytoskeleton, forming actin tails that allow the passage to neighbor cells, being important in the spreading of the infection. The formation of actin tails is not present in all species of *Rickettsia*. Bacteria from the TG cannot form actin tails, multiplying in the cytosol until the lysis of the cell with the subsequent spreading of the infection (Raoult, 2015; Van Kirk et al., 2000).

Apoptosis is an important defense mechanism in cells to prevent infection in the host. Pathogens have evolved several ways to modulate cell death pathways, contributing to their pathogenesis (Curto, Riley, et al., 2019b). Curto and colleagues have demonstrated that *Rickettsia* can modulate macrophages upon infection, delaying the apoptotic events. THP-1 macrophages infected with *Rickettsia* present downregulation of apoptotic process genes (Curto, Riley, et al., 2019b). *R. conorii* infection significantly reduces cleaved Poly (ADP-ribose) polymerase (PARP)-positive THP-1 cells, protecting against apoptosis (Curto, Riley, et al., 2019b). These results suggests that *R. conorii* actively modulates apoptotic signaling in order to maintain host cell viability (Curto, Riley, et al., 2019b).

Economic globalization, changes in land use and urbanization, increase in travel, and global warming have all been postulated to raise the distribution and incidence of diseases caused by *Rickettsia* (El-Sayed & Kamel, 2020; Wu et al., 2017). Accordingly, there is a growing concern about rickettsioses and their impact on global health (El-Sayed & Kamel, 2020; Parola et al., 2008). All *Rickettsia* are susceptible to antibiotics of the class tetracycline, which inhibit protein synthesis, such as doxycycline (Rolain et al., 1998). However, there are few antibiotics that treat rickettsial diseases and a study demonstrated that one point mutation in the RNA polymerase β-subunit-encoding gene (rpoB) sequence leads to rifampicin resistance in rifampicin-susceptible species (Drancourt & Raoult, 1999). Due to this, it is important to discover new targets to treat rickettsial diseases. To find these targets, it is important to identify and characterize virulence factors of *Rickettsia*.

1.5.1 *Rickettsia* moonlight virulence factors

Rickettsia presents virulence factors that exhibit moonlight activity such as OmpB, Adr2, PrsA and Sca2. These proteins are important in several steps of *Rickettsia* infection including adhesion, invasion, and immune evasion.

Rickettsial OmpB is an autotransporter protein that is a major component of the rickettsial outer membrane (Riley et al., 2012), and for which several functions have been described. Adherence and subsequent invasion of host cells are crucial for establishing rickettsial infection (Chan et al., 2009). rOmpB mediates the adherence and invasion of non-phagocytic cells by binding specifically to Ku70, a receptor present in the membrane of host cells (Walker & Ismail, 2008). rOmpB-Ku70 mediated bacterial uptake relies on actin polymerization, protein tyrosine kinase, and phosphoinositide 3 (PI3)-kinase-dependent activities and microtubule stability. Additionally, bacterial entry into the host cells is also dependent on endocytic pathway proteins c-Cbl, clathrin, and caveolin-2, suggesting their contribution to the rOmpB-Ku70 mediated internalization process (Chan et al., 2009). Tick histone H2B is a component of the nucleosome that is also present on the surface of tick cells. Thepparit and colleagues demonstrated that rOmpB binds H2B and that the depletion of this histone results in significant inhibition of *R. felis* infection (Thepparit et al., 2010). The complement system is a crucial component of innate immunity that, in response to the recognition of molecular components, becomes sequentially activated, causing a proteolytic cascade that converges with the formation of C3 convertase that cleaves C3 (Merle et al., 2015). This activation leads to the generation of proinflammatory mediators (anaphylatoxins), opsonization of pathogens mediated by opsonins, and targeted lysis of the pathogen through the formation of a membrane attack complex (MAC) (Dunkelberger & Song, 2009). Riley and colleagues demonstrated that rOmpB exerts an additional function, mediating serum resistance through interaction with Factor H (Riley et al., 2012). Factor H is a protein that acts as a regulator of the alternative pathway of the complement by disrupting C3 convertase activity. Depletion of factor H from normal human serum diminishes rickettsial survival, and factor H-binding results in lower deposition of C3 and MAC on the surface of *Rickettsia*. These results show that factor H binding partially

inhibits the alternative pathway, contributing to *R. conorii* survival in serum. Finally, expression of the cleaved form of rOmpB (rOmpB β-peptide) in the outer membrane of *E. coli* is sufficient to protect the bacteria against the bactericidal properties of human serum, further supporting rOmpB role in immune evasion (Riley et al., 2012). Recently, Engström and colleagues demonstrated that rOmpB also promotes autophagy evasion (Engström et al., 2019). rOmpB prevents ubiquitination of bacterial surface proteins and subsequent recognition by autophagy receptors and is required to form a capsule-like layer. As previously mentioned, this work shows that rOmpB is essential for *R. parkeri* growth in macrophages and organ colonization in mice by acting as a protective shield to inhibit antimicrobial autophagy (Engström et al., 2019).

Parvulin-like peptidyl-prolylcis-transisomerase (PrsA) is an outer membrane-anchored protein that acts as a foldase, important in folding secreted proteins, including toxins and virulence factors (Emelyanov & Demyanova, 1999; Jakob et al., 2015). Expression of the *R. prowazekii* homolog in *E. coli* confirmed its peptidyl-prolyl cis/trans isomerase activity (Emelyanov & Loukianov, 2004). As observed in rOmpB, PrsA also interacts with histone H2B, facilitating infection in a tick cell line and suggesting an additional role in adhesion (Thepparit et al., 2010).

Adr2 is a rickettsial outer membrane protein that has been identified in all pathogenic species of *Rickettsia*. Garza and colleagues demonstrated that Adr2 expression in *E. coli* is sufficient to mediate serum resistance, suggesting its role in immune evasion through interaction with vitronectin, a glycoprotein that inhibits the formation of MAC, inhibiting bacterial lysis (Garza et al., 2017). Furthermore, it has been suggested Adr2 role as an adhesin, in *R. prowazekii* and *R. rickettsii* (Vellaiswamy et al., 2011). However, the expression of Adr2 in a non-adherent strain of *E. coli* is not sufficient to mediate adherence to mammalian endothelial cells (Garza et al., 2017). Therefore, Adr2's role in adhesion and invasion is still conflicting and needs to be further elucidated.

Surface cell antigen 2 (Sca2), a surface protein of SFG *Rickettsia,* is another example of a protein with moonlight activity. Cardwell and Martinez showed that expression of Sca2 in a heterologous system is sufficient to mediate adherence and

invasion of mammalian epithelial and endothelial cells (Cardwell & Martinez, 2009). Additionally, it has been demonstrated that Sca2 is a bacterial actin assembly factor that functionally mimics eukaryotic formin proteins (Haglund et al., 2010; Madasu et al., 2013). Sca2 nucleates unbranched actin filaments that are observed in *Rickettsia* and associates with growing barbed ends. Furthermore, this protein requires profilin (an actin-binding protein that promotes assembly) for efficient elongation (Haglund et al., 2010). Sca2 also inhibits the activity of capping protein, promoting actin filaments growth. These results demonstrate Sca2's role in promoting actin filament nucleation and elongation to assemble actin tails, important in *Rickettsia* motility (Haglund et al., 2010; Madasu et al., 2013).

1.5.2 Aspartic protease from *Rickettsia conorii* (APRc)

Previous work from our laboratory identified an aspartic protease that is highly conserved in *Rickettsia*, named aspartic protease from *Rickettsia conorii* (APRc) (R. Cruz et al., 2014). APRc is a membrane-embedded protein that presents an intramembrane region and a soluble region that is present in the outer side of the cell **(Figure 3).** This protease shares several features with other retropepsin-like proteases. In order to be functional, APRc needs to be in a symmetric homodimer and presents an active site where each monomer contributes one catalytic aspartate.

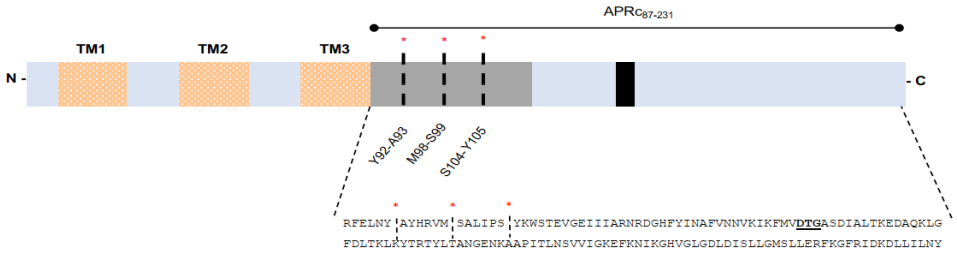

Figure 3: Schematic representation of full-length aspartic protease APRc. APRc is predicted to present three transmembrane domains at the N-terminal (TM1, TM2 and TM3) and a soluble domain at the C terminus ($APRc_{87-231}$). Dashed lines with red * represent the cleavage sites of APRc autocatalytic activity identified by Edman degradation. The black box represents the catalytic active site DTG. Image obtained from (Teixeira & Simões, Unpublished).

Li and colleagues demonstrated that APRc monomer folding is similar to the canonical form of retropepsins, despite the low sequence similarity (Li et al., 2015). However, the quaternary structure of APRc dimer diverges from the canonical form of retropepsins because the catalytic aspartate residues of each monomer are not close. The formation of this structure can be due to the presence of an extended C terminus, where the His tag is present, a crystallization artifact, or a combination of both since this does not support the previously reported APRc enzymatic activity (Li et al., 2015). APRc presents autoprocessing activity *in vitro* upon incubation of its recombinant soluble domain fused with GST (rGST-APRc$_{87-231}$) at pH 6.0, appearing intermediate cleavage products APRc$_{93-231}$ and APRc$_{99-231}$, and the activated form APRc$_{105-231}$ **(Figure 4)**, whose cleavage sites were confirmed through Edman sequencing: Tyr92-Ala93, Met98-Ser99, and Ser104-Tyr105 **(Figure 3)**. On the other hand, when the catalytic aspartate was mutated (D140A), changing the aspartic acid by alanine, there was an impairment of the APRc multistep processing of the recombinant soluble domain of APRc **(Figure 4)**. These results demonstrate that the autoprocessing activity is dependent on the catalytic aspartate residue. Additionally, APRc autocatalytic activity using rGST-APRc$_{87-231}$ has also been observed in *E. coli* and in eukaryotic cells (Teixeira and Simões, Unpublished). In these systems the final putative form APRc$_{105-231}$ was detected, without the formation of the intermediate forms, suggesting that APRc autoprocessing is faster *in vivo* than *in vitro*. Furthermore, in the presence of oxidized insulin B chain, a substrate usually cleaved by aspartic proteases, there is the appearance of insulin fragments concomitant with the appearance of the activation product APRc$_{105-231}$, demonstrating rGST-APRc$_{87-231}$ enzymatic activity and suggesting that the protein needs to undergo processing in order to be active towards the substrate. In the presence of the protease inhibitor EDTA and specific inhibitors of the retropepsin human immunodeficient virus-1 protease (HIV-1 PR) that is important in HIV maturation, APRc is significantly inhibited, supporting that APRc is a retropepsin-like protease (R. Cruz et al., 2014). On the other hand, APRc is insensitive to the presence of the classical aspartic protease inhibitor pepstatin A.

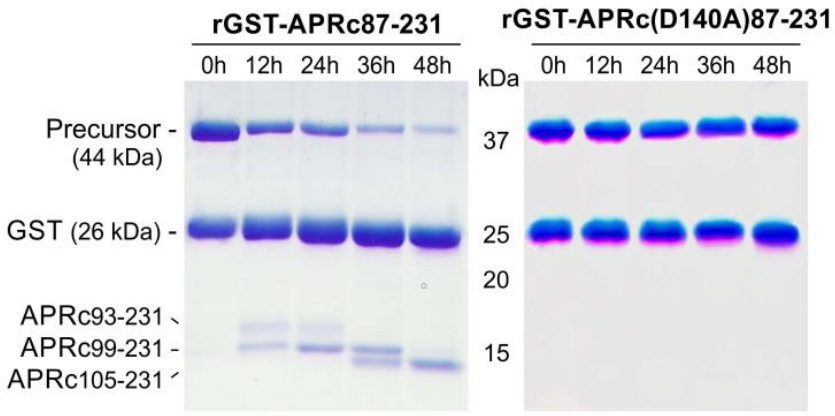

Figure 4: APRc autoprocessing activity *in vitro*. SDS-page with Coomassie blue staining of the recombinant soluble domain of APRc fused with GST (rGST-APRc$_{87-231}$) produced in *E. coli*. APRc$_{87-231}$ (44 kDa) presents autoprocessing activity resulting in the formation of three products: intermediate forms APRc$_{93-231}$ and APRc$_{99-231}$ and final form APRc$_{105-231}$. The catalytic aspartate mutant rGST-APRc(D140A)$_{87-231}$ was also evaluated but as opposite as observed in the wild-type form, there is not the formation of cleavage products, demonstrating impairment of the autocatalytic activity. Image obtained from (R. Cruz et al., 2014).

Cruz and colleagues have demonstrated that APRc catalyzes the *in vitro* processing of Sca5/OmpB and Sca0/OmpA autotransporter proteins that mediate adhesion and invasion of host cells by *Rickettsia*, suggesting its role as a modulator of rickettsial surface virulence factors (R. Cruz et al., 2014). Transactivation assays using total membrane fractions of *E. coli* enriched in rOmpB incubated with the activated APRc soluble domain (APRc$_{105-231}$) demonstrated that in the presence of APRc$_{105-231}$ there is a decrease of the full-length form of rOmpB and an increase of rOmpB-βbarrel, the cleaved form of OmpB (R. Cruz et al., 2014). Additionally, when the active site mutant form of APRc was used, the rOmpB proprotein was not cleaved. These results were also obtained when using rOmpA (R. Cruz et al., 2014).

As mentioned before, *Rickettsia* can modulate the host cells, preventing apoptosis. In fact, APRc might be involved in the modulation of cell death processes during rickettsial infection (Teixeira and Simões, Unpublished). When the GFP_APRc-fusion WT constructs were expressed and active in mammalian cells it caused morphological alterations that are observed in cell death processes such as nuclear condensation, membrane blebbing, and the presence of fragmented cellular material (Teixeira and Simões, Unpublished). Cells expressing the previously mentioned

construct also present a significant increase in cleaved caspase-3 positive cells and cleaved PARP was slightly increased. Additionally, it was observed an increase in the percentage of annexin V-APC^{+}/DAPI^{-} cells (Teixeira and Simões, Unpublished). These data support that APRc may trigger apoptosis. Although, it is necessary to perform additional assays in order to confirm this cell death phenotype.

Bacterial surface proteins that display non-immune Ig binding activity are important in immune evasion because they confer protection against complement attack, decreasing opsonization and phagocytosis (Sidorin & Solov'eva, 2011). Curto and colleagues have shown that APRc presents non-immunogenic Ig-binding activity and is involved in serum resistance (Curto et al., 2021). *R. africae* and *R. massiliae* can bind human IgG at the cell surface, both from isolated human IgG and normal human serum (NHS). Total protein extracts from *R. montanensis*, *R. massiliae*, *R. parkeri*, and *R. africae* probed with human IgG antibody presented protein bands with molecular weights similar to the molecular weights of APRc. Indeed, when the protein extracts from the previously mentioned species were incubated with APRc-blocked human IgG antibody there was an impairment of IgG binding, suggesting APRc interaction with IgG (Curto et al., 2021). Moreover, APRc can bind IgG from different species (human, rabbit, and mouse) in a concentration-dependent manner and can bind different classes of Ig (IgG, IgM, IgA), presenting stronger interaction with IgG. APRc interacts with the Fab region of the antibodies, being one of APRc interacting regions between the amino acids 150-166. Additionally, the binding is independent of the catalytic activity. Interestingly, *E. coli* expressing the full-length protease or the catalytic mutant display resistance to complement-mediated killing, although the differences in protection (higher in the WT) suggest that APRc interferes with other serum components. Furthermore, IgG contributes to the observed serum resistance. Its deposition is increased on the surface of APRc-expressing *E. coli* and when IgG and IgM are depleted there is increased C3 deposition on *R. massiliae* surface (Curto et al., 2021). Taken together, APRc-Ig interaction is important for immune evasion, possible acting as a shield to protect against complement deposition.

As previously referred, *Rickettsia* is transmitted by arthropod vectors to the host, being the serum one of the first barriers that bacteria encounters. Pull-down assays

using recombinant APRc$_{110-231}$HisShort and APRc$_{110-231}$HisShort(D140N) incubated with NHS demonstrate differences between the two forms of APRc (Curto et al., 2021). It is visible a difference between the profiles of the eluted proteins of APRc$_{110-231}$HisShort and APRc$_{110-231}$HisShort(D140N) in the region between 50 and 75 kDa, presenting an additional protein band and less intensity in the wild type form **(Figure 5)**. Taken together these and the results of the serum resistance assays, we hypothesize that APRc potentially binds and cleaves other proteins from human serum. Furthermore, the protein bands of the mentioned region were excised from the gel and analyzed by mass spectrometry in order to identify putative substrates. Preliminary data suggests that complement proteins C3 and C4 might be candidate APRc substrates.

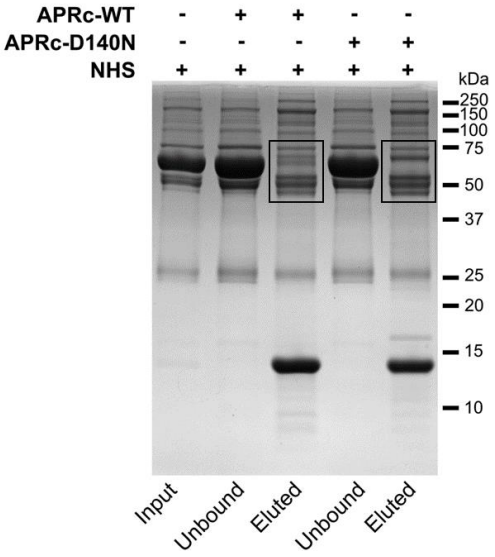

Figure 5: APRc targets components from human serum. SDS-page stained with Coomassie blue of normal human serum (NHS), not-linked (unbound) and eluted samples of the soluble form of APRc (APRc-WT) and the soluble form of the catalytic aspartate mutant (APRc-D140N) fractions. The black boxes represent the regions that present different protein profiles in APRc-WT when comparing with APRc-D140N, suggesting that this aspartic protease presents substrates in human serum. APRc protein band is present at approximately 14 kDa in the eluted samples. Image obtained from (Curto et al., 2021)

1.6 Research objectives

Moonlighting proteins represent a vast group of virulence factors in many pathogenic bacteria. Given the reduced genomes of the organisms belonging to the genus *Rickettsia*, understanding the importance of this multitasking phenomenon to expand their virulence landscape is of paramount relevance. Since proteases can be involved in different stages of bacterial pathogenesis (Marshall et al., 2017), rickettsial protease APRc might also present this purpose and possibly present moonlight activity, performing more than one function in the bacterial infectious process and progression. These characteristics, along with the previously mentioned results, support APRc moonlighting, being a good target to develop new therapies against rickettsioses. However, there is a need to explore more about APRc protein-protein interactions as well as its substrates to acknowledge its moonlight activity.

Curto and colleagues study demonstrated that APRc-Ig interaction promotes immune evasion, and that this interaction occurs mainly with the antibody's Fab region. Furthermore, this study suggests that APRc presents substrates in human serum (Curto et al., 2021). Preliminary data suggests that C3 and C4 are putative substrates/interactors. As previously mentioned, it has been described that the classical and MBL pathways regulator C4BP can mediate immune evasion in relevant pathogens, such as *S. pyogenes* and *S. aureus* (Hair et al., 2013; Jenkins et al., 2006). Moreover, it has been described few proteins that bind both C4BP and Ig, including proteins M22 and Arp4 from *S. pyogenes* (Carlsson et al., 2003; Johnsson et al., 1996; Pleass et al., 2001, p. 89). Since APRc has the ability to bind IgG, C4BP rises as a potential substrate of this aspartic protease.

Therefore, this work aims to unveil APRc moonlighting by further analyzing APRc non-immune Ig-binding and by analyzing C3, C4, and C4BP as putative APRc substrates in serum. Recombinant soluble and biotinylated APRc constructs will be expressed in *E. coli* and purified. APRc binding to different IgG isoforms will be assessed. Additionally, APRc binding to light chains, a component of the Fab region, will be evaluated. C3, C4 and C4BP surface deposition on *E. coli* and *Rickettsia* will be assessed. Furthermore, APRc binding and cleavage of these complement proteins will be evaluated in the presence of isolated proteins and in a more complex system (human serum). The

potential contribution of IgG to these interactions will be also assessed. Finally, the formation of C3 and C4 complexes at the surface of bacteria, as well as APRc's impact on the activation of complement pathways will be evaluated.

Chapter II – Material and Methods

2.1. Materials

The rabbit polyclonal anti-C3 antibody (PA5-21349), the anti-mouse IgG (whole molecule)-Peroxidase antibody (A9044), the anti-rabbit IgG (whole molecule)-Peroxidase antibody (A0545), IgG from human serum (I2511), IgG1 κ light chain from human myeloma plasma (I5154), IgG1 λ light chain from human myeloma plasma (I5029) and κ light chains (Free) from human myeloma sera (K3388) were purchased from Sigma-Aldrich (St. Louis, MO, USA). The goat anti-mouse IgG (H+L) Highly Cross-Adsorbed Secondary Antibody, fluorescein isothiocyanate (FITC; A16079), the goat anti-rabbit IgG (H+L) Highly Cross-Adsorbed Secondary Antibody, FITC (F-2765) and the rabbit anti-goat IgG (H+L) Secondary Antibody, HRP (#81-1620) were produced by Invitrogen (Carlsbad, CA, USA). The purified mouse anti-human C3a/C3a(desArg)/C3 antibody (#518102) and biotin mouse anti-human C3a/C3a(desArg)/C3 antibody (#518002) were purchased from Biolegend Way (San Diego, CA, USA). The mouse anti-human C4BPα (sc-398720), the mouse anti-human C4BPβ (sc-514553), the mouse anti-C4α (sc-271181), and the mouse anti-human C3 (sc-28294) were acquired from Santa Cruz Biotechnology (Dallas, TX, USA). Human IgG1 (31R-1087), IgG2 (31-AI18), IgG3 (31-AI19) and IgG4 (31-1009) antibodies were produced by Fitzgerald Industries International (Acton, MA, U.S.A). The goat anti-human C3 (A213) and the goat anti-human C4 (A205) were produced by Complement Technology (Tyler, TX, U.S.A). The rabbit polyclonal anti-APRc raised towards the sequence Cys-Tyr-Thr-Arg-Thr-Tyr-Leu-Thr-Ala-Asn-Gly-Glu-Asn-Lys-Ala was produced by GenScript (Piscataway, NJ, EUA).

The purified complement proteins C4 (A105), C4BP (A109) and pre-activated Zymosan from *Saccharomyces cerevisae* (B400) were purchased from Complement Technology were produced by Complement Technology (Tyler, TX, U.S.A). Normal Human Serum (from male AB clotted whole blood; H6914) and complement C3 from human serum (C2910) were purchased from Sigma-Aldrich (St. Louis, MO, USA). Human complement IgG/IgM depleted serum (34010) and Human Serum Type AB Sterile Male Off-Clot Pooled (34006) were purchased from Pel-Freez (Rogers, AR, U.S.A). Umbilical Cord Serum was donated by Crioestaminal (Cantanhede, Portugal). Streptavidin-

Horseradish peroxidase (HRP; #3999S) was purchased from Cell Signalling Technology (Danvers, MA, EUA). WIESLAB® Complement System Screen RUO kit (COMPL300RUO) was purchased from Svar Life Science (Lundavägen, Malmö, Sweden). *E. coli* TOP10F' and BL21 Star (DE3) competent cells were prepared according with the calcium chloride method.

2.2 Expression and purification of the soluble forms of APRc

2.2.1 Protein expression

To purify the wildtype and corresponding catalytic mutant soluble forms of APRc ($APRc_{110-231}$), competent BL21 Star (DE3) *E. coli* were transformed with pET23a plasmids encoding $APRc_{110-231}$ WT and $APRc_{110-231}$ D140N with a Histag in the C-terminal ($APRc_{110-231}$ HisShort). *E. coli* were grown in LB medium pH 7.4 containing 100 µg/mL of ampicillin at 37ºC with agitation until the $O.D_{600nm}$ was between 0.6 and 0.7. When the culture reached this absorbance, protein expression was induced by the addition of 0.1 mM isopropyl-β-d-thiogalactopyranoside (IPTG) for 4h at 30ºC with agitation. The cultures were centrifuged at 2246 x *g* for 20 min at 4ºC in an Avanti J-26S XPI Centrifuge using a JLA 8.1000 rotor. Supernatant was discarded and the pellets (corresponding to 2L of expression) were resuspended in 40 mL of 20 mM sodium phosphate containing 500 mM NaCl and 10 mM Imidazole pH 7.4 (Buffer A) and stored in -20ºC.

2.2.2 Bacterial lysis followed by immobilized metal affinity chromatography (IMAC) using Ni Sepharose

The pellets were thawed at room temperature and added to an Emulsiflex-C3 (Avestin, ON, Canada) previously washed and equilibrated in Buffer A, where the cells were mechanically lysed using high-pressure. After, the lysates were harvested at 17418 x *g* for 20 min at 4ºC in an Avanti J-26S XPI Centrifuge using a JA 25.50 rotor. The supernatant was collected and ultracentrifuged at 144028 x *g* for 20 min at 8ºC in an Optima™ L-100 XP Ultracentrifuge (Beckman Coulter) using a 90Ti rotor. The supernatant was collected and loaded in a previously charged and equilibrated in Buffer A Histrap HP 5 mL column (GE Healthcare Life Sciences). The column was subjected to

a program of four-step gradient of imidazole (50 mM, 150 mM, 200 mM, and 500 mM) using 20 mM sodium phosphate containing 500 mM NaCl and 500 mM Imidazole pH 7.4 at a flow of 5 mL/min in an ÄKTA FPLC system (Amersham Biosciences). Absorbance was measured at 280 nm. Since imidazole presents absorbance at 280 nm, prior to the purification the newly charged Histrap HP 5 mL column with Ni Sepharose™ High Performance was subjected to the previously mentioned program, to evaluate the baseline absorbance on each gradient step. The collected protein (200 mM imidazole step) was dialyzed overnight in a 3.5 kDa Spectra/Por®3 dialysis membrane in 5L 20 mM HEPES pH 7.4 at 4^{o}C with agitation. This allows to decrease NaCl and Imidazole concentration in the samples and exchange the buffer to HEPES.

2.2.3 Cationic Exchange Chromatography

The next day, the dialyzed samples were ultracentrifuged at 144028 x *g* for 20 min at 8^{o}C in an Optima™ L-100 XP Ultracentrifuge (Beckman Coulter) using a 90Ti rotor. The supernatant was collected and injected into a MonoS™ 5/50L column of cationic exchange (GE17-5168-01; GE Healthcare) previously equilibrated in 20 mM HEPES pH 7.4. A program with a linear gradient of NaCl (0 to 1M) was performed using the buffer 20 mM HEPES containing 1M NaCl pH 7.4 at a flow of 0.75 mL/min in an ÄKTA FPLC system (Amersham Bioscience). Absorbance was measured at 280 nm. Eluted fractions were evaluated by SDS-PAGE as described in section 2.11. Protein concentration of each fraction was evaluated using a NanoDrop 1000 spectrophotometer (Thermo Fisher Scientific) and samples were frozen at -80^{o}C.

2.2.4 Size exclusion chromatography (SEC)

The oligomerization state of the constructs was assessed by analytical-size exclusion chromatography using a high-pressure liquid chromatography (HPLC) system (Shimadzu). The collected fractions were injected in a Superdex 200 5/150 GL column (Cytiva) previously equilibrated in 20 mM HEPES pH 7.4 containing 100 mM NaCl. An isocratic program was conducted with the mentioned buffer at a flow of 0.25 mL/min and measured at an absorbance of 220 nm. To estimate the size of our protein,

ribonuclease A (13.69 kDa) and carbonic anhydrase (29 kDa) were also injected in the column.

2.3 Expression and purification of biotinylated APRc

2.3.1 Protein expression

To purify biotinylated APRc, competent BL21 Star *E. coli* containing the pDW363ΔMBP (encoding the biotin protein ligase birA) were transformed with a pCoofy plasmid expressing the soluble form of APRc with the N-terminal containing a Histag and the C-terminal containing a biotin accepting peptide (avi-tag; HisAPRc$_{110-231}$-avi). BirA ligase recognizes the avi-tag present in the APRc construct, promoting biotinylation in the presence of biotin. *E. coli* were grown in LB medium containing 100 µg/mL of ampicillin, 50 µg/mL of kanamycin and 50 µM biotin at 37^{o}C with agitation. When the culture reached an O.D$_{600nm}$ between 0.6 and 0.7, protein expression was induced at a final concentration of 0.1 mM IPTG overnight at 20^{o}C with agitation. After, the cultures were centrifuged at 2246 x *g* for 20 min in an Avanti J-26S XPI Centrifuge using a JLA 8.1000 rotor centrifuge. Supernatant was discarded and the pellets corresponding to 2L of expression were resuspended in Buffer A and stored in -20^{o}C until further use.

2.3.2 Bacterial lysis followed by IMAC using Ni Sepharose

The pellets were thawed at room temperature, and the bacterial lysis and centrifuge steps were conducted as previously described for the APRc$_{110-231}$His construct in section 2.2.2. The supernatant was applied in a Histrap HP 5 mL column (GE Healthcare Life Sciences) where it was subjected to a four-step gradient of imidazole (50 mM, 150 mM, 200 mM, and 500 mM) using 20 mM sodium phosphate containing 500 mM NaCl and 500 mM Imidazole pH 7.4 at a flow of 5 mL/min in an ÄKTA FPLC system (Amersham Biosciences). Absorbance was measured at 280 nm. Previously, the newly charged Histrap HP 5 mL column with Ni Sepharose™ High Performance was subjected to the same program to evaluate the baseline absorbance on each level of the gradient. The collected samples (150 mM imidazole step) were dialyzed overnight in a 3.5 kDa

Spectra/Por®3 dialysis membrane in 5L of 20 mM Tris-HCl pH 8 at 4ºC with agitation. This allows to decrease the concentration of NaCl and Imidazole in the samples and exchange the buffer to Tris-HCl.

2.3.3 Anionic Exchange Chromatography

The next day, the samples were ultracentrifuged at 144028 x *g* for 20 min at 8ºC in an Optima™ L-100 XP Ultracentrifuge (Beckman Coulter) using a 90Ti rotor. The supernatant was collected and injected into a MonoQ™ 5/50 GL column of anionic exchange (GE17-5166-01; Amersham Biosciences) previously equilibrated in 20 mM Tris-HCl pH 8. A program with increasing gradient of NaCl (0 to 1M) using the buffer 20 mM Tris-HCl containing 1 M NaCl pH 8 at a flow of 0.75 mL/min was performed in an ÄKTA FPLC system (Amersham Biosciences). Absorbance was measured at 280 nm.

2.3.4 3C protease digestion and histidine chains removal

The collected fractions were incubated overnight with 50 mM Tris-HCl pH 7.5 containing 150 mM NaCl and 1 mg/mL of HRV 3C protease at 4ºC. The 3C protease recognizes the consensus cleavage site downstream the histidine chains sequence, cleaving them from the constructs. To evaluate histidine chains cleavage, samples from each pool were denatured and assessed by SDS-PAGE as described in section 2.11. In order to remove the histidine chains and HRV 3C protease from the solution, the digestion was incubated with previously washed in 20 mM Tris-HCl pH 8.0 Ni Sepharose™ High Performance beads (GE17-5268-01, Cytiva) for 15 minutes at room temperature with agitation. The supernatant was filtered by Whatman Puradisc syringe 0.2 µm filter to remove the Ni Sepharose High Performance beads. The filtered solution was dialysed twice against 5 L PBS pH 7.4 in a 3.5 kDa Spectra/Por®3 dialysis membrane for 2 h and overnight at 4ºC with agitation. The next day, a sample of the fractions was denatured and assayed by SDS-PAGE following Coomassie blue staining as described in section 2.11. Protein concentration of each fraction was evaluated using a NanoDrop 1000 spectrophotometer (Thermo Fisher Scientific) and the samples were frozen at -80ºC.

2.4 Flow cytometry

Flow cytometry assay was used to analyze C3, C4, and C4BP deposition on the surface of *Rickettsia massiliae* and APRc-expressing *E. coli*. *R. massiliae* were fixed in 4% paraformaldehyde (PFA) for 20 minutes at room temperature with agitation. After, the bacteria were washed twice in 1 mL phosphate-buffered saline (PBS; 137 mM NaCl, 2.7 mM KCl, 10 mM Na_2HPO_4, and 1,8 mM KH_2PO_4, pH 7.4) and incubated with 100 µL of Hanks' Balanced Salt Solution (HBSS), 50% Normal Human Serum (NHS) and 50% Normal NHS depleted in IgG and IgM (NHSΔIgG/IgM) for 1h at 37°C with rotation. Serum sensitive BL21 Star (DE3) *E. coli* were transformed with the empty backbone vector pET28a, full-length active site mutant APRc and full-length wild type APRc. The transformed bacteria were grown at 37°C with agitation in LB medium containing 50 µg/mL kanamycin and when the $O.D_{600nm}$ was between 0.6 and 0.7, the protein expression was induced with 0.1 mM IPTG overnight at 20°C with agitation. At the end, an $O.D_{600nm}$ of 2 in 4 mL of each construct was centrifuged at 3000 rpm for 20 minutes at 4°C using a Megafuge 40R centrifuge (Thermo Scientific). Supernatant was discarded and the cells were resuspended in 4 mL of ice-cold PBS and 1 mL was dispensed per condition. *E. coli* were centrifuged and fixed in 4% PFA for 20 minutes at room temperature with agitation and washed twice in 1 mL PBS. Fixed *E. coli* were resuspended in 100 µL of HBSS, 40% NHS and 40% NHSΔIgG/IgM for 20 min at 37°C with rotation. All preparations were washed twice in PBS and blocked in PBS containing 2% bovine serum albumin (BSA) for 1h at RT with agitation. Samples were probed with 100 µL of the rabbit polyclonal anti-C3 (PA5-21349; 1:100); the mouse anti-C4BPα (sc-398720; 1:250); the mouse anti-C4BPβ (sc-514553; 1:250) or the mouse anti-C4α (sc-271181; 1:250) in PBS, 2% BSA, for 1h at RT with agitation and washed three times in PBS. After washing, samples were incubated with 150 µL of the anti-rabbit IgG FITC (F-2765; 1:500) or the anti-mouse IgG FITC (A16079; 1:500) conjugated secondary antibodies for 1h at RT with agitation, washed three times in PBS and resuspended in 300 µL of PBS. Results were analyzed with a Becton Dickinson Accuri™ C6 cell analyzer instrument and with FlowJo software 10.3. Each condition presents about 10000 counts.

To confirm protein expression in *E. coli*, an $O.D_{600nm}$ of 1 was harvested for 3 min at 16 000 x *g* at RT and resuspended in 100 µL BugBuster Protein Extraction Reagent

(Novagen) for 20 min at room temperature with agitation. The samples were denatured with 6x SDS sample buffer for 10 min at 90ºC and evaluated by Western blot analysis with rabbit anti-APRc antibody as described in the section 2.12.

2.5 Enzyme-linked immunosorbent assay (ELISA)

To confirm the biotinylation of purified APRc fractions, Nunc MaxiSorp high protein-binding capacity 96 well ELISA plates (Thermo Fisher Scientific) were incubated with 1 µg/well of BSA and hIgG for 2 h at 37ºC. The wells were washed three times in PBS containing 0.05% Tween (PBS-T) and blocked in 200 µL PBS-T containing 3% BSA for 2h at 37ºC. The wells were washed 4 times in PBS-T and 100 µL of each fraction of biotinylated APRc (200 µg/mL) were added per well for 1h at 37ºC. Wells were washed 4 times in PBS-T and were incubated in 1:2000 HRP-conjugated Streptavidin (#3999S, Cell Signaling Technology) in PBS-T containing 3% milk for 1h at 37ºC. After incubation, the wells were washed four times in PBS-T and were incubated with 100 µL TMB ELISA substrate (34028, Thermo Fisher Scientific) for 15-30 minutes at room temperature, protected from light, and the reaction was stopped with the addition of 100 µL 2M sulfuric acid. The plate was read at an absorbance of 450nm in a BioTek PowerWave Microplate Spectrophotometer. Experiment was performed with triplicates.

To analyze APRc effect in C3a production in serum, Nunc MaxiSorp high protein-binding capacity 96 well ELISA plates (Thermo Fisher Scientific) were incubated overnight at room temperature with 5 µg/mL purified anti-human C3a (518102, BioLegend). The wells were washed three times in PBS-T and blocked in 200 µL PBS-T containing 3% BSA for 2h at 37ºC. The wells were washed 4 times in PBS-T and 100 µL of the samples were added per well for 1h at 37ºC. The serum samples were previously incubated with $APRc_{110-231}$ HisShort in human umbilical cord serum (UCS) for 1h at 37ºC with agitation and were diluted 1:1000 in PBS. As a positive control was used Zymosan (1:20 in serum, Complement Technology), and as a negative control was used PBS. The wells were washed four times in PBS-T buffer and probed with 1 µg/mL of biotinylated anti-human C3a (518002, BioLegend) for 1h at 37ºC. Wells were washed 4 times in PBS-T and were incubated in 1:2000 HRP-conjugated Streptavidin (#3999S, Cell Signaling Technology) in PBS-T containing 3% milk for 1h at 37ºC. After incubation, the wells were

washed four times in PBS-T and were incubated with 100 µL TMB ELISA substrate (34028, Thermo Fisher Scientific) for 15-30 minutes at room temperature, protected from light, and the reaction was stopped with the addition of 100 µL 2M sulfuric acid. The plate was read at an absorbance of 450 nm in a BioTek PowerWave Microplate Spectrophotometer. Experiment was performed with triplicates and significance was determined through one-way ANOVA with Tukey's multiple comparisons test using GraphPad Prism v 8.0.2 263 (GraphPad Software, Inc., CA, USA).

To analyze APRc interaction with complement proteins, IgG1 light chains, free κ light chain and IgG isotypes (1, 2, 3 and 4), Nunc MaxiSorp high protein-binding capacity 96 well ELISA plates (Thermo Fisher Scientific) were incubated with 1 µg/well of negative control BSA and complement proteins (C3, C4, C4BP), IgG1 light chains and free κ light chains, or IgG1, IgG2, IgG3 and IgG4 for 2h at 37ºC. The wells were washed three times with PBS-T and blocked with PBS-T, 3% BSA. After blocking, the wells were washed four times and coated with different concentrations of biotinylated $APRc_{110-231}$ (0 µg/well, 1 µg/well, 2.5 µg/well, 10 µg/well, 22.5 µg/well, 30 µg/well, 40 µg/well) for 1h at 37ºC. For the experiments testing APRc-binding to the complement proteins, the wells were also incubated with hIgG (20 µg/well, Sigma-Aldrich) in this step. Wells were washed four times with PBS-T and were incubated with 1:2000 HRP-conjugated Streptavidin (#3999S, Cell Signaling Technology) in PBS-T containing 3% milk for 1h at 37ºC. Wells were washed four times in PBS-T and were incubated with 100 µL TMB ELISA substrate (34028, Thermo Fisher Scientific) for 15-30 minutes at room temperature, protected from light, and the reaction was stopped with the addition of 100 µL 2M sulfuric acid. The plate was read at an absorbance of 450nm in a BioTek PowerWave Microplate Spectrophotometer. Experiment was performed with triplicates and significance was determined through one-way ANOVA with Tukey's multiple comparisons test or Kruskal-Wallis with Dunn's multiple comparisons test using GraphPad Prism v 8.0.2 263 (GraphPad Software, Inc., CA, USA).

2.6 APRc-κ light chains complex formation assay

To evaluate the formation of APRc-κ light chains complexes, APRc and κ light chains were incubated in different APRc:κ light chains molar ratios (1:1, 2:1 and 3:1) diluted in PBS for 1h at 37ºC with agitation. APRc and κ light chains alone were used as controls. The samples were injected in a Superdex 200 5/150 GL column (Cytiva) previously equilibrated in PBS pH 7.4 using a HPLC system (Shimadzu) and evaluated by SEC. The performed program used the mentioned buffer at a flow of 0.25 mL/min and absorbance was measured at 220 nm. Carbonic anhydrase (29 kDa) was injected in the column as a reference to evaluate $APRc_{110-231}$HisShort dimerization.

2.7 Pull-down assay with HisMag Sepharose Nickel beads

2.7.1 Human Serum

Pull-down assays using HisMag Sepharose Nickel beads were performed to evaluate complement proteins C3, C4 and C4BP as APRc substrates. Previously washed 30 µL of His Mag Sepharose™ Nickel beads slurry (GE28-9673-90, Cytiva) were incubated with 300 µL PBS and 85 µg of $APRc_{110-231}$ HisShort or $APRc_{110-231}$ HisShort D140N for 1h30min at room temperature with agitation. These constructs present a histidine tag that has affinity for nickel, resulting in a specific interaction with the beads. After incubation, the beads were washed three times with 1 mL PBS and incubated with 240 µL of Human Umbilical Cord Serum (UCS; Crioestaminal), NHS (H6914, Sigma-Aldrich), NHS (34006, Pel-freez) or NHSΔIgG/IgM (34010, Pel-freez) diluted 15x in PBS for 4h at 37ºC with agitation. The supernatant was collected before the incubation (T_0), and the beads were sequentially washed with 1 mL PBS, 1 mL PBS containing 200 mM NaCl and 1 mL PBS containing 0.1% Tween to remove non-specific interactions. The beads were eluted in 50 µL of 6x SDS sample buffer diluted in PBS and denatured at 90ºC for 10 minutes. Finally, the magnetic beads were separated in a MagRack™ 6 (GE28-9489-64, Cytiva) and the supernatant containing APRc and bounded proteins (T_{eluted}) was collected. Denatured samples were loaded into 12.5% polyacrylamide gel and assessed by SDS-PAGE and Western Blot as described in the sections 2.11 and 2.12, respectively.

2.7.2 Purified complement proteins

APRc pull-down assays with purified C3, C4 and C4BP were conducted using HisMag Sepharose nickel beads. Previously washed 10 µL of His Mag Sepharose Nickel beads slurry (GE28-9673-90, Cytiva) were incubated with 150 µL PBS and 28 µg of $APRc_{110-231}$HisShort or $APRc_{110-231}$HisShort D140N for 1h at room temperature with agitation. After incubation, the beads were washed three times with 1 mL PBS and incubated with 7 µg of C3, C4 or C4BP with and without 7 µg of hIgG (I2511, Sigma-Aldrich) for 5h at 37ºC with agitation. A condition of 7 µg of the purified complement proteins with and without 7 µg hIgG in PBS was used as a control. Before the incubation, a sample from the supernatant was collected (T_0). After incubation, beads were sequentially washed with 1 mL PBS, 1 mL PBS containing 200 mM NaCl and 1 mL PBS containing 0,1% Tween to remove non-specific interactions. The beads were eluted in 50 µL of 6x SDS sample buffer diluted in PBS and denatured at 90ºC for 10 minutes. Finally, the magnetic beads were separated in a MagRack™ 6 (GE28-9489-64, Cytiva) and the supernatant containing APRc and bounded proteins (T_{eluted}) was collected. Denatured samples were loaded into a 12.5% polyacrylamide gel and assessed by SDS-PAGE and Western Blot as described in section 2.11 and 2.12, respectively.

2.8 Incubation assay with HisMag Sepharose Nickel beads

APRc incubation assays with purified C3, C4 and C4BP were conducted using HisMag Sepharose nickel beads. Previously washed 10 µL of His Mag Sepharose Nickel beads slurry (GE28-9673-90, Cytiva) were incubated with 150 µL PBS and 28 µg of $APRc_{110-231}$HisShort or $APRc_{110-231}$HisShort D140N for 1h at room temperature with agitation. After incubation, the beads were washed three times with 1 mL PBS and incubated with 7 µg of C3, C4 or C4BP with and without 7 µg of hIgG (I2511, Sigma-Aldrich) for 5h at 37ºC with agitation. A condition of 7 µg of the purified complement proteins with and without 7 µg hIgG in PBS was used as a control. Before the incubation, a sample from the supernatant was collected (T_0). After incubation, the solution was denatured (T_{final}) and assessed by SDS-PAGE and Western Blot, as described in sections 2.11 and 2.12, respectively.

2.9 C3, C4 complex formation at the surface of bacteria

To identify cross-linking between C4 and C3 proteins and bacteria, 2.56 x 10^8 *R. massiliae* and an $O.D_{600nm}$=1 of *E. coli* expressing the empty backbone vector pET28a, full-length D140N APRc and full-length APRc WT were suspended in HBSS and incubated with HBSS or 40% NHS (Pel-Freez) for 1h at 37ºC with rotation. Bacteria were washed twice in 1 mL of HBSS and resuspended in a final volume of 60 µL. Samples were denatured, and results were obtained by performing SDS-PAGE and Western Blot analysis, as described in sections 2.11 and 2.12, using polyclonal anti-C3 (A213), polyclonal anti-C4 (A205) and rabbit polyclonal anti-APRc antibodies.

2.10 Complement System activation assay

To determine APRc effect in the activation of complement pathways was used the WIESLAB® Complement System Screen RUO (COMPL300RUO; Svar Life Science). This kit is used for the determination of complement deficiencies in human sera and qualitative determination of functional classical, alternative and MBL pathways. The assay combines the specific activation of each complement pathway with the use of labeled antibodies against the terminal complex C5b-9, whose levels are proportional to the complement activity. Previously washed 10 µL of His Mag Sepharose™ Nickel beads slurry (Cytiva) were incubated in 150 µL PBS and 28 µg of $APRc_{110-231}$ HisShort or $APRc_{110-231}$ HisShort D140N for 1h at room temperature with agitation. After incubation, the beads were washed three times with 1 mL PBS and incubated with 25 µL of NHS (34006, Pel-freez) for 1h at 37ºC with agitation. Serum and the positive and negative controls were diluted according to the kit protocol: 1:101 in classical pathway diluent, 1:101 in MBL pathway diluent and 1:18 in alternative pathway diluent. Samples diluted with the MBL pathway diluent were left at room temperature for 25 minutes. Ninety-six-wells plate coated with human IgM (classical pathway), coated with mannan (MBL pathway) and coated with lipopolysaccharide (LPS; alternative pathway) was incubated with 100 µL of the corresponding diluted samples and diluents (blank) per well for 1h at 37ºC. The wells were washed three times in washing buffer and incubated with 100 µL of the conjugate to each well and incubated for 30 min at room temperature. After incubation,

the wells were washed three times in washing buffer and were incubated with 100 µL of substrate solution for 30 minutes at room temperature, protected from light. The reaction was stopped with the addition of 100 µL 5 mM EDTA and the plate was read at an absorbance of 405 nm in a BioTek PowerWave Microplate Spectrophotometer. Experiment was performed with duplicates.

2.11 SDS-PAGE

To separate protein samples by size was performed a SDS-polyacrylamide gel electrophoresis (SDS-PAGE). Samples were denatured using 6x SDS sample solution (4× Tris-HCl, 30% glycerol, 10% SDS, 0.012% bromophenol blue, 0.6 M dithiothreitol [DTT] pH 6.8) at 90^{o}C for 10 min and were applied onto a 12.5% polyacrylamide gel. The gel electrophoresis was run using running buffer (100 mM Bicine, 100 mM Tris base) for 15 min at 120V and after at 170V in a Mini-PROTEAN Tetra Cell system (Bio-Rad). The gel was stained with Coomassie Brilliant Blue solution (50% methanol, 10% acetic acid, 0.2% Coomassie Brilliant Blue), followed by unstaining with a solution containing 25% methanol and 5% acetic acid. Images were obtained using a VWR imager (VWR international). To evaluate the proteins molecular weight, was used the Precision Plus Protein™ All Blue Prestained Protein Standards (Biorad) with the following known molecular weights: 250 kDa, 150 kDa, 100 kDa, 75 kDa, 50 kDa, 37 kDa, 25 kDa, 20 kDa, 15k Da and 10 kDa.

2.12 Western Blot analysis

To detect specific proteins and potential cleavage fragments in the samples was performed Western Blot analysis. After the SDS-PAGE, the proteins were electrotransfered to a previously activated in methanol Amersham Hybond 0.2 µm PVDF membrane (Cytiva) using a Trans-Blot Electrophoretic Transfer cell (Bio-Rad) with the buffer containing 25 mM Tris, 192 mM glycine and 20% methanol, for 1h40min at 100V, at 4^{o}C. The membrane was blocked with the proteins upwards with Tris-buffer saline (TBS; 20 mM Tris and 137 mM NaCl) containing 2% BSA for 1 h at room temperature with agitation. After, the membrane was probed with one of the following primary

antibodies for 1h at room temperature with agitation: rabbit polyclonal anti-C3 antibody (1:2000 in TBS-T, 2% BSA; PA5-21349) produced by Sigma-Aldrich, mouse anti-human C3 (1:500 in TBS-T, 2% BSA; sc-28294), mouse anti-human C4α (1:500 in TBS-T, 2% BSA; sc-271181), mouse anti-human C4BPα (1:500 in TBS-T, 2% BSA; sc-398720) or mouse anti-human C4BPβ (1:500 in TBS-T, 2% BSA; sc-514553) purchased from Santa Cruz Biotechnology, goat polyclonal anti-C3 (1:64000 in TBS-T, 2% BSA; A213) or the goat polyclonal anti-C4 (1:64000 in TBS-T, 2% BSA; A205) obtained from Complement technology or the anti-APRc (1:500 in TBS-T, 2% BSA) produced by GenScript. The membrane was washed five times (each 5 minutes) in TBS-T and incubated with the corresponding secondary antibody for 1h with agitation: anti-Mouse IgG (1:5000 in TBS-T, 2% BSA; A9044), anti-rabbit IgG (1:40000 in TBS-T, 2% BSA; A0545) or anti-goat IgG (1:5000 in TBS-T, 2% BSA, #81-1620). Finally, the membrane was washed five times (each 5 minutes) using TBS-T. The membrane was incubated with the NZY advanced ECL substrate (NZYTech) for 3 minutes, and chemiluminescence was detected using a VWR imager. Molecular weights were inferred by comparison with the Precision Plus Protein™ All Blue Prestained Protein Standards (Biorad).

Chapter III – Results

3.1 Purification of the soluble form of recombinant APRc

In order to conduct this study a shorter soluble form of APRc ($APRc_{110-231}$HisShort) containing a histidine tag was purified. This construct presents the C-terminal histidine tag directly fused to the APRc sequence since previous experiments from our laboratory demonstrated that the use of a linker sequence had an impact in APRc binding to non-immune Ig. $APRc_{110-231}$HisShort and the respective catalytic dead mutant ($APRc_{110-231}$HisShort_D140N) were recombinantly expressed in *E. coli* and purified by immobilized metal affinity chromatography (IMAC) with Ni Sepharose and cationic exchange chromatography. Oligomerization state of APRc was evaluated by size exclusion chromatography (SEC).

BL21 star strain of *E. coli* presenting the plasmid pET28a_$APRc_{110-231}$HisShort_D140N or pET28a_$APRc_{110-231}$HisShort were grown until an $O.D_{600nm}$ between 0.6 and 0.7, protein expression was induced for 4h at 30^{o}C and the pellets were collected and frozen. Bacteria were lysed and the soluble part of cellular extracts was subjected to IMAC. The histidine-tag presents affinity for the nickel ions in the column, allowing the separation of the recombinant proteins from the other soluble components. Proteins were subjected to a four-step gradient of imidazole (50 mM, 150 mM, 200 mM, and 500 mM) at a flow of 5 mL/min and absorbance was measured at 280 nm. As shown in the **Figure 6A,D**, the recombinant proteins were eluted in the step of 200 mM Imidazole (region between the dotted lines). Previous purifications have demonstrated that APRc dimeric forms are eluted in this imidazole step.

The collected samples from each construct were independently dialysed overnight against 20 mM HEPES buffer pH 7.4. Samples were ultracentrifuged to remove any precipitates and were applied in a cationic-exchange column. The histidine tag present in the constructs $APRc_{110-231}$HisShort and $APRc_{110-231}$HisShort_D140N gives them positive charge at a pH 7.4, enabling their binding to the column. Each construct was subjected to an increase gradient of NaCl (0 to 1M), competing with the Na^{+} ions and resulting in their elution. Fractions were collected from the region between the dashed lines, as shown in the chromatograms of **Figure 6B,E**, and were evaluated by SDS-PAGE.

The soluble domain of APRc presents a molecular weight of approximately 14 kDa **(Figure 6C,F)**. The weak homodimerization of this protease makes it difficult to visualize the dimer under these conditions.

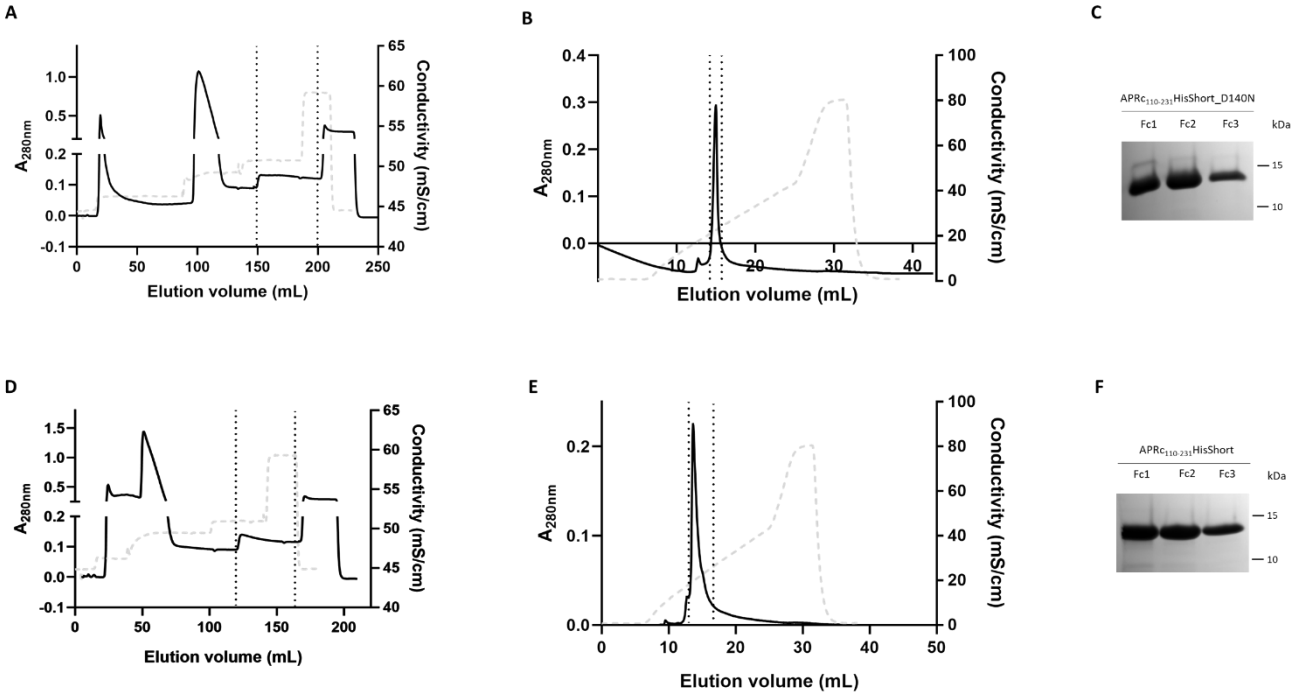

Figure 6: Purification of APRc$_{110-231}$HisShort_D140N and APRc$_{110-231}$HisShort by IMAC using Ni Sepharose and cationic exchange chromatography. (A) Supernatant containing APRc$_{110-231}$HisShort_D140N or **(D)** APRc$_{110-231}$HisShort was loaded in a Histrap HP 5 mL column previously equilibrated in buffer 20 mM sodium phosphate, 500 mM NaCl, 10 mM Imidazole pH 7.4. Soluble protein pool was subjected to a four-step gradient of imidazole (50 mM, 150 mM, 200 mM, and 500 mM; grey dashed line) using the buffer 20 mM sodium phosphate, 500 mM NaCl, 500 mM Imidazole pH 7.4 with a flow of 5 mL/min and measured at 280 nm. The black dashed lines indicate the region where the protein was eluted (200 mM). **(B,E)** Collected fractions from the previous step were dialyzed overnight in 5L 20 mM HEPES pH 7.4 at 4^{o}C and were injected in a MonoS column previously equilibrated in 20 mM HEPES pH 7.4 and cationic exchange chromatography was conducted. A linear NaCl gradient (0 to 1 M; grey dashed line) using the buffer 20 mM HEPES containing 1M NaCl pH 7.4 at a flow of 0.75 mL/min was performed. Absorbance was measured at 280 nm. The black dashed lines represent the collected pool of purified APRc forms. **(C)** SDS-PAGE followed by Coomassie blue staining of the three collected fractions of APRc$_{110-231}$HisShort_D140N or **(F)** APRc$_{110-231}$HisShort after cationic-exchange chromatography (Fc1, Fc2, Fc3).

Since APRc needs to be in a homodimer to present catalytic activity (R. Cruz et al., 2014), the oligomerization state of the purified fractions of histidine tagged APRc were evaluated by analytical SEC. The purified proteins were injected in a Superdex column previously equilibrated in 20 mM HEPES buffer pH 7.4 containing 100 mM NaCl.

Proteins were subjected to a program with the mentioned buffer at a flow of 0.25 mL/min and absorbance was measured at 220 nm. Molecular weight of each construct was estimated by running the standard molecular weight proteins carbonic anhydrase (29 kDa) and ribonuclease (13.69 kDa). As expected, dimeric $APRc_{110-231}$HisShort and $APRc_{110-231}$HisShort_D140N (hereby named APRc) present approximately 25 kDa, eluting closer to carbonic anhydrase elution volume. Fractions 1 and 2 from both constructs represent the most concentrated purified fractions **(Figure 7A,B)**. For the following experiments the dimeric fractions 1 and 2 from $APRc_{110-231}$HisShort and $APRc_{110-231}$HisShort_D140N were used.

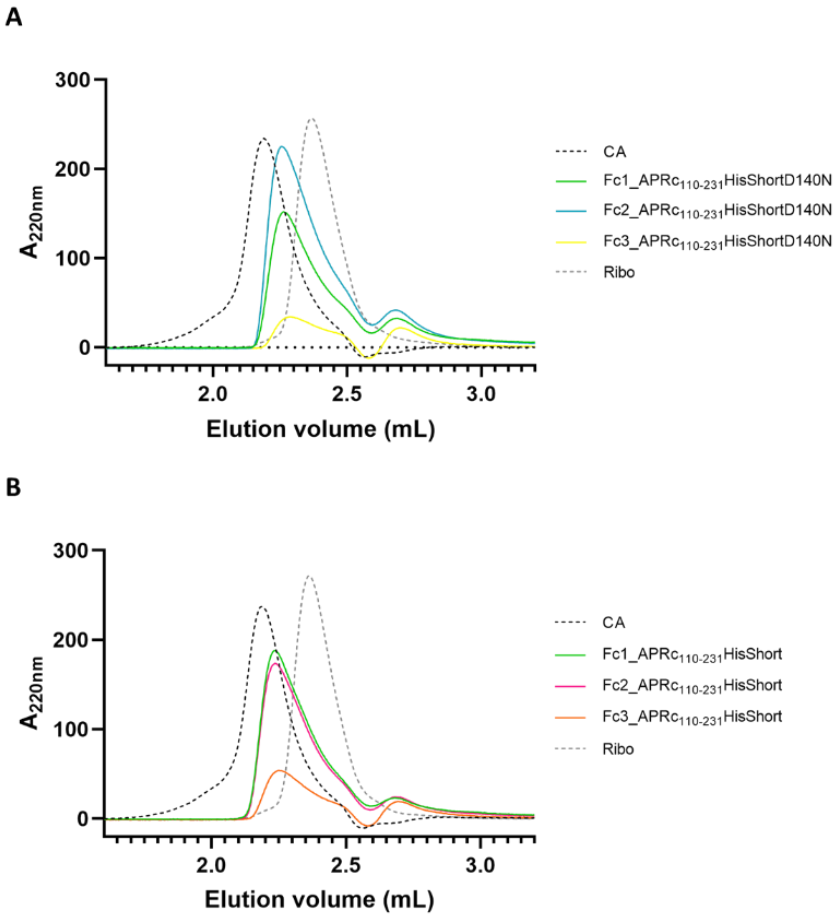

Figure 7: Evaluation of APRc oligomerization state by size exclusion chromatography. (A) The three purified fractions of $APRc_{110-231}$HisShortD140N and the **(B)** three purified fractions of $APRc_{110-231}$HisShort were analysed by analytical size exclusion chromatography using a Superdex column previously equilibrated in 20 mM HEPES buffer pH 7.4 containing 100 mM NaCl. The program used the mentioned buffer at a flow of 0.25 mL/min and absorbance was measured at 220 nm. To estimate the molecular weight of the fractions, carbonic anhydrase (CA; 29 kDa) and ribonuclease (Ribo; 13.69 kDa) were also injected in the column for reference.

3.2 Purification of biotinylated APRc soluble form

HisAPRc$_{110-231}$avi was recombinantly expressed in *E. coli* and purified by IMAC with Ni Sepharose and anionic exchange chromatography. The histidine tag from the construct was cleaved by HRV 3C protease and removed with Ni beads. Finally, samples were dialyzed against PBS pH 7.4.

BL21 star strain of *E. coli* containing the plasmid pDW363ΔMBP and encoding the plasmid pCoofy1_APRc110-231 were grown until an O.D$_{600nm}$ between 0.6 and 0.7, protein expression was induced overnight at 20^{o}C and the pellets were collected and frozen. Bacteria were lysed and the soluble part of the cellular extracts was subjected to IMAC. This construct also presents a histidine-tag, allowing the binding to the column. Proteins were subjected to a four-step gradient of imidazole (50 mM, 150 mM, 200 mM, and 500 mM), and the fraction eluted at the 150 mM imidazole step was selected **(Figure 8A).**

The collected samples from each construct were independently dialysed against 20 mM Tris-HCl pH 8 overnight, ultracentrifuged and applied in an anionic-exchange column. HisAPRc$_{110-231}$avi presents negative charge at pH 8, which enables the binding to the column. Each protein was subjected to an increase gradient of NaCl (0 to 1M), competing with the Cl^- ions and resulting in their elution **(Figure 8B)**. Three different pools corresponding to the first peak, second peak and descendent from the second peak were collected **(Figure 8B)** and evaluated by SDS-PAGE **(Figure 8C)**.

To remove the histidine-tag from the construct, the three pools were incubated with HRV 3C Protease overnight at 4^{o}C. This protease recognizes the consensus cleavage site downstream the histidine tag sequence, cleaving it. The cleavage was assayed by SDS-PAGE. As seen in **Figure 8D**, after digestion there is the appearance of a protein band with approximately 14 kDa (corresponding to APRc) and the appearance of a protein bands below 10 kDa (corresponding to the histidine tags). The cleaved histidine tags and the HRV 3C protease were removed by using Ni beads and the proteins were dialyzed in PBS pH 7.4 for 2h and overnight **(Figure 8E)**.

The biotinylation of the purified pools of APRc was assessed by ELISA. In this assay a 96-well plate was incubated with BSA and human IgG and was incubated with 200 μg/mL of APRc of each pool. Human IgG was used as coating since it is known that

APRc is a Ig-binding protein (Curto et al., 2021). Only the Pools 2 and 3 present signal, confirming their biotinylation **(Figure 9).** Pool 3 presents higher signal than Pool 2, however the protein concentration is much lower. Due to this, for the following ELISA experiments the Pool 2 of biotinylated APRc was used.

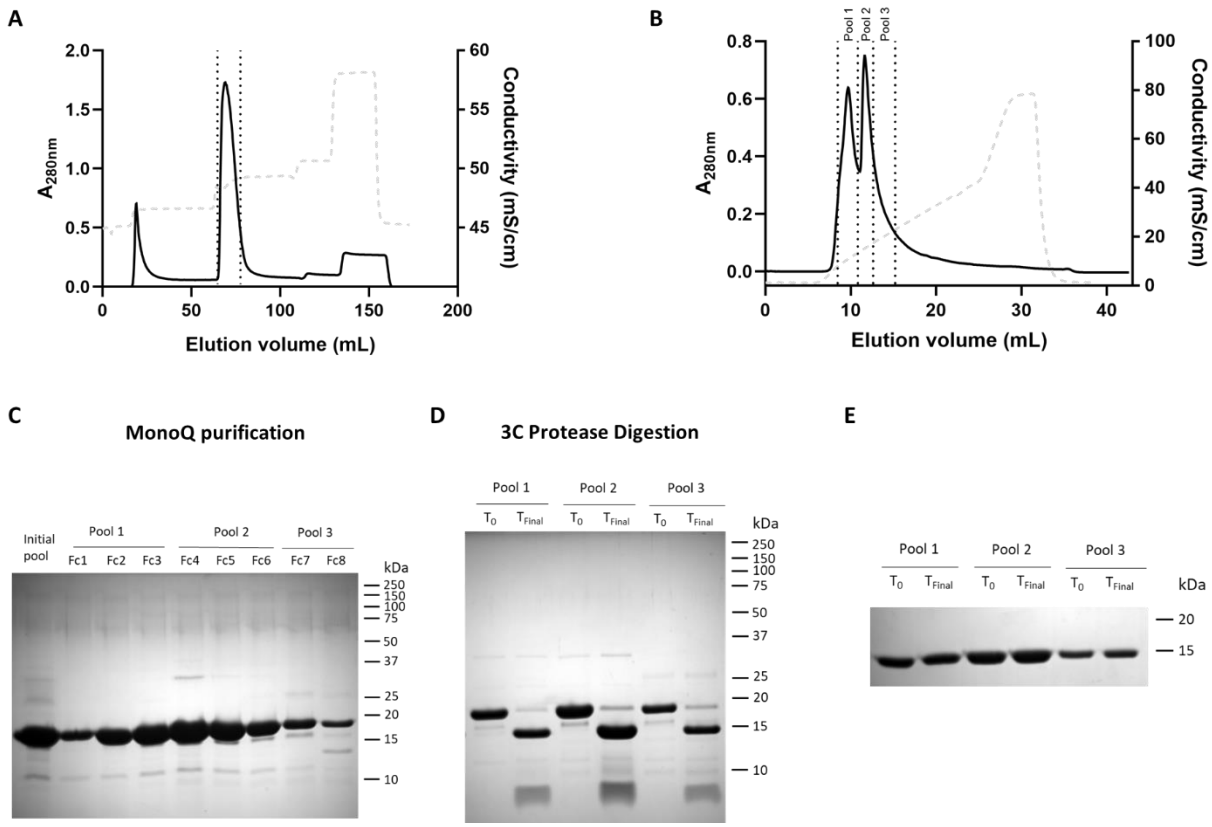

Figure 8: Purification of biotinylated APRc by IMAC with Ni Sepharose and anionic exchange chromatography. (A) Supernatant containing HisAPRc$_{110-231}$avi was loaded in a Histrap HP 5 mL column previously equilibrated in buffer 20 mM sodium phosphate, 500 mM NaCl, 10 mM Imidazole pH 7.4. Protein pool was subjected to a four-step gradient of imidazole (50 mM, 150 mM, 200 mM, and 500 mM; grey dashed line) using the buffer 20 mM sodium phosphate, 500 Mm NaCl, 500 mM Imidazole pH 7.4 with a flow of 5 mL/min. Absorbance was measured at 280 nm. The black dashed lines indicate the region where the protein was eluted (150 mM imidazole). **(B)** Collected fractions were dialyzed overnight in 5L 20 mM Tris-HCl pH 8 at 4ºC and were injected in a MonoS column previously equilibrated in buffer 20 mM Tris-HCl pH 8 and anionic exchange chromatography was conducted. A linear NaCl gradient (0 to 1 M; grey dashed line) using the buffer 20 mM Tris-HCl containing 1M NaCl pH 8 at a flow of 0.75 mL/min was performed. Absorbance was measured at 280 nm. The black dashed lines represent the three collected pools (pool1, pool 2, pool 3) with the biotinylated HisAPRc$_{110-231}$ construct. **(C)** SDS-PAGE followed by Coomassie blue staining of the fractions of the three collected pools of biotinylated HisAPRc$_{110-231}$ before (Initial pool; dialyzed pool from 150 mM imidazole step) and after ultracentrifugation (Fc1, Fc2, Fc3, Fc4, Fc5, Fc6, Fc7, Fc8). **(D)** SDS-PAGE followed by Coomassie blue staining of the three collected pools before (T_0) and after digestion with 3C protease to cleave the histidine tag (T_{final}).

(E) SDS-PAGE followed by Coomassie blue staining of the three collected pools upon 3C protease and histidine tag removal, before (T_0) and after (T_{final}) dialysis with PBS pH 7.4 for 2h and overnight.

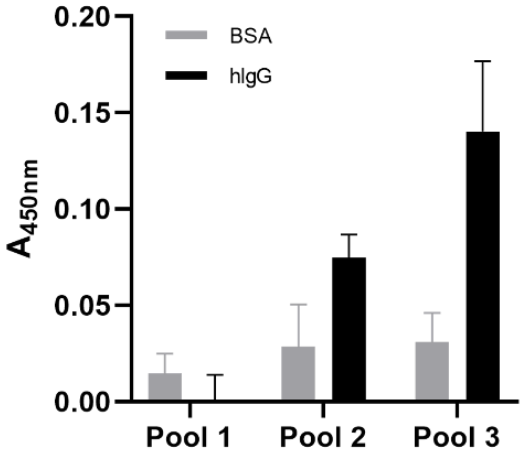

Figure 9: Evaluation of the biotinylation of purified recombinant APRc by ELISA. 96-well plates were incubated with 1 µg of BSA and human IgG (hIgG) and were incubated with 200 µg/mL of APRc. The three pools of purified APRc were tested. To detect the signal streptavidin-HRP at 450 nm was used. Results are represented in mean ± standard deviation from three replicates.

3.3 Evaluation of APRc binding to different IgG isoforms

Previous work from our laboratory demonstrated that APRc binds to different types of immunoglobulins, presenting more interaction with IgG (Curto et al., 2021). To further unveil APRc binding to IgG, the interaction with the four isoforms of this immunoglobulin (IgG1, IgG2, IgG3 and IgG4) was evaluated. These isoforms present over 90% homology, mainly differing in the hinge region and the N-terminal CH2 domain, a component of the heavy chain (Vidarsson et al., 2014). Ninety-six-well plates were coated with IgG1, IgG2, IgG3 and IgG4 and incubated with different concentrations of APRc: 0 µg/well, 1 µg/well, 2.5 µg/well, 10 µg/well, 22.5 µg/well, 30 µg/well, 40 µg/well. APRc binds to the IgG1, IgG2 and IgG3 in a concentration-dependent manner, binding preferentially to IgG1 and IgG3 **(Figure 10A,B)**. On the other hand, IgG4 binding is similar to the control BSA, being observed differences only after the 22.5 µg/well concentration. Although the absorbance values of IgG1, IgG2 and IgG3 are higher in **Figure 10A** than IgG1 and IgG4 absorbance values in **Figure 10B**, they cannot be compared since different incubation times with the substrate were used. To compare them and to further confirm APRc

preference, a 96-well was coated with IgG1, IgG2, IgG3, and IgG4 and incubated with 22.5 µg/well and 40 µg/well of APRc. As previously observed, APRc binds more to isoforms 1 and 3 in both concentrations, although there are no statistical differences in the 22.5 µg/well condition. The isoforms 2 and 4 do not present statistical differences when compared to BSA in both concentrations, although both absorbance values increase in the 40 µg/well **(Figure 10C)**.

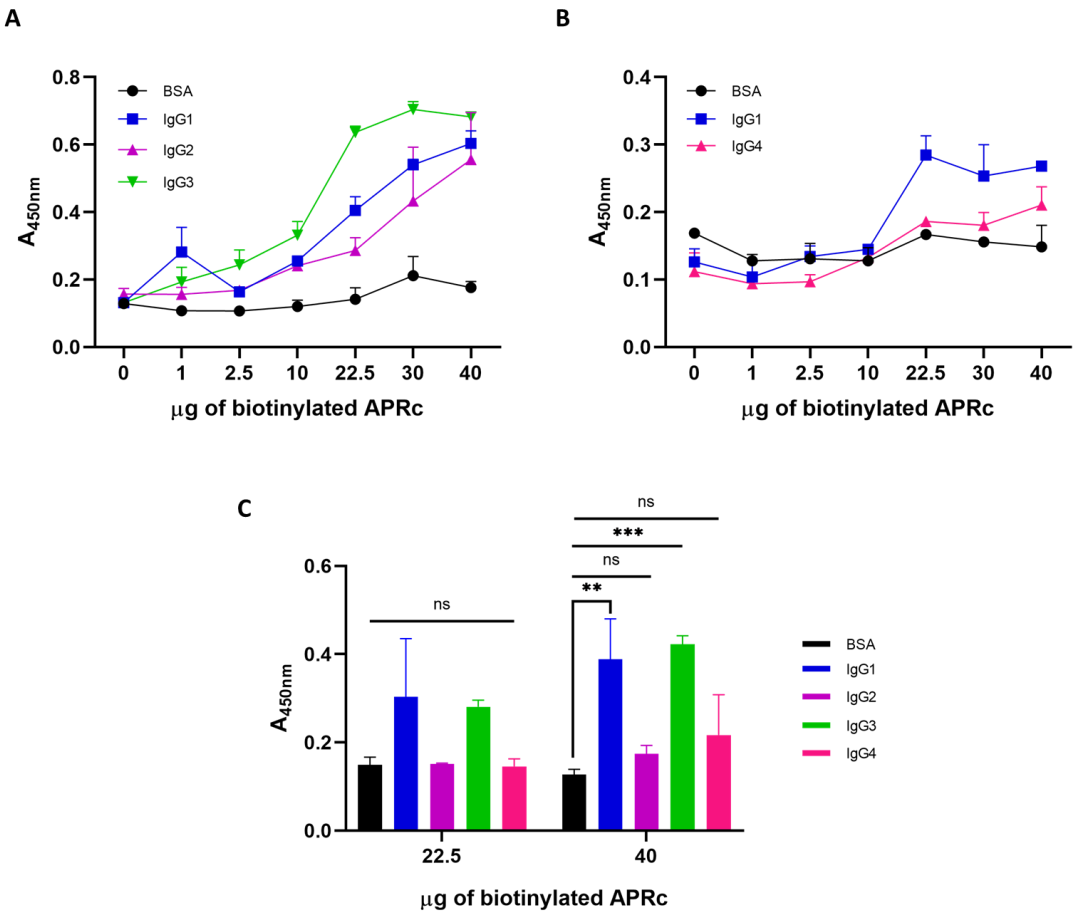

Figure 10: APRc ability to bind different IgG isoforms was evaluated by ELISA. (A) 96-well plates were coated with 1 µg/well of BSA and IgG isoforms (1,2,3) and incubated with different concentrations of biotinylated APRc. **(B)** 1 µg/well of BSA, IgG1 and IgG4 were used as coating in a 96-well plate and incubated with different concentrations of biotinylated APRc. To detect the signal was used streptavidin-HRP at 450 nm. Results are represented in mean ± standard deviation from three replicates. **(C)** 96-well plate were coated with 1 µg/well of BSA and IgG isoforms (1,2,3,4) and incubated with two different concentrations of biotinylated APRc (22,5 µg/well and 40 µg/well). To detect the signal was used streptavidin-HRP at 450 nm. Results are represented in mean ± standard deviation from three replicates. Significance was determined using a one-way ANOVA followed by Tukey's multiple comparisons test using GraphPad Prism 8 (ns, non-significant; *, $P < 0.05$; **, $P < 0.01$; ***, $P < 0.001$).

3.4 Evaluation of APRc binding to the antibody light chains

Previous work from our laboratory also demonstrated that APRc binds preferentially to the antibody Fab region (Curto et al., 2021). This region is responsible to bind the antigen and is composed by one variable and one constant domain from each light and heavy chain (Charles A Janeway et al., 2001). To further analyse this interaction, 96-well plates were coated with BSA, IgG1 with κ light chains and IgG1 with γ lights chains and incubated with different concentrations of APRc. Obtained results demonstrate that APRc binds to both IgG1 with κ light chains and IgG1 with γ lights chains in a concentration-dependent manner, binding preferentially to the antibody with κ light chains by ~2-fold **(Figure 11A)**. A part of this binding could be due to interaction with the antibody heavy chains, however it's clear that changing only the type of light chains alter the binding. To further validate APRc-κ light chains interaction, 96-well plates were coated with BSA, IgG1 with κ light chains and free κ lights chains and incubated with 22.5 µg/well and 40 µg/well of APRc. At the lower used concentration, there is a statistical difference between the IgG1 with κ light chains and free κ lights chains when compared to the BSA control **(Figure 11B)**. Furthermore, there are no visible differences between the two experimental groups, however, when the concentration increases IgG1 with κ light chains presents higher binding to APRc than the free κ lights chains conditions. These results demonstrate that APRc binds to κ light chains alone, although this protease can also interact with other antibody regions.

To confirm APRc-κ light chains complexes formation, APRc was incubated with κ light chains at different molar ratios and evaluated by SEC. The profile of the used fraction of $APRc_{110\text{-}231}$HisShort presents two peaks, being one of them in a dimeric form **(Figure 11C)**. For two of the tested APRc:κ molar ratios we observe a shoulder at lower elution volumes (~2mL), that is not present when both proteins were independently run **(Figure 11D)**. These results suggest the formation of higher molecular weight complexes between both proteins.

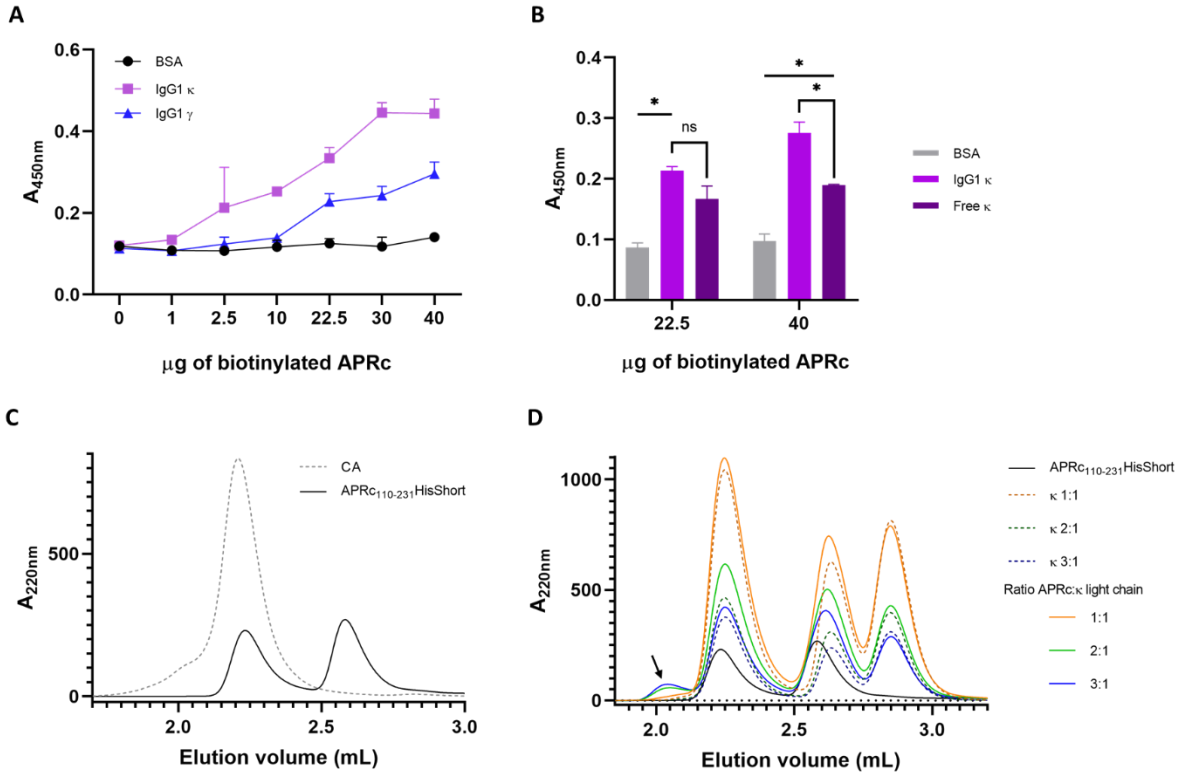

Figure 11: APRc ability to bind κ and γ light chains was evaluated by ELISA. (A) 96-well plates were coated with 1 µg/well of BSA IgG1 κ light chain and IgG1 γ light chain and incubated with different concentrations of biotinylated APRc. To detect the signal was used Streptavidin-HRP at 450 nm. Results are represented in mean ± standard deviation from three replicates **(B)** To further assess APRc binding to κ light chains, 96-well plates were coated with 1µg/well of BSA, IgG1 κ light chains and free κ light chains incubated with 22.5 µg/well and 40 µg/well of biotinylated APRc. Bars represent the mean value ± standard deviation. Significance was determined using a one-way ANOVA followed by Tukey's multiple comparisons test using GraphPad Prism 8 (ns, non-significant; *, $P < 0.05$). **(C)** Formation of APRc-κ light chains complexes was evaluated by size-exclusion chromatography (SEC). $APRc_{110-231}$HisShort dimerization was assessed by comparing with carbonic anhydrase (CA; 29 kDa). **(D)** APRc and κ light chains were incubated in PBS with varying molar ratios APRc: κ light chain (1:1, 2:1, 3:1) in PBS and injected in a Superdex column previously equilibrated in PBS pH 7.4. Proteins were subjected to an isocratic run at a flow of 0.25 mL/min in the same buffer. Absorbance was measured at 220 nm. The black arrow highlights the appearance of a shoulder.

3.5 Evaluation of complement proteins as APRc interactors/substrates

Preliminary data demonstrates that C3 and C4 proteins are potential APRc substrates from human serum. Additionally, it has been reported a few bacterial proteins that bind Ig as well as complement protein C4BP, causing immune evasion (Carlsson et al., 2003; Johnsson et al., 1996; Pleass et al., 2001, p. 89). Since APRc

presents Ig-binding activity, we hypothesize that it might also bind C4BP. In these following experiments we wanted to unveil if C3, C4, and C4BP are APRc substrates.

First it was evaluated the binding of the three potential substrates (C3, C4, and C4BP) to the surface of *Rickettsia* by flow cytometry. *R. massiliae* were fixed and incubated with Hanks' Balanced Salt Solution (HBSS), 50% Normal Human Serum (NHS) and 50% Normal NHS depleted in IgG and IgM (NHSΔIgG/IgM). The latter one was used to assess the impact of IgG and IgM depletion in the binding of the complement proteins. Blocked bacteria were probed with antibodies against each of the complement proteins and further probed with a FITC-coupled antibody. *R. massiliae* binds to all the tested complement proteins, although binding is more evident for C3. *R. massiliae* binds to C3 in both NHS and NHSΔIgG/IgM, presenting more deposition in the NHSΔIgG/IgM condition **(Figure 12A)**. These results anticipate that IgG binding by *Rickettsia* may exert a protective effect reducing C3 binding at the surface of the bacteria. On the other hand, we observe binding of C4 and C4BP only in the NHS condition, suggesting that the depletion of IgG and IgM impacts their deposition **(Figure 12B,C)**. However, for C4BP the low protein levels detected in the NHSΔIgG/IgM serum **(Figure S2)** can limit this deposition, making it difficult to draw any conclusion.

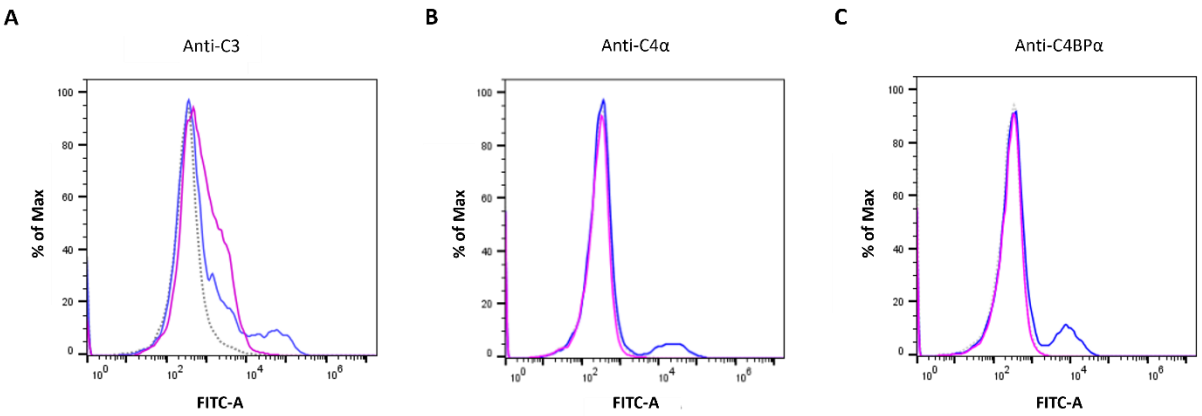

Figure 12: Flow cytometry analysis of C3, C4 and C4BP deposition at the surface of *Rickettsia massiliae*. *R. massiliae* were fixed and incubated with HBSS (grey trace), 50% NHS (blue trace), or 50% NHSΔIgG/IgM (pink trace). After incubation, samples were blocked at RT, washed, and incubated with **(A)** anti-C3 antibody, **(B)** anti-C4α antibody or **(C)** anti-C4BPα antibody at RT for 1h. Each condition was incubated with anti-rabbit IgG FITC-conjugated antibody for 1h at RT and resuspended in PBS. Results were obtained with the FL1-A channel (FITC). Each condition presents about 10000 counts.

3.5.1 Evaluation of C3 as an APRc substrate

After acknowledging that C3 binds to *Rickettsia* surface, we wanted to assess if C3 binds specifically to the protease APRc. To do this, we used the surrogate model of *E. coli* expressing this protease. It has been demonstrated that the full-length APRc integrates in the outer membrane of *E. coli* and presents the soluble catalytic domain oriented to the extracellular site (R. Cruz et al., 2014).

E. coli expressing the empty vector, full-length APRc and the corresponding catalytic dead mutant were fixed and incubated with HBSS, 40% NHS and 40% NHSΔIgG/IgM. Blocked bacteria were incubated with anti-C3α antibody and probed with a FITC-coupled antibody. Full-length APRc expression was confirmed with the protein band with ~25 kDa, presenting more expression of the mutant than the wild-type form **(Figure 13A)**. Bacteria expressing the empty vector present C3 deposition in both serums, presenting more binding in the serum depleted in IgG and IgM (Positive % 26.02 vs 41.19, respectively; **Figure 13B**). Bacteria expressing APRcFL_D140N and APRcFL present deposition only when the IgG and IgM are depleted **(Figure 13C,D)**. One plausible explanation for this result is that APRc binding to IgG may be competing with APRc-C3 binding in NHS. Furthermore, C3 binds more to the surface of *E. coli* expressing the wild-type protease than the mutant form (Positive % 34.88 vs 23.3 respectively), suggesting that the proteolytic activity increases C3 binding/deposition. However, the observed binding in both APRc forms is lower than the control with the empty vector.

APRc-binding to complement protein C3 was also evaluated by ELISA. Ninety-six-well plates were incubated with BSA and C3 and incubated with different concentrations of APRc. The results demonstrate that APRc binds to C3 in a concentration-dependent manner, however this interaction seems to saturate at the concentration 22.5 µg/well **(Figure 14A)**. Moreover, APRc-C3 interaction seems to be unstable/transient since it decreases in the 10 µg/well concentration. To analyse the potential role of IgG in this interaction, 96-well plate was incubated with BSA and C3 and incubated with 22.5 µg/well and 40 µg/well of APRc and 20 µg/well of human IgG. As previously observed APRc binds to C3 in both concentrations, although it is not statistically different. Furthermore, the conditions with C3 and IgG also increase absorbance when compared to the control BSA with IgG, being slightly lower than the condition with only C3 **(Figure**

14B). Therefore, under the tested conditions, the presence of IgG have no positive impact on APRc-C3 interaction.

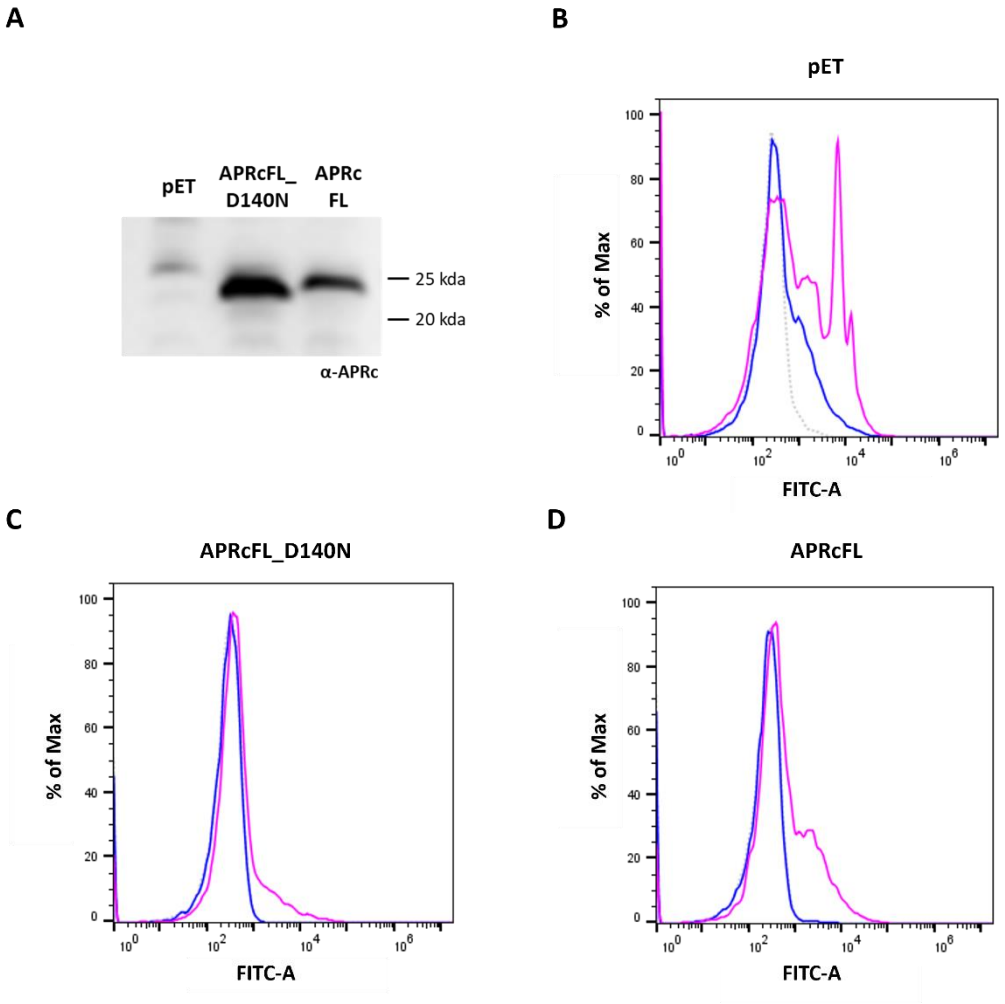

Figure 13: **Flow cytometry analysis of C3 deposition on the surface of *E. coli* expressing APRc. (A)** Western blot analysis with anti-APRc antibody of total protein extracts equivalent to an OD_{600nm} of 1 from BL21 Star DE3 strain of *E. coli* expressing empty vector backbone pET28a (pET), full-length active site mutant APRc (APRcFL_D140N) and full-length APRc (APRcFL). **(B)** BL21 Star DE3 *E. coli* expressing pET, **(C)** APRcFL_D140N and **(D)** APRcFL were fixed and incubated with HBSS (grey trace), 40% NHS (blue trace), or 40% NHSΔIgG/IgM (pink trace). After incubation, samples were blocked at RT, washed, and incubated with primary anti-C3α antibody at RT for 1h. Each condition was incubated with anti-rabbit IgG FITC-conjugated secondary antibody for 1h at RT and resuspended in PBS. Results were obtained with the FL1-A channel (FITC). Each condition presents about 10000 counts.

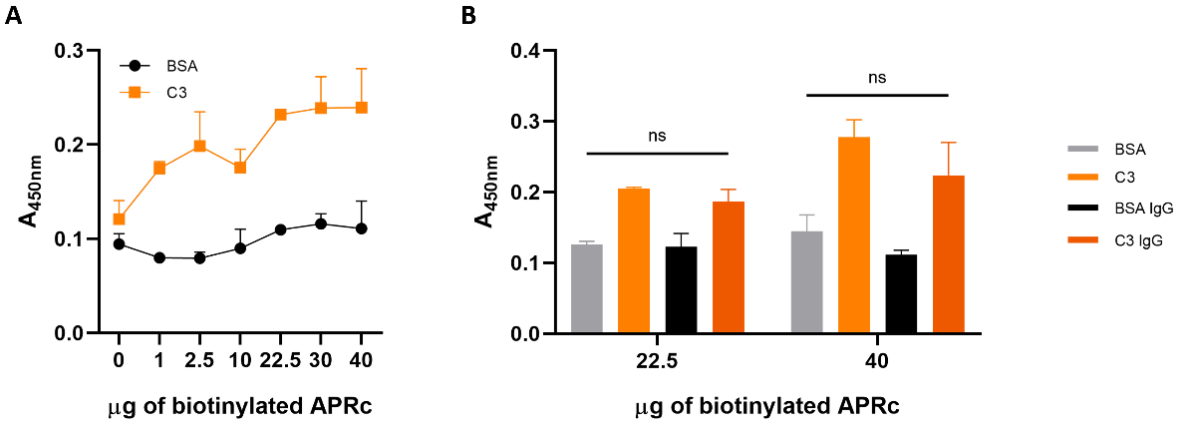

Figure 14: APRc ability to bind C3 in the presence and absence of human IgG was evaluated by ELISA. (A) 96-well plate were coated with 1 µg/well of BSA and purified C3 and incubated with different concentrations of biotinylated APRc. To detect the signal was used streptavidin-HRP at 450 nm. Results are represented in mean ± standard deviation from three replicates. **(B)** 1 µg/well of BSA and purified C3 were used as coating in a 96-well plate and incubated with different concentrations of biotinylated APRc and 20 µg/well of IgG. To detect the signal was used streptavidin-HRP at 450 nm. Results are represented in mean ± standard deviation from three replicates. Significance was determined using a Kruskal-wallis with Dunn's multiple comparisons test using GraphPad Prism 8 (ns, non-significant).

To further evaluate APRc binding to C3 and its potential to cleave this complement protein pull-down assays were performed. Previously incubated beads with the wild-type and active site mutant APRc were incubated with four different serums: UCS, NHS from Sigma, NHS from Pel-Freez and NHS depleted in IgG/IgM. After incubation the beads were washed, and APRc-bounded proteins were assessed.

C3 presents a molecular weight of 190 kDa and is composed by an α-chain (115 kDa) and a β-chain (75 kDa) (Pollack et al., 2021) **(Figure S3)**. The used antibody against C3 recognizes the C-terminal region downstream of the thioester binding that enables the interaction of C3 with the target upon C3 activation **(Figure 15A)**. With this antibody, binding and cleavage of fragments containing the following regions may be visible: α-chain (115 kDa), C3b α'-chain (101 kDa) and iC3b/C3c α'-chain fragment 2 (39 kDa) (Pollack et al., 2021). In the latter region the thioester binding is not present.

In the four serum profiles, the α-chain and potentially the C3c/iC3b α-chain fragment 2 (~39 kDa) are observed. Although theoretically the antibody only detects the C3 α-chain, a band with 75 kDa is detected in the UCS and NHSΔIgG/IgM that corresponds to the expected molecular weight of the β-chain, anticipating some

unspecific binding. Both forms of APRc bind to C3 in the tested sera **(Figure 15B-E)**. NHS Sigma appears more degraded in the protein profile from the initial input comparing with the other sera (presents a more intense band between 50 and 37 kDa and a more tenuous band between 150 and 100 kDa). In all sera there is a decrease intensity of the band between 50 and 37 kDa in the APRc-WT eluted fraction when compared to the APRc_D140N. Furthermore, one (NHS Sigma) or more protein bands (UCS, NHS PF and NHSΔIgG/IgM) are additionally observed, suggesting C3 cleavage. Indeed, for both NHS samples an additional protein band with ~37 kDa is detected. According to the antibody-recognized region, one can assume that APRc is cleaving C3 in the region encompassing the C3c/iC3b α-chain fragment 2. However, further studies are required to confirm this and if the fragment is being generated from cleavage of the α-chain (115 kDa) or C3b α'-chain (101 kDa), as this may impact C3 activation and the exposure of the reactive thioester bond. Moreover, when the IgG and IgM are depleted the protein bands are more intense, suggesting that this depletion leads to increased binding to the APRc_WT form, consistent with our previous observations by flow cytometry **(Figure 13)**.

APRc cleavage of C3 β-chain **(Figure S3)** was also evaluated. Pull-down assays were conducted as previously described, being used an antibody that recognizes the portion of C3 that encompasses a region of the β- and a region of the α-chain **(Figure 16A)**. As expected, in each serum, a protein band that corresponds to the β-chain (75 kDa) is detected, confirming APRc binding to C3 **(Figure 16B-E)**. Contrary to the α-chain, there are no new protein bands or smears, apart from the UCS incubation where is visible a smear below 75 kDa. APRc-WT appears to bind more to the C3 in the UCS, NHS Pel-Freez and NHS depleted in IgG and IgM when compared to the APRc-D140N, as shown previously with the α-chain.

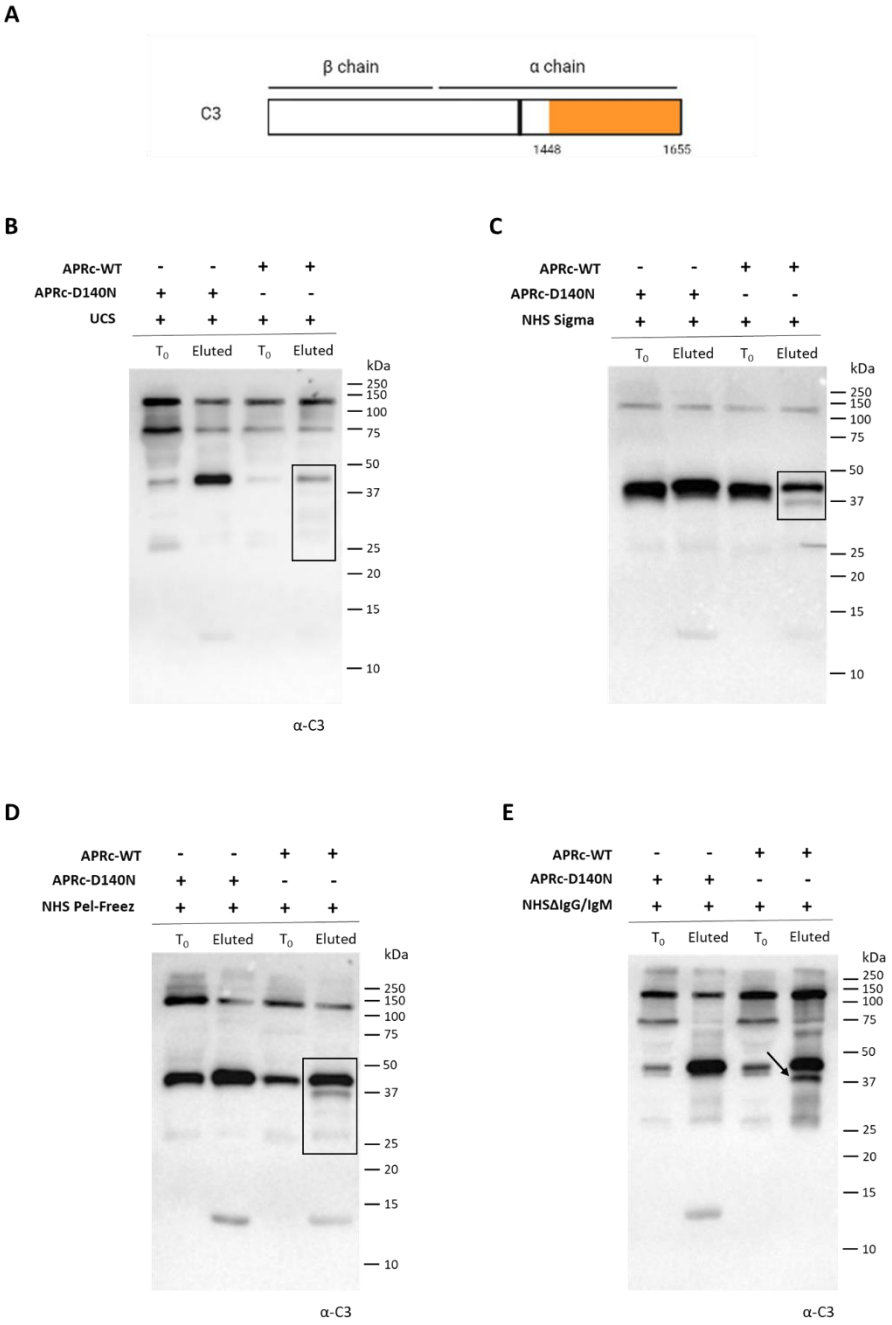

Figure 15: APRc binding and cleavage of C3 α-chain was evaluated by pull-down assays using human serum. Pull-down assays using HisMag Sepharose Nickel beads were independently incubated with the dimeric soluble form of APRc wildtype (APRc-WT) and the corresponding active site mutant (APRc-D140N). After binding, the beads were incubated with human serum diluted 15x in PBS pH 7.4 for 5 hours at 37ºC with agitation. In this step was taken a sample of the initial input (T_0). The beads were washed and denatured with SDS sample buffer diluted 6x in PBS buffer (Eluted). Input and eluted samples were loaded into a 12.5% polyacrylamide gel and C3 detection was conducted by Western Blot. **(A)** Schematic representation of the C3 protein. The black line represents the isoglutamyl cysteine thioester that enables the binding to the target. The orange box represents the region that the anti-C3 antibody encompasses (aa 1448-1655). **(B)** Western blot of the pull-down assay with UCS, **(C)** NHS from Sigma, **(D)** NHS from Pel-Freez and **(E)** NHS depleted in IgG and IgM (NHSΔIgG/IgM) probed with anti-human C3α. The black boxes represent the smear consistent with additional cleavage products. The black arrow highlights a new protein band.

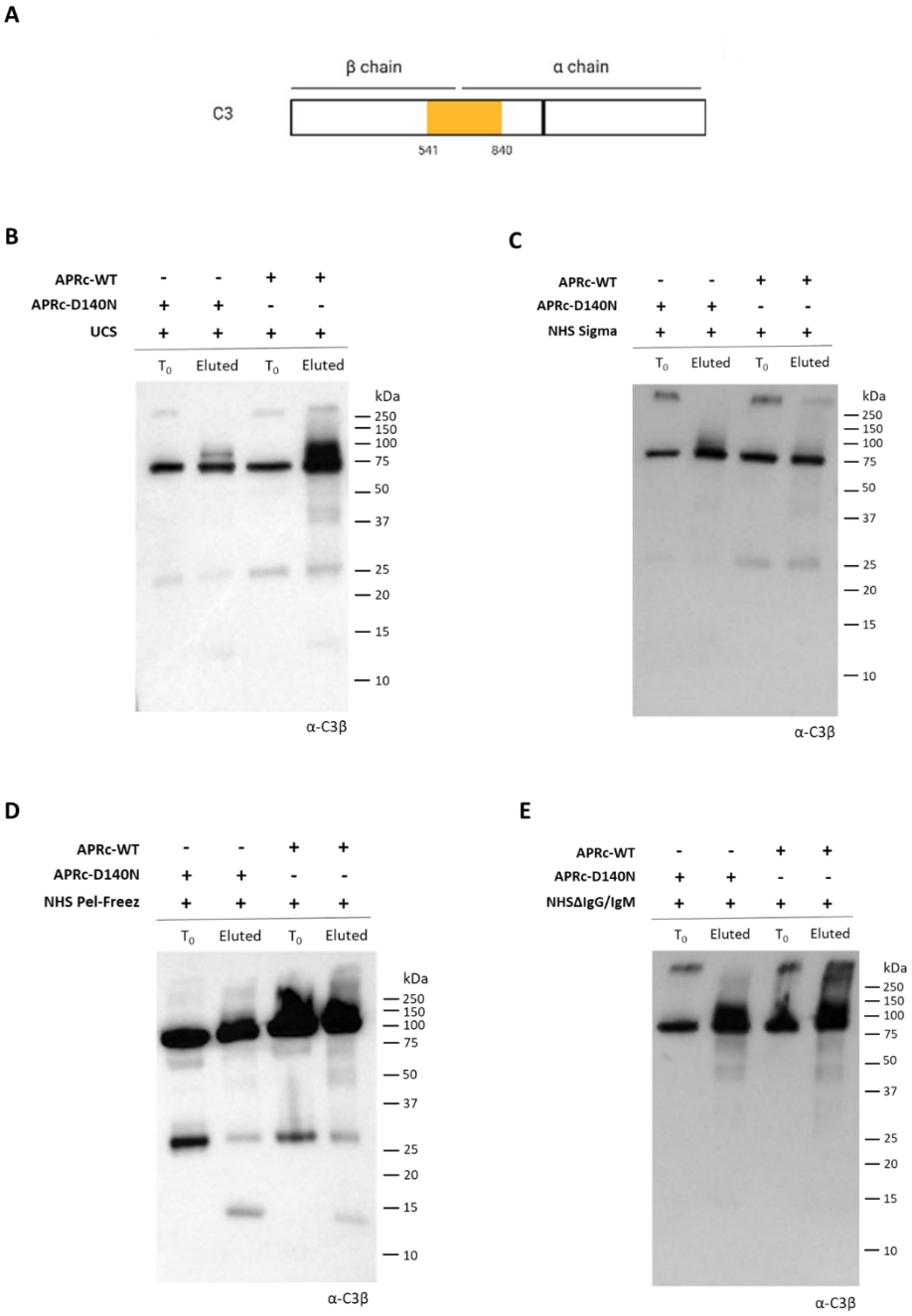

Figure 16: APRc binding and cleavage of C3 β-chain was evaluated by pull-down assays using human serum. Pull-down assays using HisMag Sepharose Nickel beads were independently incubated with the dimeric soluble form of APRc wildtype (APRc-WT) and the corresponding active site mutant (APRc-D140N). After binding, the beads were incubated with human serum diluted 15x in PBS pH 7.4 for 5 hours at 37ºC with agitation. In this step was taken a sample of the initial input (T_0). The beads were washed and denatured with SDS sample buffer diluted 6x in PBS buffer (Eluted). Input and eluted samples were loaded into a 12.5% polyacrylamide gel and C3 detection was conducted by Western Blot. **(A)** Schematic representation of the C3 protein. The black line represents the isoglutamyl cysteine thioester that enables the binding to the target. The orange box represents the region that the anti-C3 antibody encompasses (aa 541-840). **(B)** Western blot of the pull-down assay with UCS, **(C)** NHS from Sigma, **(D)** NHS from Pel-Freez and **(E)** NHS depleted in IgG and IgM (NHSΔIgG/IgM) probed with anti-human C3β.

Taken together, these results demonstrate that APRc interacts and cleaves C3 in serum and that the cleavage likely occurs in the α-chain. We next ought to evaluate if this is also seen in a less complex system, doing the pull-down assay with the protease and purified C3 protein. IgG contribution in this interaction was also assessed. In the Coomassie-stained SDS-PAGE there are no obvious differences between the two forms of APRc in the presence and absence of IgG **(Figure 17A)**. However, in all eluted fractions there is a band with about 25 kDa that corresponds to the dimeric form of APRc, which is less intense in the presence of IgG **(Figure 17B)**. This is consistent with previous data showing that APRc forms high-molecular weight complexes in the presence of IgG (Curto et al., 2021). In the incubations with only C3, there are a few differences in the protein profiles when comparing the eluted fraction of both APRc forms **(Figure 17C)**. However, the activity towards the α-chain, if any, appears to be lower than that observed in the context of NHS **(Figure 15)**. Contrary to our previous observations, in the presence of IgG, APRc WT binds more to C3 than the mutant form. Moreover, there are no visible differences between the conditions when probed with the C3 β-chain antibody **(Figure 17D)**.

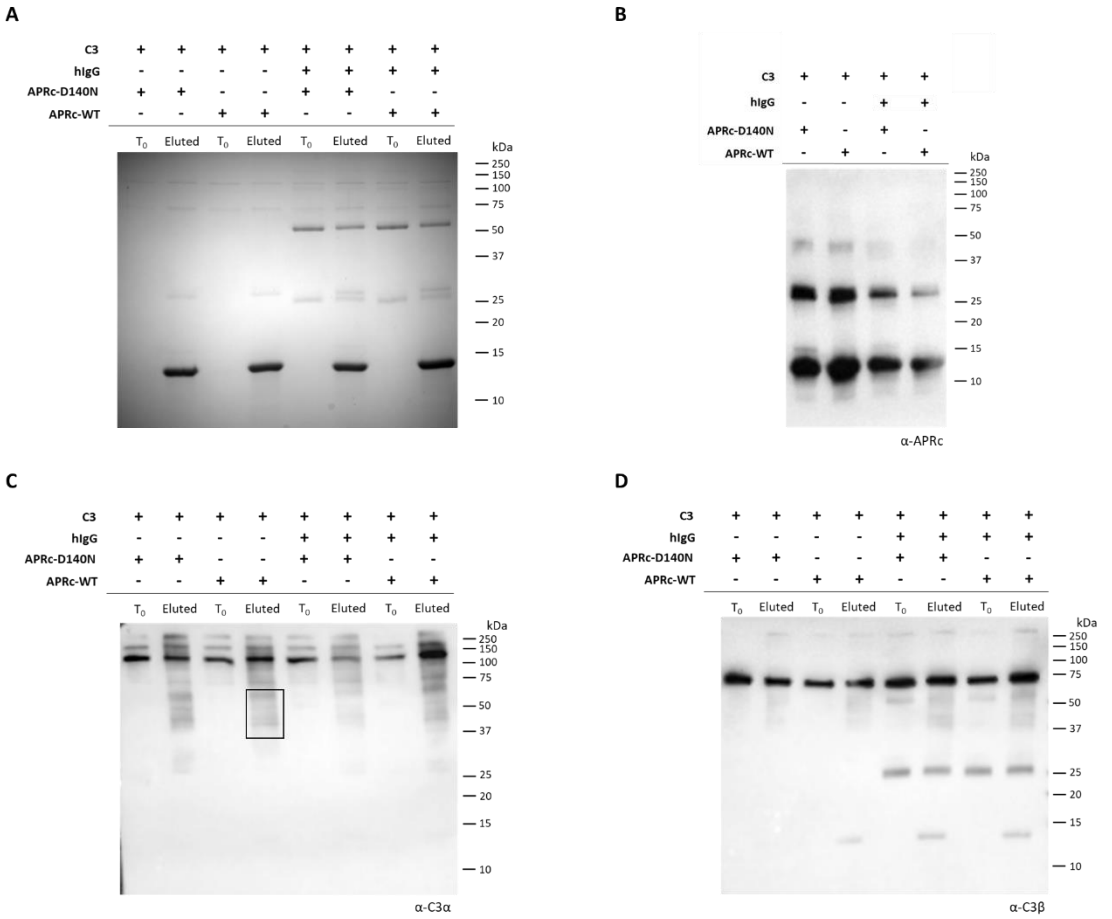

Figure 17: APRc binding and cleavage of C3 was evaluated by pull-down assays with purified C3. Pull-down assays using HisMag Sepharose Nickel beads were independently incubated with the dimeric soluble form of APRc wildtype (APRc-WT) and the corresponding active site mutant (APRc-D140N). After binding, the beads were incubated with 7 µg of C3 purified protein with or without 7 µg human IgG (hIgG) diluted in PBS pH 7.4 for 5 hours at 37ºC with agitation. In this step was taken a sample of the initial input (T_0). The beads were washed and denatured with SDS sample buffer diluted 6x in PBS buffer (Eluted). Input and eluted samples were loaded into a 12.5% polyacrylamide gel. **(A)** SDS-PAGE stained with Coomassie blue of the input and eluted samples of wildtype and mutant APRc fractions. **(B)** Western Blot analysis with anti-APRc antibody of the eluted fractions. **(C)** Western Blot analysis with anti-C3α antibody and **(D)** anti-C3β antibody.

In the pull-down assays, we evaluate only the profiles of APRc-bounded proteins, without evaluating the total protein sample. To analyse the total protein, additional incubation assays were performed. Nickel-magnetic beads with the wild-type and active site mutant APRc were independently incubated with purified C3 with or without human IgG. After incubation, the samples were denatured and assessed. In the SDS-PAGE there are no visible differences between the presence and absence of IgG, as well as between

the two forms of APRc **(Figure 18A,B)**. In the absence of IgG, there is the appearance of a band between 50 and 37 kDa in the APRc-WT **(Figure 18C)**. In the presence of IgG, it is also visible the formation of a band between 50 and 37 kDa **(Figure 18D)**.

Anaphylatoxin C3a is a proinflammatory mediator whose levels increase with complement system activation. Although a protein band with 9.6 kDa corresponding to the C3a molecular weight was not visible in the previous assays, it could be due to the used anti-C3a antibody (data not shown). To analyse if C3 cleavage by APRc impacts the production of the anaphylatoxin C3a, a sandwich ELISA assay was performed. Ninety-six-well plates were incubated with purified anti-human C3a and incubated with serum samples previously incubated alone, with wild-type APRc or zymosan. Zymosan is a macromolecule from the wall of *Saccharomyces cerevisiae* that can activate the complement system (Smith et al., 1982), being used as a positive control. The wells were probed with biotinylated anti-human C3a, and the signal was detected with Strep-HRP. As expected, UCS preincubated with zymosan results in the production of C3a consistent with complement activation. However, the values of serum preincubated with APRc-WT do not differ from those observed for the UCS, suggesting that APRc does not impact C3a production under the conditions tested **(Figure 19)**.

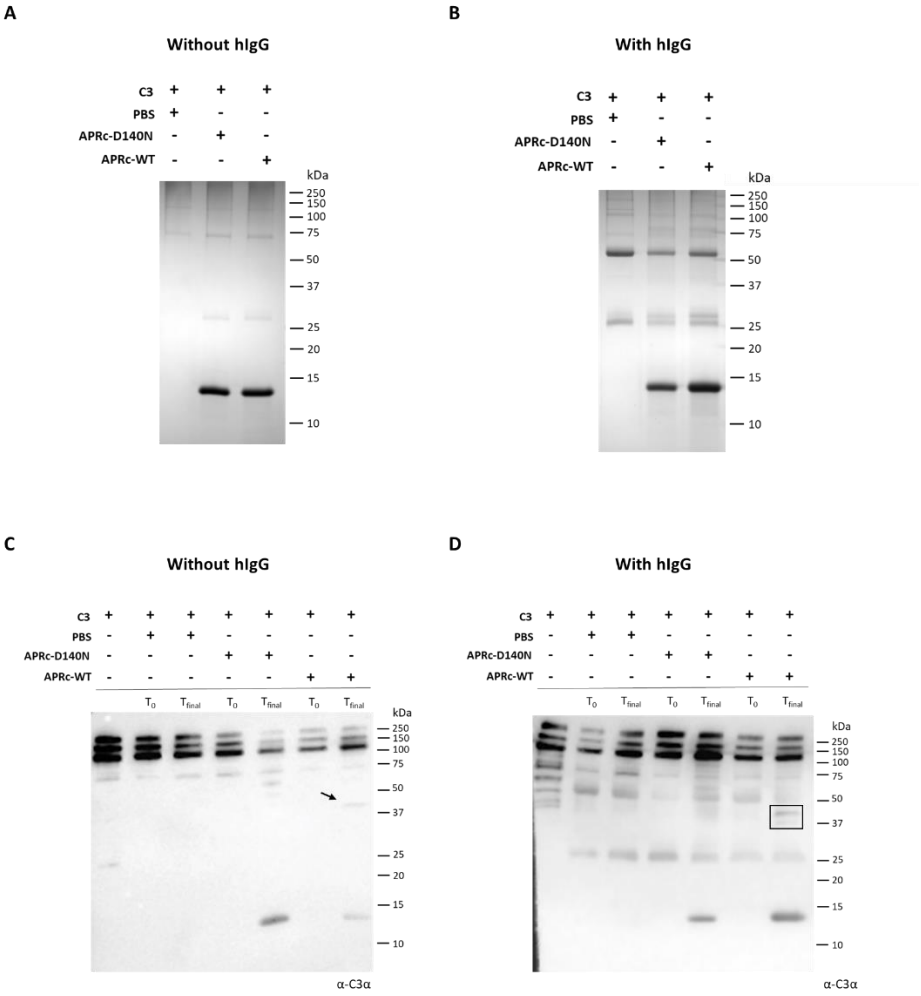

Figure 18: APRc cleavage of C3 was evaluated by incubation assays with purified C3. Incubation assays using HisMag Sepharose Nickel beads were independently incubated with the dimeric soluble form of APRc wildtype (APRc-WT) and the corresponding active site mutant (APRc-D140N). After binding, the beads were incubated with 7 µg of C3 purified protein with or without 7 µg human IgG (hIgG) diluted in phosphate-buffered saline (PBS) for 5 hours at 37ºC with agitation. In this step was taken a sample of the initial input (T_0). 7 µg of C3 purified protein diluted in PBS was used as a control. The beads were washed and denatured with SDS sample buffer diluted 6x in PBS buffer (T_{Final}). Input and eluted samples were loaded into a 12.5% polyacrylamide gel. **(A)** SDS-PAGE stained with Coomassie blue of the T_{final} samples incubated without hIgG. **(B)** SDS-PAGE of the T_{final} samples incubated with IgG. **(C)** Western Blot analysis with anti-C3α of the PBS and APRc samples incubated without hIgG. **(D)** Western Blot analysis with anti-C3α of the PBS and APRc samples incubated with hIgG.

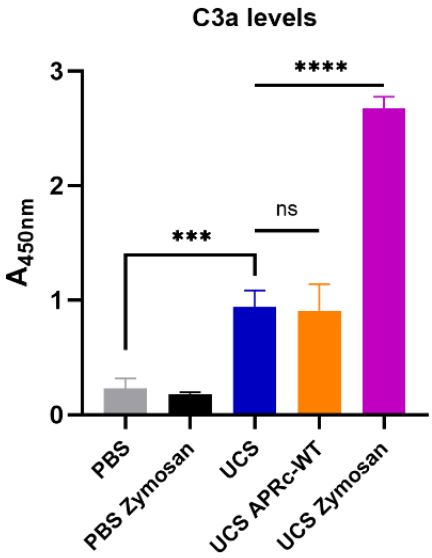

Figure 19: APRc impact in C3a production evaluated by ELISA. 96-well plates were coated with 5 µg/mL of anti-human C3a and incubated with serum samples previously incubated for 4h at 37ºC. PBS conditions were used as a negative control and Zymosan (0.5 mg/mL) was used as a positive control. Biotinylated anti-human C3a followed by streptavidin-HRP was used to detect the signal at 450 nm. Results are represented in mean ± standard deviation from three replicates. Significance was determined using a one-way ANOVA followed by Tukey's multiple comparisons test using GraphPad Prism 8 (ns, non-significant; ***, P < 0.001; ****, P < 0.0001).

3.5.2 Evaluation of C4 as an APRc substrate

Since C4 binds to some level to the rickettsial surface, it was evaluated if this complement protein could bind specifically to APRc using flow cytometry. This experiment was conducted as previously described for C3 in section 3.5.1. APRc expression was confirmed with the protein band with ~25 kDa, presenting slightly more expression of the mutant than the wild type form **(Figure 20A)**. Bacteria expressing the empty vector present C4 deposition in the serum depleted in IgG and IgM **(Figure 20B)**. Bacteria-expressing APRcFL_D140N and APRcFL do not bind to C4 in the NHS condition, however some very residual binding of C4 is observed when the IgG and IgM are depleted **(Figure 20C,D)**.

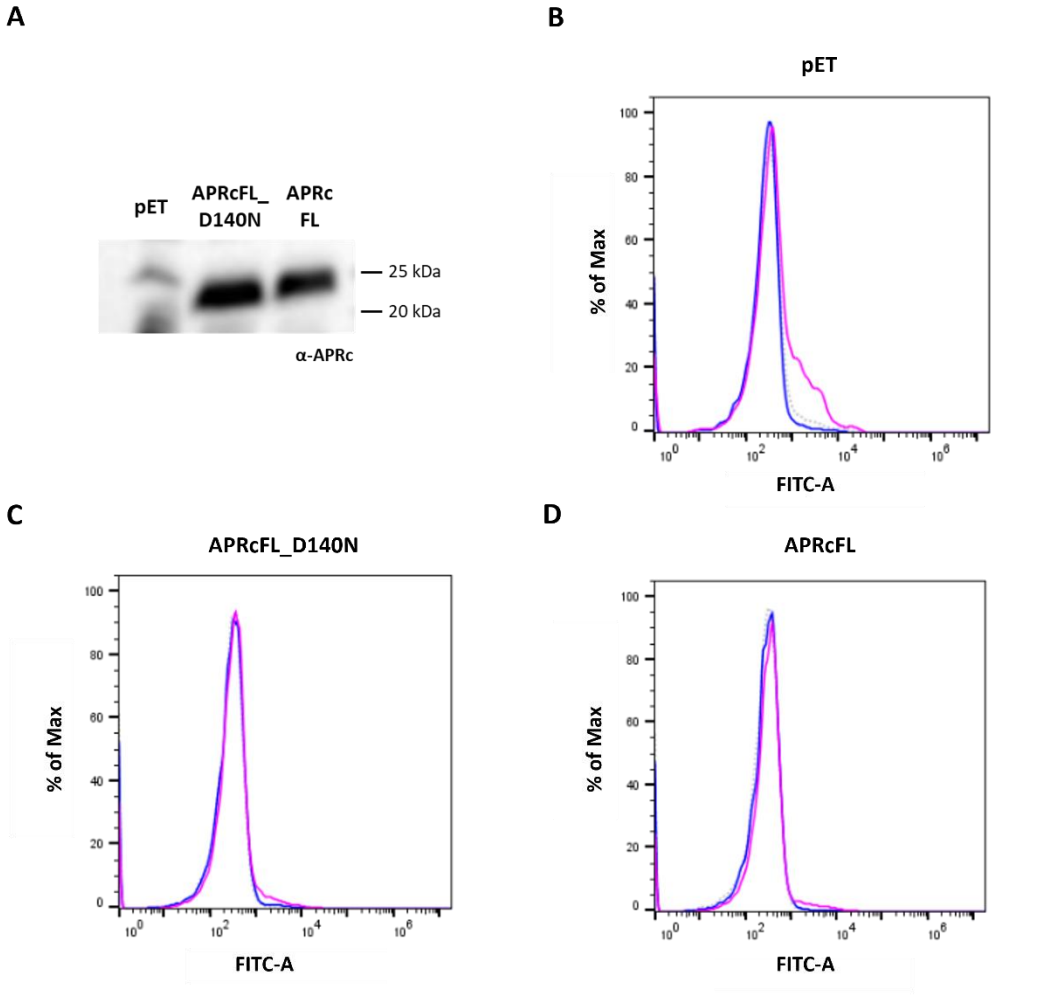

Figure 20: Flow cytometry analysis of C4 deposition on *E. coli* expressing APRc. (A) Western blot analysis with anti-APRc antibody of total protein extracts equivalent to an OD_{600nm} of 1 from BL21 Star DE3 strain of *E. coli* expressing empty vector backbone pET28a (pET), full-length active site mutant APRc (APRcFL_D140N) and full-length APRc (APRcFL). **(B)** BL21 Star DE3 *E. coli* expressing pET, **(C)** APRcFL_D140N and **(D)** APRcFL were fixed and incubated with HBSS (grey trace), 40% NHS (blue trace), or 40% NHSΔIgG/IgM (pink trace). After incubation, samples were blocked at RT, washed, and incubated with primary anti-C4α antibody at RT for 1h. Each condition was incubated with anti-mouse IgG FITC-conjugated secondary antibody for 1h at RT and resuspended in PBS. Results were obtained with the FL1-A channel (FITC). Each condition presents about 10000 counts.

To further validate APRc-binding to complement protein C4, 96-well plates were incubated with BSA and C4 and incubated with different concentrations of APRc. The results confirm that APRc binds to C4 in a concentration-dependent manner **(Figure 21A)**. To analyse IgG role in this interaction, 96-well plate was incubated with BSA and C4 and incubated with different concentrations of APRc and 20 µg/well of human IgG. As previously observed in **Figure 21A**, APRc binds to C4 under both conditions, with no significant alterations when IgG is present **(Figure 21B)**.

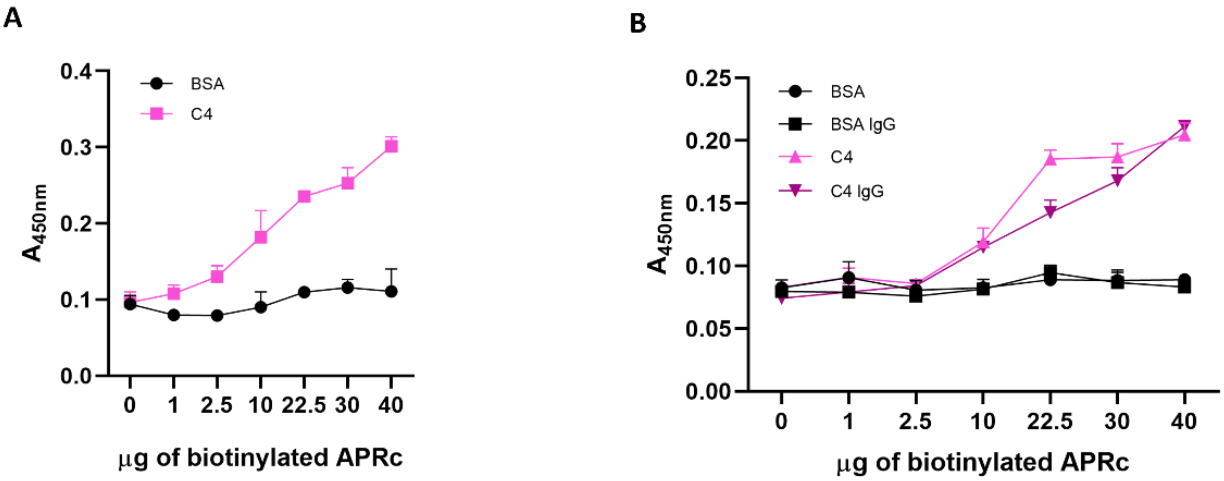

Figure 21: APRc ability to bind C4 in the presence and absence of human IgG was evaluated by ELISA. (A) 96-well plate were coated with 1 µg/well of BSA and purified C4 and incubated with different concentrations of biotinylated APRc. **(B)** 1 µg/well of BSA and purified C4 were used as coating in a 96-well plate and incubated with different concentrations of biotinylated APRc and 20 µg/well of IgG. To detect the signal was used streptavidin-HRP at 450 nm. Results are represented in mean ± standard deviation from three replicates.

Complement C4 protein is composed by a γ-chain (30 kDa), an α-chain (95 kDa) and a β-chain (75 kDa) (H. Wang & Liu, 2021) **(Figure S4)**. The used antibody detects the α-chain and C4 processing derivates C4b α-chain (95 kDa) and C4d α-chain (45 kDa) (H. Wang & Liu, 2021, p. 4), all containing the thioester binding that is crucial to bind to the target **(Figure 22A)**. All sera, apart from the NHS Sigma, present the C4 α-chain in the input fractions. Furthermore, it is seen in all tested sera the presence of a band with approximately 50 kDa, that could correspond to the C4d α-chain. In the UCS incubation, it is not visible a major difference between the eluted fractions of the two forms of APRc, appearing a slight increase of C4-binding in the wild type APRc **(Figure 22B)**. On the other hand, in a more degraded serum there is the decrease of the band between 50 and 37 kDa, suggesting C4 degradation **(Figure 22C)**. In the NHS Pel-Freez and in the depletion of IgG and IgM there is increased APRc-WT binding to C4, and in the latter one there is the formation of new protein bands below 75 kDa **(Figure 22D,E)**. These results further corroborate APRc-C4 binding in more complex samples as NHS, and suggest that APRc proteolytic activity appears to favour interaction (although this was not previously observed in the flow cytometry analysis).

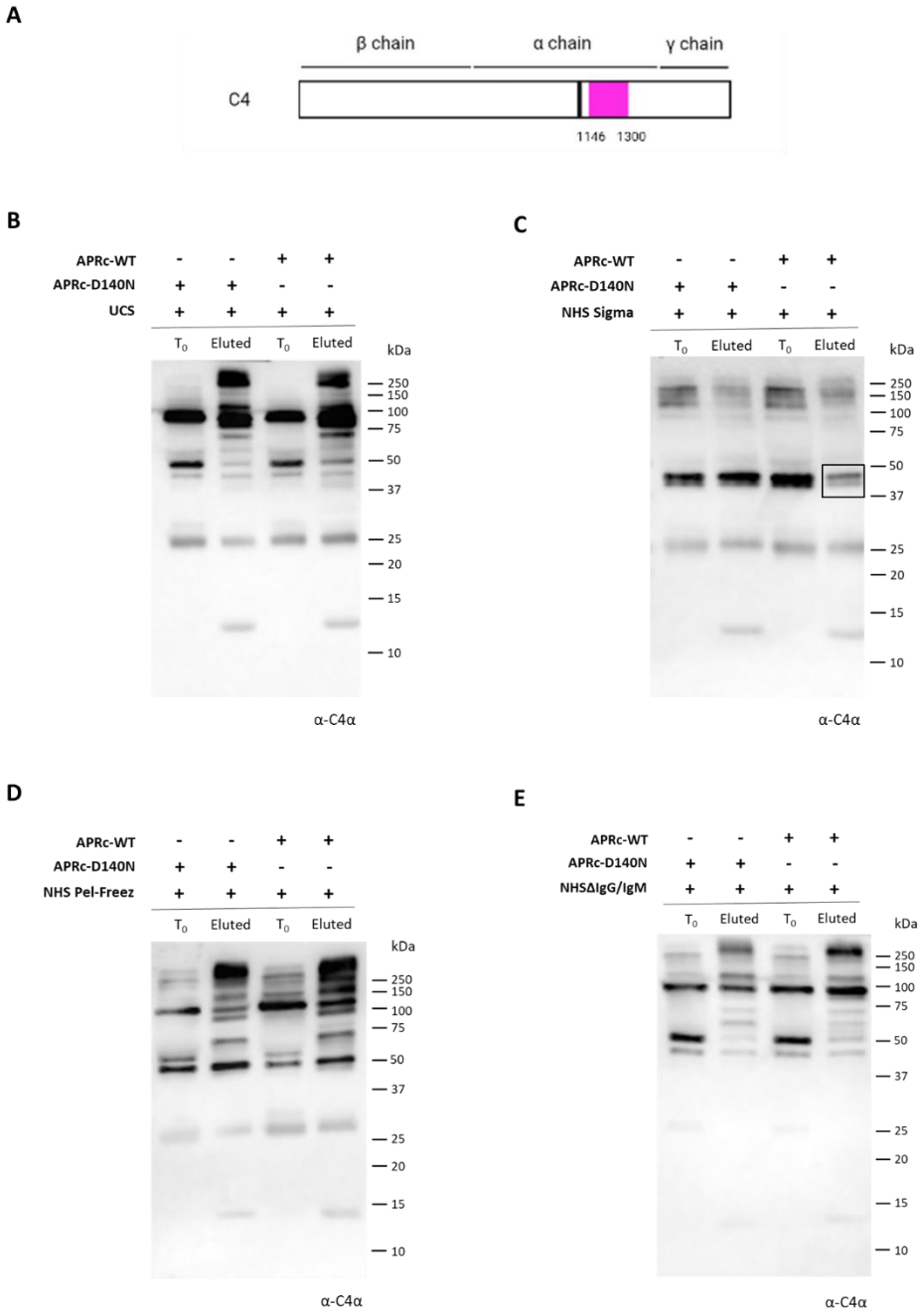

Figure 22: APRc binding and cleavage of C4 was evaluated by pull-down assays using human serum. Pull-down assays using HisMag Sepharose Nickel beads were independently incubated with the dimeric soluble form of APRc wildtype (APRc-WT) and the corresponding active site mutant (APRc-D140N). After binding, the beads were incubated with human serum diluted 15x in phosphate-buffered saline (PBS) for 5 hours at 37ºC with agitation. In this step was taken a sample of the initial input (T_0). The beads were washed and denatured with SDS sample buffer diluted 6x in PBS buffer (Eluted). Input and eluted samples were loaded into a 12.5% polyacrylamide gel and C4 detection was conducted by Western Blot. **(A)** Schematic representation of the C4 protein. The black line represents the isoglutamyl cysteine thioester that enables the binding to the target. The pink box represents the region that the anti-C4α antibody encompasses (aa 1146-1300). **(B)** Western blot of the pull-down assay with UCS, **(C)** NHS from Sigma, **(D)** NHS from Pel-Freez and **(E)** NHS depleted in IgG and IgM (NHSΔIgG/IgM) probed with anti-human C4α.

To analyse APRc effect in the total proteins and APRc-binding to isolated C4 additional incubation assays were performed. This assay was performed as previously mentioned in C3 in section 3.5.1. There are no differences in protein profiles in the SDS-PAGE **(Figure 23A)** or in the Western Blot assay both in the absence or presence of IgG (**Figure 23B,C**), with no proteolytic activity observed under these conditions.

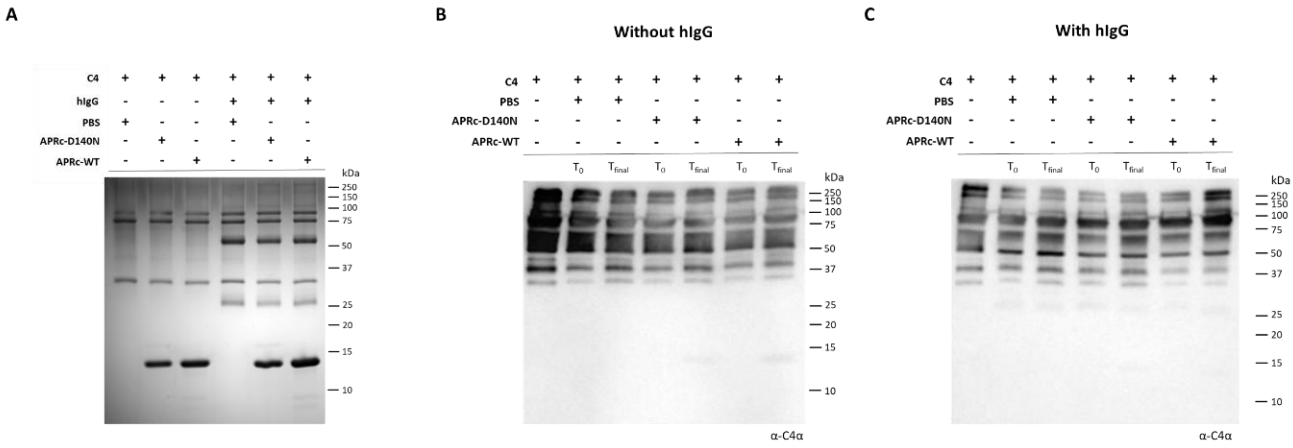

Figure 23: APRc cleavage of C4 was evaluated by incubation assays with purified C4. Incubation assays using HisMag Sepharose Nickel beads were independently performed with the dimeric soluble form of APRc wildtype (APRc-WT) and the corresponding active site mutant (APRc-D140N). After binding, the beads were incubated with 7 µg of C4 purified protein with or without 7 µg human IgG (hIgG) diluted in phosphate-buffered saline (PBS) for 5 hours at 37ºC with agitation. In this step a sample of the initial input (T_0) was taken. 7 µg of C4 purified protein diluted in PBS was used as a control. The beads were washed and denatured with SDS sample buffer diluted 6x in PBS buffer (Eluted). Input and eluted samples were loaded into a 12.5% polyacrylamide gel. **(A)** SDS-PAGE followed Coomassie Blue staining of the eluted fractions of the control and experimental groups. **(B)** Western Blot analysis with anti-C4α of the PBS and APRc samples incubated without and **(C)** with hIgG.

3.5.3 Evaluation of C4BP as an APRc substrate

C4BP binding to APRc was evaluated by flow cytometry. The most common C4BP isoform is composed by seven α-chains and one β-chain (Meri et al., 2004), and we initially evaluated C4BP deposition with anti-C4BP α-chain antibody. This experiment was conducted as previously described for C3 in section 3.5.1. APRc expression was confirmed with the protein band with ~25 kDa, presenting more expression of the wild-type form than the mutant **(Figure 24A)**. Bacteria expressing the empty vector present C4BP deposition in both sera, being higher in the NHSΔIgG/IgM **(Figure 24B).** Bacteria

expressing APRcFL_D140N and APRcFL only present deposition when IgG and IgM are depleted **(Figure 24C,D).** The deposition of C4BP in the wild-type form is higher than in the mutant form (Positive % 17.8 vs 6.7, respectively). However, given the higher protein levels of the wild-type form, we cannot infer if proteolytic activity affects this interaction or not. As seen in the previous tested complement proteins, this deposition is lower than the control with the empty vector.

C4BP deposition was also evaluated by flow cytometry using an anti-β-chain antibody. APRc expression was confirmed by Western Blot, presenting slightly more expression of the wild-type form than the mutant **(Figure 25A)**. As seen for the α-chain, bacteria expressing pET present C4BP deposition in both sera but more in the IgG/IgM-depleted serum **(Figure 25B)**. Additionally, bacteria-expressing both APRc forms also bind to C4BP in the NHS depleted in IgG and IgM **(Figure 25C,D)**. The deposition of C4BP β-chain deposition is similar between the APRcFL and APRcFL_D140N (Positive % 12.3 vs 14.8, respectively). Once again, the C4BP deposition in these conditions is lower than in bacteria expressing the empty vector.

To validate APRc-C4BP interaction, 96-well plates were incubated with BSA and C4BP and incubated with different concentrations of APRc. The results demonstrate that APRc binds to C4BP in a concentration-dependent manner, starting to saturate at the 30 μg/well concentration (**Figure 26A)**. The impact of IgG in this interaction was also analysed by ELISA. Ninety-six-well plates were incubated with BSA and C4BP and incubated with different concentrations of APRc and 20 μg/well of human IgG. As previously observed APRc also binds to C4BP, but no major differences in binding are observed **(Figure 26B)**, suggesting no impact of IgG under the conditions tested.

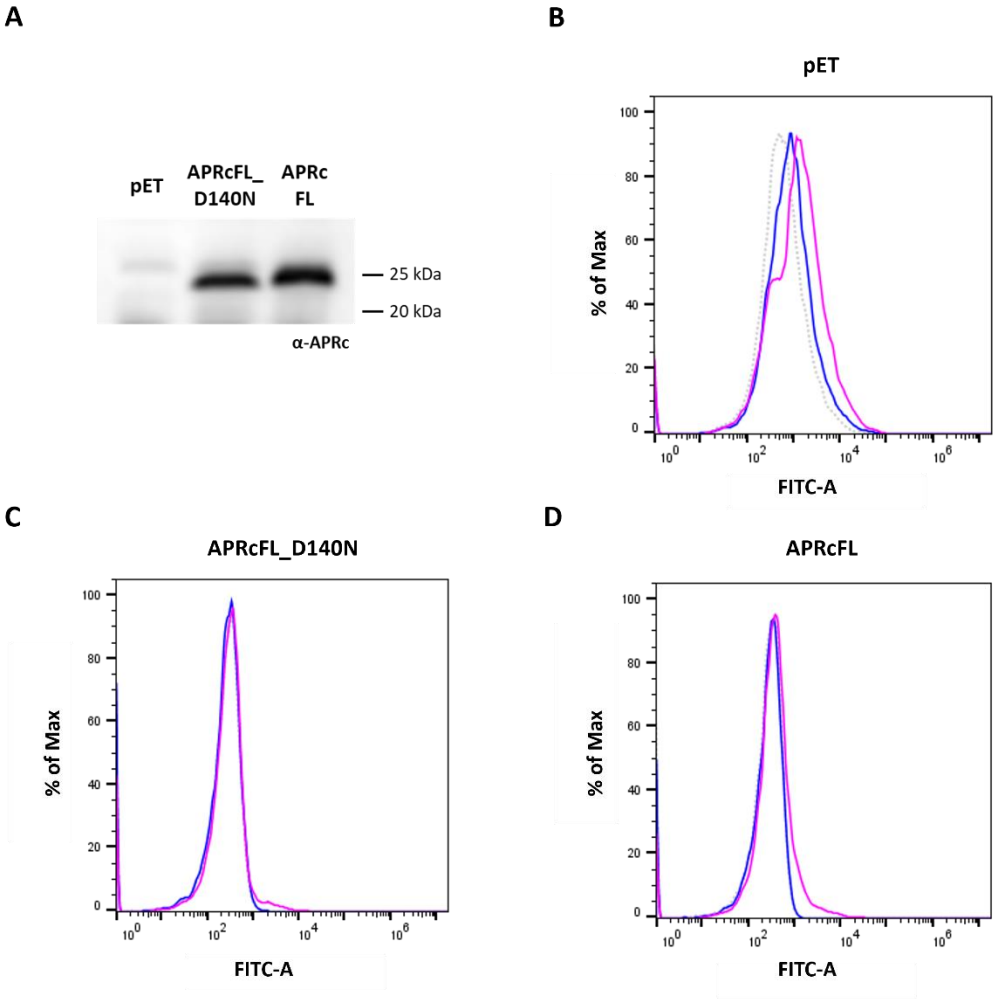

Figure 24: Flow cytometry analysis of C4BPα deposition on *E. coli* expressing APRc. (A) Western blot analysis with anti-APRc antibody of total protein extracts equivalent to an OD_{600nm} of 1 from BL21 Star DE3 strain of *E. coli* expressing empty vector backbone pET28a (pET), full-length active site mutant APRc (APRcFL_D140N) and full-length APRc (APRcFL). **(B)** BL21 Star DE3 *E. coli* expressing pET, **(C)** APRcFL_D140N and **(D)** APRcFL were fixed and incubated with HBSS (grey trace), 40% NHS (blue trace), or 40% NHSΔIgG/IgM (pink trace). After incubation, samples were blocked at RT, washed, and incubated with primary anti-C4BPα antibody at RT for 1h. Each condition was incubated with anti-rabbit IgG FITC-conjugated secondary antibody for 1h at RT and resuspended in PBS. Results were obtained with the FL1-A channel (FITC). Each condition presents about 10000 counts.

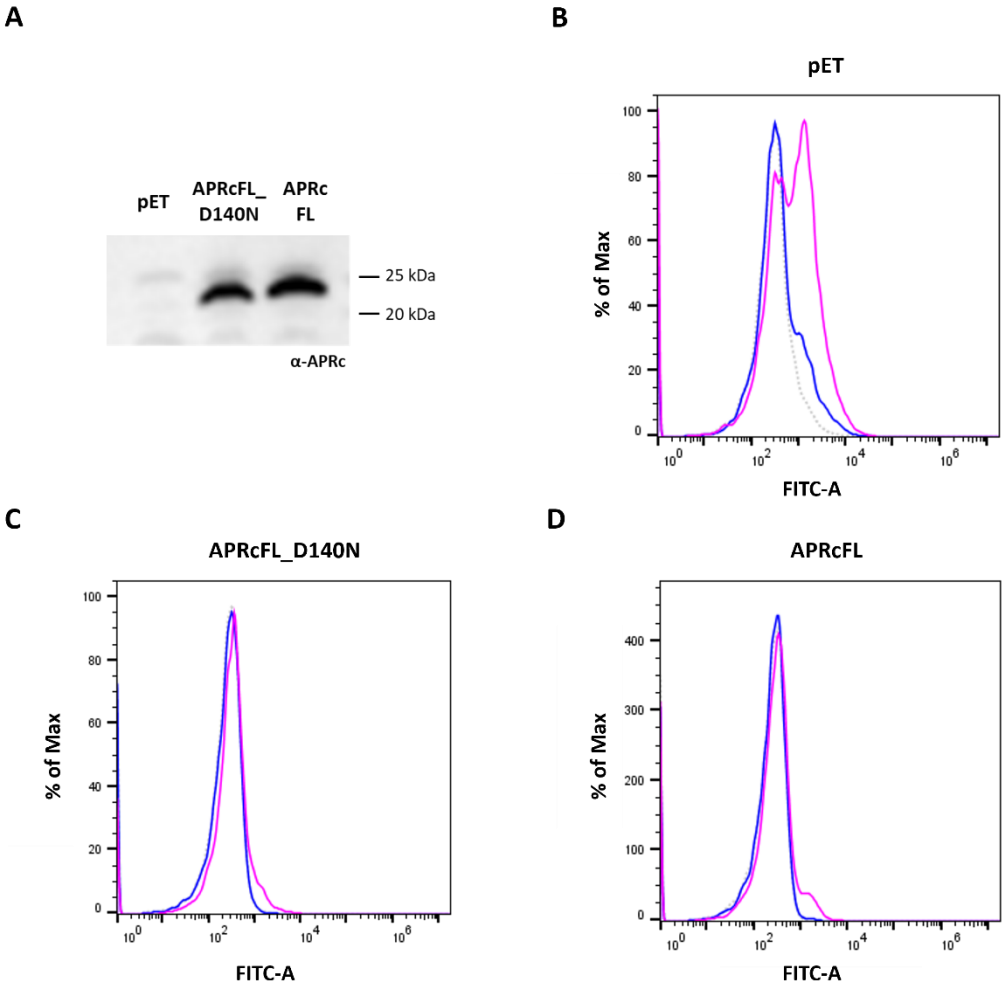

Figure 25: Flow cytometry analysis of C4BPβ deposition on *E. coli* expressing APRc. **(A)** Western blot analysis with anti-APRc antibody of total protein extracts equivalent to an OD_{600nm} of 1 from BL21 Star DE3 strain of *E. coli* expressing empty vector backbone pET28a (pET), full-length active site mutant APRc (APRcFL_D140N) and full-length APRc (APRcFL). **(B)** BL21 Star DE3 *E. coli* expressing pET, **(C)** APRcFL_D140N and **(D)** APRcFL were fixed and incubated with HBSS (grey trace), 40% NHS (blue trace), or 40% NHSΔIgG/IgM (pink trace). After incubation, samples were blocked at RT, washed, and incubated with primary anti-C4BPβ antibody at RT for 1h. Each condition was incubated with anti-rabbit IgG FITC-conjugated secondary antibody for 1h at RT and resuspended in PBS. Results were obtained with the FL1-A channel (FITC). Each condition presents about 10000 counts.

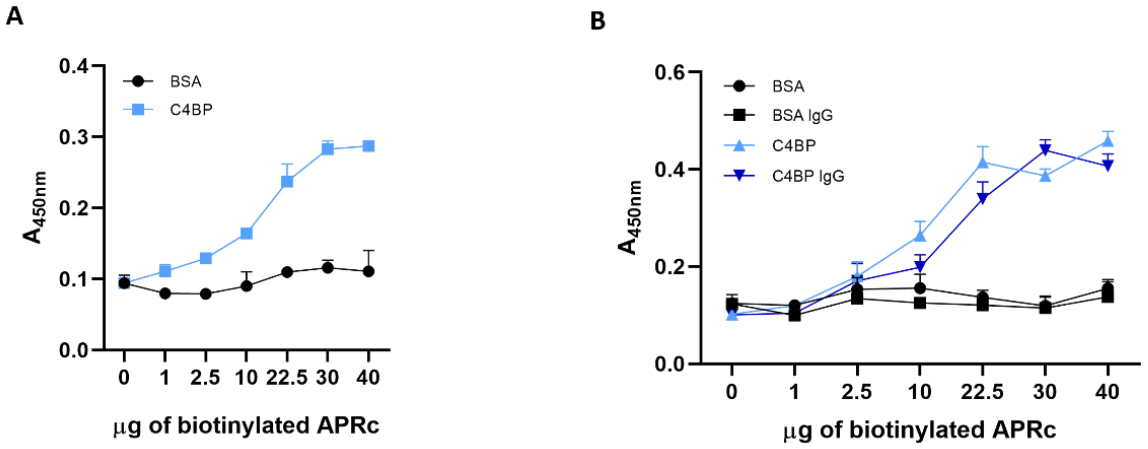

Figure 26: APRc ability to bind C4BP in the presence and absence of human IgG was evaluated by ELISA. (A) 96-well plate were coated with 1 µg/well of BSA and purified C4BP and incubated with different concentrations of biotinylated APRc. **(B)** 1 µg/well of BSA and purified C4BP were used as coating in a 96-well plate and incubated with different concentrations of biotinylated APRc and 20 µg/well of IgG. To detect the signal streptavidin-HRP was used at 450 nm. Results are represented in mean ± standard deviation from three replicates.

C4BP presents a molecular weight of 570 kDa and is composed by seven α-chains (75 kDa) and one β-chain (45 kDa) (Meri et al., 2004) **(Figure S5)**. The used antibody encompasses a region that detects the C4BP α-chain **(Figure 27A)**, visible in all sera a band with 75 kDa. However, in the NHSΔIgG/IgM condition the signal is very faint **(Figure 27E)**. This is due to the lower C4BP levels in this serum profile **(Figure S2)**. In the UCS and NHS Pel-Freez sera, the APRc-WT eluted fraction presents increased binding to the C4BP, illustrated by the increased signal of the α-chain, especially in the latter serum **(Figure 27B,D)**. Also, in UCS, NHS Sigma, and NHS Pel-Freez there is the appearance of a smear between 50 and 37 kDa **(Figure 27B-D)** in the pull-down samples with APR-WT, which may indicate some proteolytic cleavage of C4BP α-chain.

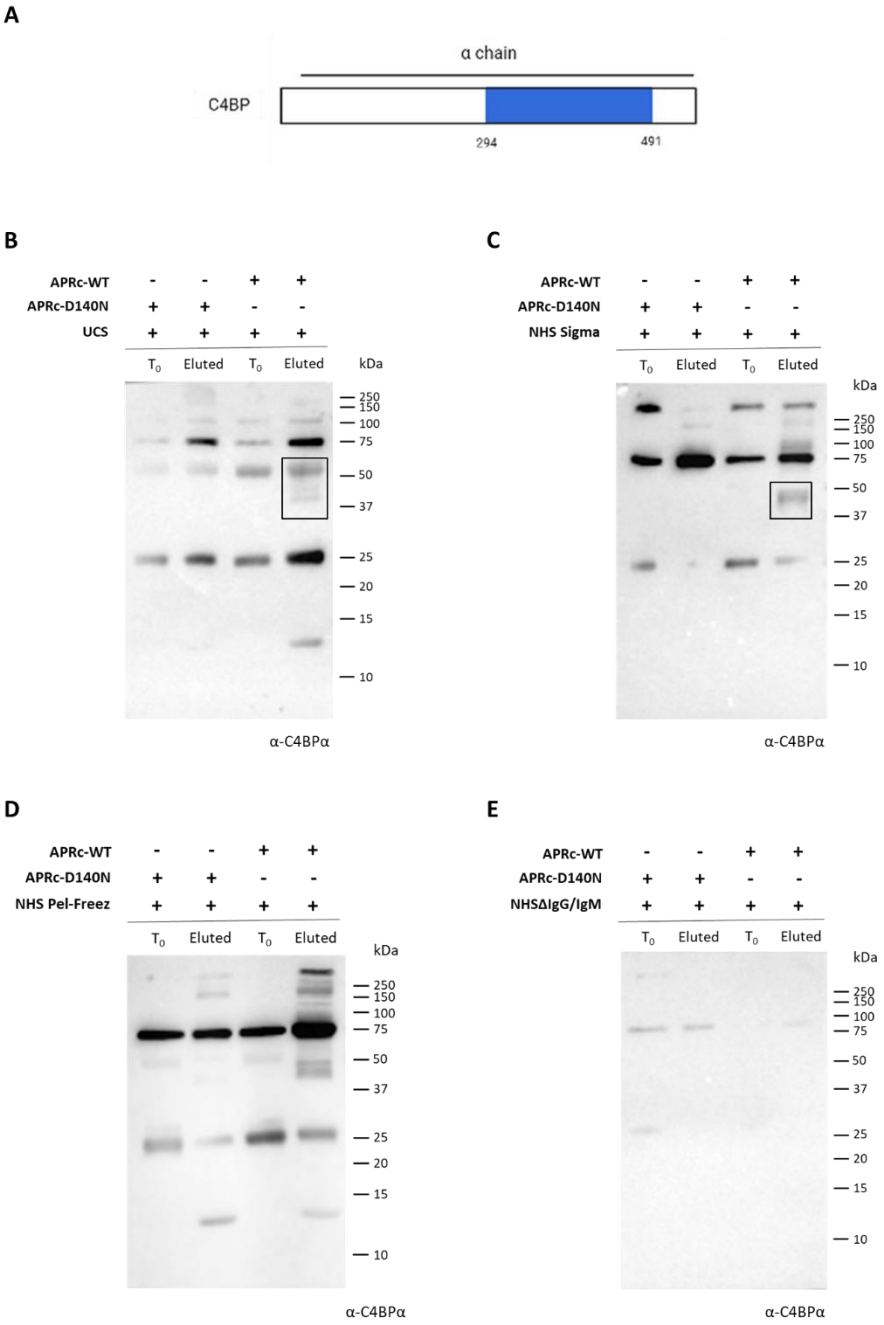

Figure 27: APRc binding and cleavage of C4BP was evaluated by pull-down assays using human serum. Pull-down assays using HisMag Sepharose Nickel beads were independently incubated with the dimeric soluble form of APRc wildtype (APRc-WT) and the corresponding active site mutant (APRc-D140N). After binding, the beads were incubated with human serum diluted 15x in phosphate-buffered saline (PBS) for 5 hours at 37ºC with agitation. In this step a sample of the initial input (T_0) was taken. The beads were washed and denatured with SDS sample buffer diluted 6x in PBS buffer (Eluted). Input and eluted samples were loaded into a 12.5% polyacrylamide gel and C4BP detection was conducted by Western Blot. **(A)** Schematic representation of the C4BP α-chain. The blue box represents the region that the anti-C4BPα antibody encompasses (aa 294 - 491). **(B)** Western blot of the pull-down assay with UCS, **(C)** NHS from Sigma, **(D)** NHS from Pel-Freez and **(E)** NHS depleted in IgG and IgM (NHSΔIgG/IgM) probed with anti-human C4BPα.

APRc-binding and cleavage of C4BP was also evaluated in a less complex system by performing pull-down assays with the purified protein. IgG impact in the interaction was also assessed. SDS-PAGE stained with Coomassie Blue was performed to assess if there are visible differences between the eluted fractions. In fact, there is a visible decrease of the α-chain in the APRc-WT in the absence of IgG, which is not observed in with the mutant or in the same condition with IgG **(Figure 28A)**. This difference is also visible in the Western Blot, presenting a less intense protein band with 75 kDa **(Figure 28B)**. Moreover, it appears that there is an increased smear below the C4BP α-chain upon incubation with APRc-WT than in with APRc-D140N **(Figure 28A,B)**, supporting that this protease may cleave C4BP in the absence of IgG. As previously observed, there are no visible differences between the eluted fractions of both APRc forms in the presence of IgG **(Figure 28C)**.

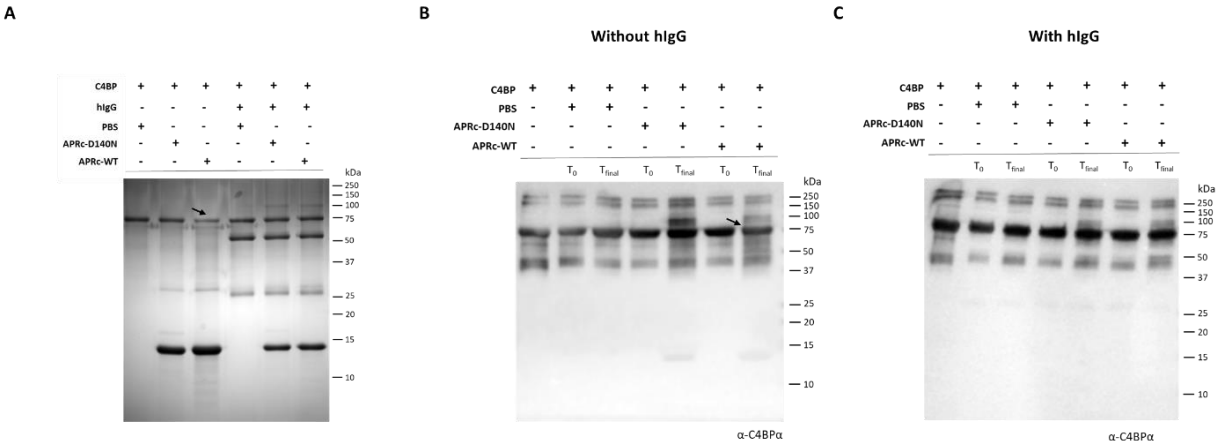

Figure 28: APRc binding and cleavage of C4BP was evaluated by pull-down assays with purified C4BP. Pull-down assays using HisMag Sepharose Nickel beads were independently incubated with the dimeric soluble forms of APRc wildtype (APRc-WT) and the corresponding active site mutant (APRc-D140N). After binding, the beads were incubated with 7 µg of C4BP purified protein with or without 7 µg human IgG (hIgG) diluted in phosphate-buffered saline (PBS) for 5 hours at 37ºC with agitation. In this step was taken a sample of the initial input (T_0). The beads were washed and denatured with SDS sample buffer diluted 6x in PBS buffer (Eluted). Input and eluted samples were loaded into a 12.5% polyacrylamide gel. **(A)** SDS-PAGE stained with Coomassie blue of the Input and eluted samples of wildtype and mutant APRc fractions. **(B)** Western Blot analysis with the input and eluted fractions without and **(C)** with hIgG probed with anti-C4BPα. Black arrows highlight the regions where is visible decreasing intensity of the protein band present in eluted fractions of APRc-WT.

Total protein fractions of APRc-C4BP incubation assays were assessed by Coomassie staining and Western blot analysis. Contrary to previous results, it is not visible a decrease of the α-chain in the APRc-WT without IgG, however in the presence of IgG there is the appearance of band below 75 kDa **(Figure 29A)**. Somewhat surprisingly, the observed protein band in the Coomassie-stained gel is not obvious in the Western blot **(Figure 29B)**. Further studies are, therefore, required to evaluate if C4BP is indeed an APRc substrate.

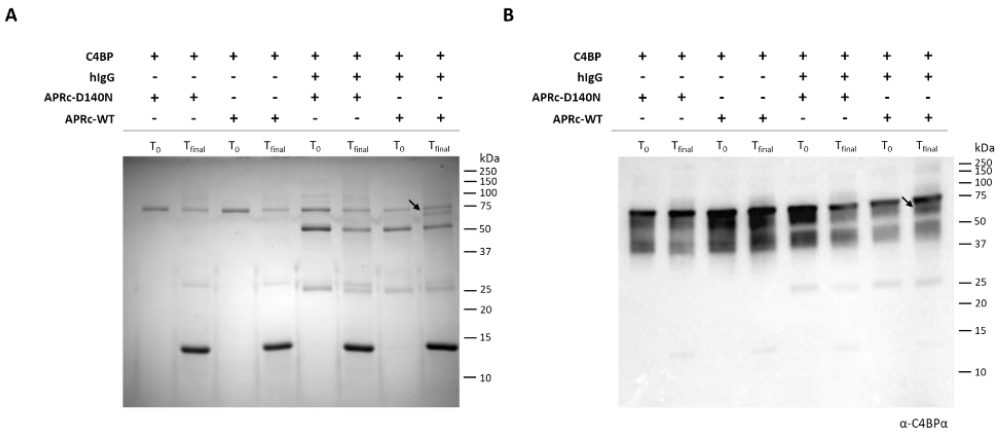

Figure 29: APRc cleavage of C4BP was evaluated by incubation assays with purified C4BP. Incubation assays using HisMag Sepharose Nickel beads were independently performed with the dimeric soluble form of APRc wildtype (APRc-WT) and the corresponding active site mutant (APRc-D140N). After binding, the beads were incubated with 7 µg of C4BP purified protein with or without 7 µg human IgG (hIgG) diluted in phosphate-buffered saline (PBS) for 5 hours at 37ºC with agitation. In this step a sample of the initial input (T_0) was taken. The beads were washed and denatured with SDS sample buffer diluted 6x in PBS buffer (T_{Final}). Input and eluted samples were loaded into a 12.5% polyacrylamide gel. **(A)** SDS-PAGE stained with Coomassie blue of the Input and eluted samples of wildtype and mutant APRc fractions. **(B)** Western Blot analysis with anti-C4BPα. Black arrows highlight the appearance of a new band in the eluted fraction APRc-WT with hIgG.

3.5.4 Assessing the formation of protein complexes between C3 and C4 proteins and bacteria

C3 and C4 proteins present a reactive thioester group which, when activated, is responsible for the covalent binding to a target molecule at the surface of bacteria and further recognition by the complement system. To start evaluating potential C3 and C4 target complexes in *R. massiliae* and *E. coli* expressing the empty vector, full-length

APRc, and the corresponding catalytic dead mutant, bacteria were independently incubated with HBSS or 40% NHS for 1h at 37ºC. After washing twice, bacterial extracts were denatured, and results were obtained by performing SDS-PAGE and Western Blot analysis, using polyclonal anti-C3 and polyclonal anti-C4 antibodies. Coomassie stained gels were performed to assess protein load. As observed in **Figure 30A**, the protein profile is different in *E. coli* expressing APRc incubated with NHS when compared to the empty vector, especially the wild-type form (where less protein is observed). These results were somewhat surprising as previous results have shown that *E. coli* expressing APRc are more resistant to the bactericidal effects of serum (Curto et al., 2021). Interestingly, no obvious difference is visible between *Rickettsia* extracts incubated with buffer and NHS **(Figure 30A)**. *Rickettsia* and *E. coli* APRc display a similar protein profile for C3 protein, presenting mainly one band with 75 kDa, a protein band between 50 and 37 kDa, and a smear for high-molecular weights (above 75 kDa), more obvious in *E. coli* and *E. coli* APRc_D140N. Accounting for the molecular weight of the C3b α'-chain (101 kDa), the expected complexes should be higher than 101 kDa (**Figure S3)**. Interestingly, these were not the predominant bands observed **(Figure 30B)**. Although we cannot exclude some anomalous migration in the gel, the observed bands at 75 kDa may likely correspond to iC3b α' 1 chain (68 kDa), which results from cleavage of C3b by factor H (cofactor) and factor I, complexed to a smaller target protein, and the second predominant band may correspond to the degradation product C3dg (39 kDa). These results anticipate a fast deposition and breakdown of C3 at the surface of bacteria, with apparent breakdown to C3dg occurring faster in *E. coli* expressing APRc. It is also quite interesting that this is the predominant profile in *R. massiliae* extracts. However, a time course analysis is required to better understand C3 deposition and complex formation.

Regarding C4*, R. massiliae* treated with NHS display a smear with several bands between 250 and 75 kDa **(Figure 30C)**. This result anticipates C4-target complexes at the surface of *Rickettsia*, as considering the molecular weight of C4b α-chain (86 kDa) protein complexes are expected to be higher than 86 kDa. The protein profile is different for *E. coli* and *E. coli* expressing APRc, with two predominant bands between 100 and 75 kDa (more intense in APRc-expressing cells). This may correspond to the C4b α-chain complexed to a smaller protein or, alternatively, to a C4d (45 kDa)-target complex. Given

the higher intensity of these bands in APRc-expressing *E. coli* and the molecular weight of APRc (~25 kDa), we next sought to evaluate if a C4d-APRc complex could account for these bands. The results obtained **(Figure 30D)** do not support this hypothesis. Although we observe a reduction in the intensity of APRc upon NHS incubation, there are no visible bands at higher molecular weight consistent with complex formation. These results need to be repeated to further understand the nature of these bands and their implication for complement activation.

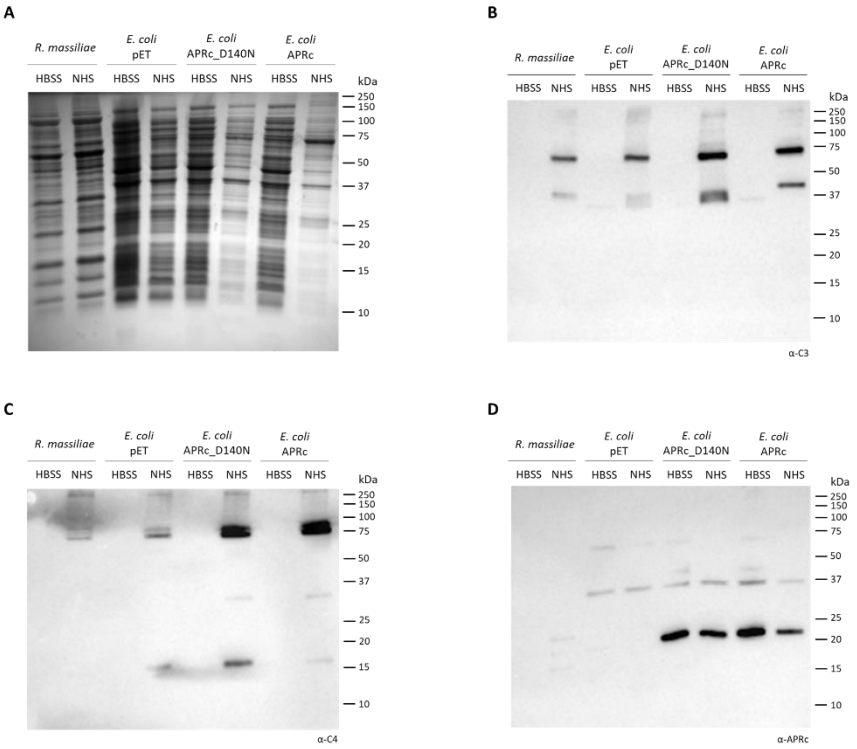

Figure 30: C3 and C4 binding and formation of target complexes at the surface of bacteria was assessed. *R. massiliae* and BL21 Star (DE3) *E. coli* strain encoding the empty vector backbone pET28a (pET), mutant form of APRc (APRc_D140N) and wild-type APRc (APRc) were incubated with 40% NHS for 1h at 37ºC, washed twice and resuspended in HBSS. Bacteria incubated with HBSS was used a negative control. **(A)** SDS-PAGE followed by Coomassie blue staining of the total bacterial extracts incubated with HBSS and serum. **(B)** Samples were analysed by Western Blotting and probed with polyclonal anti-C3, **(C)** polyclonal anti-C4, **(D)** or anti-APRc.

3.5.5 APRc impact in complement system activity

With the previous experiments we have shown that APRc binds and potentially cleaves complement proteins C3, C4, and C4BP. However, it has not been explored the physiological impact of these interactions. To do so, the activation of the classical, MBL and alternative pathways of the complement system were evaluated with a WIESLAB kit, as described by the manufacturer. This kit is generally used to assess complement deficiencies in human sera and to determine the functional classical, MBL and alternative complement pathways. NHS Pel-Freez was incubated with APRc-D140N or APRc-WT for 1h 37^{o}C prior its incubation with the coated 96-well plate. The wells are coated with specific activators of each complement pathway, and the production of C5b-9 is measured, being proportional to the complement activity. A condition with only NHS was used to evaluate the baseline complement activation. Although it is important to note that these preliminary experiments were performed in duplicates only, it is visible an impact on the activation of all pathways. In both classical and alternative pathways, the condition preincubated with wild type APRc presents lower absorbance than the mutant form, suggesting that the catalytic activity is important for the inactivation of these pathways **(Figure 31A,C)**. Interestingly, in the MBL pathway there is a marked decrease of complement activation, but there are no differences between the two forms of APRc **(Figure 31B),** suggesting that this effect is independent of APRc's proteolytic activity. Representing the values as percentage of complement activation (NHS condition with 100% of complement activation), there is a marked inhibition of activation of the complement system for all pathways. In the classical pathway there is a decrease to 87% and 58% activation in the APRc-D140N and APRc-WT conditions, respectively. In the MBL pathway both forms of APRc present the same level of activation (37%). Finally, in the alternative pathway there is a decrease to 50% for the mutant form and 16% for the wild-type form **(Figure 31D)**. These results are very exciting since we used one hour of preincubation between the serum and the protease, resulting in a large reduction of complement activation.

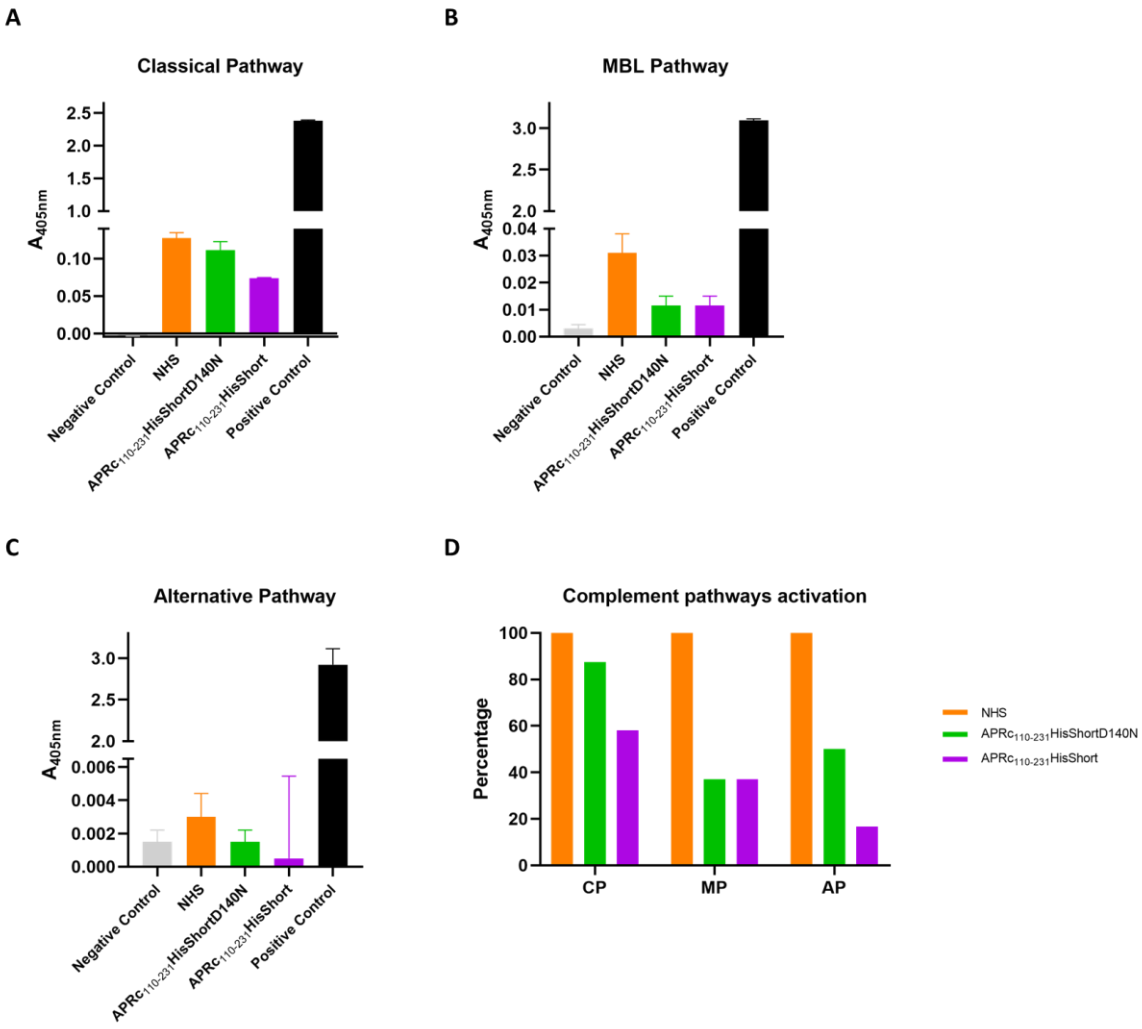

Figure 31: APRc effect in the activation of the complement system was determined by ELISA. Previously incubated NHS with the soluble catalytic aspartate mutant ($APRc_{110-231}$HisShortD140N) and the soluble wild-type APRc ($APRc_{110-231}$HisShort) was incubated in a 96-well plate coated with **(A)** human IgM (classical pathway), **(B)** mannan (MBL pathway) and **(C)** LPS (alternative pathway). A condition with only NHS was used as a control. The wells were incubated with C5b-9 antibodies and the signal was detected by using substrate solution at 405 nm. Results are represented in mean ± standard deviation from duplicates. **(D)** Representation of APRc impact in the complement pathways activation. Results are expressed in percentage. 100% corresponds to the NHS condition activation.

Chapter IV – Discussion and Future Perspectives

Moonlight proteins exert two or more functions, and are involved in many steps of infection, being considered good targets to develop new therapies and vaccines to treat bacterial diseases. *Rickettsia* is a genus of obligate intracellular bacteria transmitted through arthropod vectors, causing mild to life-threatening diseases. Currently, there is an increased concern about rickettsioses and their impact on global health because of the emerging and re-emerging of pathogens, increasing geographical distribution of its vectors, and the exponential increase of antibiotic resistance (El-Sayed & Kamel, 2020; Parola et al., 2008). Therefore, identifying and characterizing new targets is crucial to treat rickettsioses. One potential target is APRc, a highly conserved membrane-embedded retropepsin-like homologue. APRc modulates *Rickettsia* surface virulence factors Sca5/OmpB and Sca0/OmpA, binds non-immune immunoglobulins from the serum and mediates immune evasion, suggesting its moonlight activity (R. Cruz et al., 2014; Curto et al., 2021). Furthermore, preliminary data suggested that APRc presents substrates in human serum, with the complement proteins C3 and C4 emerging as putative substrates. Since moonlight proteins may be important in virulence and represent good targets to develop new therapies, it is important to acknowledge APRc moonlight activity. Therefore, additional studies to analyse APRc moonlighting by identifying and characterizing APRc substrates as well as its protein-protein interactions are crucial.

In this study we demonstrated that APRc interacts with different IgG isoforms and antibody light chains. APRc binds to IgG1, IgG2, and IgG3 in a concentration-dependent manner, presenting stronger interaction with IgG1 and IgG3. The selective binding to different IgG isoforms is observed in other bacterial proteins including the SpA virulence factor from *S. aureus* that binds IgG1, IgG2 and IgG4 and Hsp60 from *H. pylori* that binds IgG1 and IgG3 (Amini et al., 1996; A. R. Cruz et al., 2021). APRc also binds to IgG1 presenting either κ or γ light chains, binding preferentially to the IgG1 with κ light chains. Moreover, this aspartic protease can bind to the κ light chains, forming APRc- κ light chain complexes. This interaction is slightly lower than with the IgG1 with κ light chains, suggesting that APRc can bind to other antibody regions. This is in concordance with the differences observed in the binding to the different IgG isoforms

since they differ in the hinge region and a part of the heavy chain (Vidarsson et al., 2014). Future studies are necessary to assess the antibody portions that APRc interacts within the Fab region.

Complement proteins C3, C4, and C4BP bind to the rickettsial surface and *E. coli* expressing APRc. The binding of these complement proteins seems to be dependent of the presence of Ig, with the exception of C3 that binds more to *R. massiliae* upon depletion of IgG and IgM. When the deposition was addressed in the *E. coli* surrogate expressing APRc, it was observed C3, C4, and C4BP deposition (very residual for C4 and C4BP) only in serum depleted in IgG and IgM. This interaction seems greater in C3 in the presence of APRc-WT than the mutant APRc, suggesting that the catalytic activity increases the deposition. Curiously, all complement proteins present greater deposition in *E. coli* expressing the empty vector than in *E. coli* expressing the aspartic protease. It has been described that *E. coli* can bind to C4BP, not being unexpected the occurrence of surface deposition (Tseng et al., 2012). However, it was anticipated that APRc interaction with these complement proteins would be greater than the control. We hypothesize that this decrease may be due to a specificity for APRc or to the competition with other human serum components such as IgG. Furthermore, C4BP deposition in the depletion of IgG and IgM may be compromised since its protein levels are much lower than in the other used sera. In any case, additional studies are required to support surface binding of these complement proteins at the surface of bacteria.

Many bacterial proteins aid in the evasion of the immune system by binding and cleaving components of the complement pathways. SplB protease from *S. aureus* cleaves several complement proteins including C3, C4, and components of the MAC complex and *Neisseria meningitidis* NalP protease cleaves C3 α-chain. Additionally, SdrE and Bbp surface proteins of *S. aureus* bind to C4BP, resulting in immune evasion. APRc binding of C3, C4, and C4BP was observed in different experiments using isolated proteins and human serum. APRc binds to these complement proteins in a concentration-dependent manner. Although not exuberant, the wild-type form of this protease originates proteolytic products of C3α, and some residual products of C4α and C4BPα but not of C3β in the serum (except in UCS). In the ELISA assays the IgG presence does not change APRc binding to the complement proteins, however in the pull-down

and incubation assays IgG presence slightly increased binding to C4. The binding and cleavage of C3, C4 and C4BP is not as exacerbated when using the purified proteins, comparing to the human serum, suggesting that there is at least one lacking component from the serum that is important for APRc interaction and cleavage of these proteins. We also validated the formation of C3 and C4 complexes at the surface of *Rickettsia* and *E. coli* expressing APRc, which for C3 anticipates a fast turnover of C3b α' chain. A deeper understanding of the molecules that are targets for C3 and C4 deposition at the surface of *Rickettsia* and the implications of modulating their binding for complement activation (or not) will be critical to enhance our understanding of the complement evasion mechanisms in *Rickettsia*. Moreover, additional experiments should be performed to clarify which regions are interacting with APRc, identify their cleavage sites and unveil serum proteins that might impact APRc-binding. The role of IgG in these interactions should also be further evaluated using different concentrations of hIgG in ELISA assays.

Since APRc binds C3, C4, and C4BP it might impact production of complement products and consequently complement system activation. APRc does not change the levels of the anaphylatoxin C3a. However, we have demonstrated that APRc impacts the activation of the three complement pathways. The decreased activation is greater in the incubation with the wild-type form in both classical and alternative pathways, suggesting that the catalytic activity promotes the inactivation of these pathways. Interestingly, in the MBL pathway there are no differences between the two forms of APRc, suggesting that the marked inhibition observed is independent of the catalytic activity of APRc, and anticipating a different mechanism of action. The previously mentioned proteins from *S. aureus* and *Neisseria meningitidis* impair C5b-9 deposition (in the case of SplB protease) and C3 deposition on bacterial surface, inhibiting the final step of the complement pathways and diminishing opsonophagocytosis. Besides impacting the complement system, APRc might also impair pathogen recognition and aid in opsonophagocytosis evasion. Further studies are needed to evaluate if APRc presents these roles, by assessing the role of this protease in bacterial opsonophagocytosis *in vitro*.

With this work, we further characterized APRc interaction with IgG, unveiled human serum substrates of this protease and demonstrated that APRc inhibits the

complement system. Taken together, these results support APRc protease as an immune evasion factor from *Rickettsia* and a moonlight protein, raising exciting questions on the mechanism(s) by which this unique protease exerts its multiple functions, and further reinforcing its potential as a target to develop new therapeutic tools against rickettsioses.

Chapter V – Bibliography

Akram, S. M., Ladd, M., & King, K. C. (2021). Rickettsia Prowazekii. In *StatPearls*. StatPearls Publishing. http://www.ncbi.nlm.nih.gov/books/NBK448173/

Álvarez-Hernández, G., Roldán, J. F. G., Milan, N. S. H., Lash, R. R., Behravesh, C. B., & Paddock, C. D. (2017). Rocky Mountain spotted fever in Mexico: Past, present, and future. *The Lancet. Infectious Diseases*, *17*(6), e189–e196. https://doi.org/10.1016/S1473-3099(17)30173-1

Amblee, V., & Jeffery, C. J. (2015). Physical Features of Intracellular Proteins that Moonlight on the Cell Surface. *PloS One*, *10*(6), e0130575. https://doi.org/10.1371/journal.pone.0130575

Amdahl, H., Jongerius, I., Pasanen, T., Lehtinen, M., Van Strijp, J., Rooijakkers, S., & Jokiranta, T. S. (2010). The Secreted Ecb and Efb Proteins of Staphylococcus aureus Enhance Binding of Factor H to C3b and C3d. *Molecular Immunology - MOL IMMUNOL*, *47*, 2250–2250. https://doi.org/10.1016/j.molimm.2010.05.159

Amini, H.-R., Ascencio, F., Cruz, A., Ruiz-Bustos, E., & Wadström, T. (1996). Immunochemical properties of a 60 kDa cell surface-associated heat shock-protein (Hsp60) from Helicobacter pylori. *FEMS Immunology & Medical Microbiology*, *16*, 163–172. https://doi.org/10.1111/j.1574-695X.1996.tb00133.x

Andersson, S. G. E., Zomorodipour, A., Andersson, J. O., Sicheritz-Pontén, T., Alsmark, U. C. M., Podowski, R. M., Näslund, A. K., Eriksson, A.-S., Winkler, H. H., & Kurland, C. G. (1998). The genome sequence of Rickettsia prowazekii and the origin of mitochondria. *Nature*, *396*(6707), 133–140. https://doi.org/10.1038/24094

Barro, A. M. S. (2021). *Characterization of APRc as an immune evasion factor of Rickettsia*.

Beckmann, C., Waggoner, J. D., Harris, T. O., Tamura, G. S., & Rubens, C. E. (2002). Identification of novel adhesins from Group B streptococci by use of phage

display reveals that C5a peptidase mediates fibronectin binding. *Infection and Immunity*, *70*(6), 2869–2876. https://doi.org/10.1128/IAI.70.6.2869-2876.2002

Binder, A. M., & Armstrong, P. A. (2019). Increase in Reports of Tick-Borne Rickettsial Diseases in the United States. *The American Journal of Nursing*, *119*(7), 20–21. https://doi.org/10.1097/01.NAJ.0000569428.81917.6c

Bourdonnay, E., & Henry, T. (2016). Catch me if you can. *ELife*, *5*, e14721. https://doi.org/10.7554/eLife.14721

Brown, L. D., & Macaluso, K. R. (2016). Rickettsia felis, an Emerging Flea-Borne Rickettsiosis. *Current Tropical Medicine Reports*, *3*, 27–39. https://doi.org/10.1007/s40475-016-0070-6

Buczek, W., Koman-Iżko, A., Buczek, A. M., Buczek, A., Bartosik, K., Kulina, D., & Ciura, D. (2020). Spotted fever group rickettsiae transmitted by Dermacentor ticks and determinants of their spread in Europe. *Annals of Agricultural and Environmental Medicine*, *27*(4), 505–511. https://doi.org/10.26444/aaem/120602

Caravedo Martinez, M. A., Ramírez-Hernández, A., & Blanton, L. S. (2021). Manifestations and Management of Flea-Borne Rickettsioses. *Research and Reports in Tropical Medicine*, *12*, 1–14. https://doi.org/10.2147/RRTM.S274724

Cardwell, M. M., & Martinez, J. J. (2009). The Sca2 Autotransporter Protein from Rickettsia conorii Is Sufficient To Mediate Adherence to and Invasion of Cultured Mammalian Cells. *Infection and Immunity*, *77*(12), 5272–5280. https://doi.org/10.1128/IAI.00201-09

Carlsson, F., Berggård, K., Stålhammar-Carlemalm, M., & Lindahl, G. (2003). Evasion of Phagocytosis through Cooperation between Two Ligand-binding Regions in Streptococcus pyogenes M Protein. *The Journal of Experimental Medicine*, *198*(7), 1057–1068. https://doi.org/10.1084/jem.20030543

Chan, Y. G. Y., Cardwell, M. M., Hermanas, T. M., Uchiyama, T., & Martinez, J. J. (2009). Rickettsial Outer-Membrane Protein B (rOmpB) Mediates Bacterial Invasion through Ku70 in an Actin, c-Cbl, Clathrin and Caveolin 2-Dependent Manner. *Cellular Microbiology*, *11*(4), 629. https://doi.org/10.1111/j.1462-5822.2008.01279.x

Charles A Janeway, J., Travers, P., Walport, M., & Shlomchik, M. J. (2001). The structure of a typical antibody molecule. *Immunobiology: The Immune System in Health and Disease. 5th Edition*. https://www.ncbi.nlm.nih.gov/books/NBK27144/

Chen, C., Liu, H., Zabad, S., Rivera, N., Rowin, E., Hassan, M., Gomez De Jesus, S. M., Llinás Santos, P. S., Kravchenko, K., Mikhova, M., Ketterer, S., Shen, A., Shen, S., Navas, E., Horan, B., Raudsepp, J., & Jeffery, C. (2021). MoonProt 3.0: An update of the moonlighting proteins database. *Nucleic Acids Research*, *49*(D1), D368–D372. https://doi.org/10.1093/nar/gkaa1101

Cruz, A., Bentlage, A., Blonk, R., Haas, C. J. C., Aerts, P. c, Scheepmaker, L., Bouwmeester, I., Lux, A., Van Strijp, J., Nimmerjahn, F., Kessel, K., Vidarsson, G., & Rooijakkers, S. (2022). *Staphylococcal protein A inhibits IgG-mediated phagocytosis by blocking the interaction of IgGs with FcγRs and FcRn*. https://doi.org/10.1101/2022.01.21.477287

Cruz, A. R., Boer, M. A. den, Strasser, J., Zwarthoff, S. A., Beurskens, F. J., Haas, C. J. C. de, Aerts, P. C., Wang, G., Jong, R. N. de, Bagnoli, F., Strijp, J. A. G. van, Kessel, K. P. M. van, Schuurman, J., Preiner, J., Heck, A. J. R., & Rooijakkers, S. H. M. (2021). Staphylococcal protein A inhibits complement activation by interfering with IgG hexamer formation. *Proceedings of the National Academy of Sciences*, *118*(7), Article 7. https://doi.org/10.1073/pnas.2016772118

Cruz, R., Huesgen, P., Riley, S. P., Wlodawer, A., Faro, C., Overall, C. M., Martinez, J. J., & Simões, I. (2014). RC1339/APRc from Rickettsia conorii is a novel aspartic

protease with properties of retropepsin-like enzymes. *PLoS Pathogens*, *10*(8), e1004324. https://doi.org/10.1371/journal.ppat.1004324

Culp, E., & Wright, G. D. (2017). Bacterial proteases, untapped antimicrobial drug targets. *The Journal of Antibiotics*, *70*(4), 366–377. https://doi.org/10.1038/ja.2016.138

Curto, P., Barro, A., Almeida, C., Vieira-Pires, R. S., & Simões, I. (2021). The Retropepsin-Type Protease APRc as a Novel Ig-Binding Protein and Moonlighting Immune Evasion Factor of Rickettsia. *MBio*, *12*(6), e03059-21. https://doi.org/10.1128/mBio.03059-21

Curto, P., Riley, S. P., Simões, I., & Martinez, J. J. (2019a). Macrophages Infected by a Pathogen and a Non-pathogen Spotted Fever Group Rickettsia Reveal Differential Reprogramming Signatures Early in Infection. *Frontiers in Cellular and Infection Microbiology*, *9*. https://doi.org/10.3389/fcimb.2019.00097

Curto, P., Riley, S. P., Simões, I., & Martinez, J. J. (2019b). Macrophages Infected by a Pathogen and a Non-pathogen Spotted Fever Group Rickettsia Reveal Differential Reprogramming Signatures Early in Infection. *Frontiers in Cellular and Infection Microbiology*, *9*, 97. https://doi.org/10.3389/fcimb.2019.00097

Curto, P., Santa, C., Allen, P., Manadas, B., Simões, I., & Martinez, J. J. (2019). A Pathogen and a Non-pathogen Spotted Fever Group Rickettsia Trigger Differential Proteome Signatures in Macrophages. *Frontiers in Cellular and Infection Microbiology*, *0*. https://doi.org/10.3389/fcimb.2019.00043

Curto, P., Simões, I., Riley, S. P., & Martinez, J. J. (2016). Differences in Intracellular Fate of Two Spotted Fever Group Rickettsia in Macrophage-Like Cells. *Frontiers in Cellular and Infection Microbiology*, *6*, 80. https://doi.org/10.3389/fcimb.2016.00080

Dallo, S. F., Kannan, T. R., Blaylock, M. W., & Baseman, J. B. (2002). Elongation factor Tu and E1 beta subunit of pyruvate dehydrogenase complex act as fibronectin

binding proteins in Mycoplasma pneumoniae. *Molecular Microbiology*, *46*(4), 1041–1051. https://doi.org/10.1046/j.1365-2958.2002.03207.x

Drancourt, M., & Raoult, D. (1999). Characterization of Mutations in therpoB Gene in Naturally Rifampin-ResistantRickettsia Species. *Antimicrobial Agents and Chemotherapy*, *43*(10), 2400–2403. https://doi.org/10.1128/AAC.43.10.2400

Drexler, N. A., Dahlgren, F. S., Heitman, K. N., Massung, R. F., Paddock, C. D., & Behravesh, C. B. (2016). National Surveillance of Spotted Fever Group Rickettsioses in the United States, 2008-2012. *The American Journal of Tropical Medicine and Hygiene*, *94*(1), 26–34. https://doi.org/10.4269/ajtmh.15-0472

Du Clos, T. W., & Mold, C. (2013). 20—Complement in host deficiencies and diseases. In R. R. Rich, T. A. Fleisher, W. T. Shearer, H. W. Schroeder, A. J. Frew, & C. M. Weyand (Eds.), *Clinical Immunology (Fourth Edition)* (pp. 252–269). Elsevier. https://doi.org/10.1016/B978-0-7234-3691-1.00041-6

Dumler, J. S. (2012). Clinical Disease: Current Treatment and New Challenges. In *Intracellular Pathogens II* (pp. 1–39). John Wiley & Sons, Ltd. https://doi.org/10.1128/9781555817336.ch1

Dunkelberger, J., & Song, W.-C. (2009). Complement and its role in innate and adaptive immune response. *Cell Research*, *20*, 34–50. https://doi.org/10.1038/cr.2009.139

Eisenreich, W., Rudel, T., Heesemann, J., & Goebel, W. (2019). How Viral and Intracellular Bacterial Pathogens Reprogram the Metabolism of Host Cells to Allow Their Intracellular Replication. *Frontiers in Cellular and Infection Microbiology*, *0*. https://doi.org/10.3389/fcimb.2019.00042

El-Sayed, A., & Kamel, M. (2020). Climatic changes and their role in emergence and re-emergence of diseases. *Environmental Science and Pollution Research International*, 1–17. https://doi.org/10.1007/s11356-020-08896-w

Emelyanov, V. V., & Demyanova, N. G. (1999). Nucleotide sequence of the gene and features of the major outer membrane protein of a virulent Rickettsia prowazekii strain. *Biochemistry. Biokhimiia*, *64*(5), 494–503.

Emelyanov, V. V., & Loukianov, E. V. (2004). A 29.5 kDa heat-modifiable major outer membrane protein of Rickettsia prowazekii, putative virulence factor, is a peptidyl-prolyl cis/trans isomerase. *IUBMB Life*, *56*(4), 215–219. https://doi.org/10.1080/15216540410001699321

Engström, P., Burke, T. P., Mitchell, G., Ingabire, N., Mark, K. G., Golovkine, G., Iavarone, A. T., Rape, M., Cox, J. S., & Welch, M. D. (2019). Evasion of autophagy mediated by Rickettsia surface protein OmpB is critical for virulence. *Nature Microbiology*, *4*(12), 2538–2551. https://doi.org/10.1038/s41564-019-0583-6

Ensgraber, M., & Loos, M. (1992). A 66-kilodalton heat shock protein of Salmonella typhimurium is responsible for binding of the bacterium to intestinal mucus. *Infection and Immunity*, *60*(8), 3072–3078. https://doi.org/10.1128/iai.60.8.3072-3078.1992

Ernst, C. M., Staubitz, P., Mishra, N. N., Yang, S.-J., Hornig, G., Kalbacher, H., Bayer, A. S., Kraus, D., & Peschel, A. (2009). The bacterial defensin resistance protein MprF consists of separable domains for lipid lysinylation and antimicrobial peptide repulsion. *PLoS Pathogens*, *5*(11), e1000660. https://doi.org/10.1371/journal.ppat.1000660

Espinosa-Cantú, A., Cruz-Bonilla, E., Noda-Garcia, L., & DeLuna, A. (2020). Multiple Forms of Multifunctional Proteins in Health and Disease. *Frontiers in Cell and Developmental Biology*, *8*, 451. https://doi.org/10.3389/fcell.2020.00451

European Centre for Disease Prevention and Control. (2013). *Epidemiological situation of rickettsioses in EU/EFTA countries. Stockholm: ECDC;*

Ferreira, V. P., & Cortes, C. (2022). The Complement System. In N. Rezaei (Ed.), *Encyclopedia of Infection and Immunity* (pp. 144–169). Elsevier. https://doi.org/10.1016/B978-0-12-818731-9.00056-2

Foster, T. J. (2005). Immune evasion by staphylococci. *Nature Reviews. Microbiology*, *3*(12), 948–958. https://doi.org/10.1038/nrmicro1289

Franco-Serrano, L., Hernández, S., Calvo, A., Severi, M. A., Ferragut, G., Pérez-Pons, J., Piñol, J., Pich, Ò., Mozo-Villarias, Á., Amela, I., Querol, E., & Cedano, J. (2018). MultitaskProtDB-II: An update of a database of multitasking/moonlighting proteins. *Nucleic Acids Research*, *46*(Database issue), D645–D648. https://doi.org/10.1093/nar/gkx1066

Frank, M. M., & Sullivan, K. E. (2014). Chapter 38—Deficiencies of the Complement System. In K. E. Sullivan & E. R. Stiehm (Eds.), *Stiehm's Immune Deficiencies* (pp. 731–763). Academic Press. https://doi.org/10.1016/B978-0-12-405546-9.00038-8

Garduño, R. A., Garduño, E., & Hoffman, P. S. (1998). Surface-associated hsp60 chaperonin of Legionella pneumophila mediates invasion in a HeLa cell model. *Infection and Immunity*, *66*(10), 4602–4610. https://doi.org/10.1128/IAI.66.10.4602-4610.1998

Garza, D. A., Riley, S. P., & Martinez, J. J. (2017). Expression of Rickettsia Adr2 protein in E. coli is sufficient to promote resistance to complement-mediated killing, but not adherence to mammalian cells. *PLOS ONE*, *12*(6), e0179544. https://doi.org/10.1371/journal.pone.0179544

Haglund, C. M., Choe, J. E., Skau, C. T., Kovar, D. R., & Welch, M. D. (2010). Rickettsia Sca2 is a bacterial formin-like mediator of actin-based motility. *Nature Cell Biology*, *12*(11), 1057–1063. https://doi.org/10.1038/ncb2109

Hair, P. S., Foley, C. K., Krishna, N. K., Nyalwidhe, J. O., Geoghegan, J. A., Foster, T. J., & Cunnion, K. M. (2013). Complement regulator C4BP binds to

Staphylococcus aureus surface proteins SdrE and Bbp inhibiting bacterial opsonization and killing. *Results in Immunology*, *3*, 114–121. https://doi.org/10.1016/j.rinim.2013.10.004

Hallström, T., Jarva, H., Riesbeck, K., & Blom, A. M. (2007). Interaction with C4b-Binding Protein Contributes to Nontypeable Haemophilus influenzae Serum Resistance. *The Journal of Immunology*, *178*(10), 6359–6366. https://doi.org/10.4049/jimmunol.178.10.6359

Heilmann, C., Hartleib, J., Hussain, M. S., & Peters, G. (2005). The multifunctional Staphylococcus aureus autolysin aaa mediates adherence to immobilized fibrinogen and fibronectin. *Infection and Immunity*, *73*(8), 4793–4802. https://doi.org/10.1128/IAI.73.8.4793-4802.2005

Heilmann, C., Thumm, G., Chhatwal, G. S., Hartleib, J., Uekötter, A., & Peters, G. (2003). Identification and characterization of a novel autolysin (Aae) with adhesive properties from Staphylococcus epidermidis. *Microbiology (Reading, England)*, *149*(Pt 10), 2769–2778. https://doi.org/10.1099/mic.0.26527-0

Heinrich, N., Dill, T., Dobler, G., Clowes, P., Kroidl, I., Starke, M., Ntinginya, N. E., Maboko, L., Löscher, T., Hoelscher, M., & Saathoff, E. (2015). High Seroprevalence for Spotted Fever Group Rickettsiae, Is Associated with Higher Temperatures and Rural Environment in Mbeya Region, Southwestern Tanzania. *PLOS Neglected Tropical Diseases*, *9*(4), e0003626. https://doi.org/10.1371/journal.pntd.0003626

Henderson, B., & Martin, A. (2011). Bacterial virulence in the moonlight: Multitasking bacterial moonlighting proteins are virulence determinants in infectious disease. *Infection and Immunity*, *79*(9), 3476–3491. https://doi.org/10.1128/IAI.00179-11

Hernández, S., Franco, L., Calvo, A., Ferragut, G., Hermoso, A., Amela, I., Gómez, A., Querol, E., & Cedano, J. (2015). Bioinformatics and Moonlighting Proteins.

Frontiers in Bioengineering and Biotechnology, *3*, 90. https://doi.org/10.3389/fbioe.2015.00090

Hovingh, E. S., van den Broek, B., & Jongerius, I. (2016). Hijacking Complement Regulatory Proteins for Bacterial Immune Evasion. *Frontiers in Microbiology*, *0*. https://doi.org/10.3389/fmicb.2016.02004

Huberts, D. H. E. W., & van der Klei, I. J. (2010). Moonlighting proteins: An intriguing mode of multitasking. *Biochimica et Biophysica Acta (BBA) - Molecular Cell Research*, *1803*(4), 520–525. https://doi.org/10.1016/j.bbamcr.2010.01.022

Jagadeesan, B., Koo, O. K., Kim, K.-P., Burkholder, K. M., Mishra, K. K., Aroonnual, A., & Bhunia, A. K. (2010). LAP, an alcohol acetaldehyde dehydrogenase enzyme in Listeria, promotes bacterial adhesion to enterocyte-like Caco-2 cells only in pathogenic species. *Microbiology (Reading, England)*, *156*(Pt 9), 2782–2795. https://doi.org/10.1099/mic.0.036509-0

Jakob, R. P., Koch, J. R., Burmann, B. M., Schmidpeter, P. A. M., Hunkeler, M., Hiller, S., Schmid, F. X., & Maier, T. (2015). Dimeric Structure of the Bacterial Extracellular Foldase PrsA*. *Journal of Biological Chemistry*, *290*(6), 3278–3292. https://doi.org/10.1074/jbc.M114.622910

Jeffery, C. (2018). Intracellular proteins moonlighting as bacterial adhesion factors. *AIMS Microbiology*, *4*(2), 362–376. https://doi.org/10.3934/microbiol.2018.2.362

Jeffery, C. J. (1999). Moonlighting proteins. *Trends in Biochemical Sciences*, *24*(1), 8–11. https://doi.org/10.1016/s0968-0004(98)01335-8

Jeffery, C. J. (2015). Why study moonlighting proteins? *Frontiers in Genetics*, *6*. https://doi.org/10.3389/fgene.2015.00211

Jeffery, C. J. (2018). Protein moonlighting: What is it, and why is it important? *Philosophical Transactions of the Royal Society B: Biological Sciences*, *373*(1738), 20160523. https://doi.org/10.1098/rstb.2016.0523

Jenkins, H. T., Mark, L., Ball, G., Persson, J., Lindahl, G., Uhrin, D., Blom, A. M., & Barlow, P. N. (2006). Human C4b-binding Protein, Structural Basis for Interaction with Streptococcal M Protein, a Major Bacterial Virulence Factor*. *Journal of Biological Chemistry*, *281*(6), 3690–3697. https://doi.org/10.1074/jbc.M511563200

Johnsson, E., Thern, A., Dahlbäck, B., Hedén, L. O., Wikström, M., & Lindahl, G. (1996). A highly variable region in members of the streptococcal M protein family binds the human complement regulator C4BP. *The Journal of Immunology*, *157*(7), 3021–3029.

Jongerius, I., Köhl, J., Pandey, M. K., Ruyken, M., van Kessel, K. P. M., van Strijp, J. A. G., & Rooijakkers, S. H. M. (2007). Staphylococcal complement evasion by various convertase-blocking molecules. *The Journal of Experimental Medicine*, *204*(10), 2461–2471. https://doi.org/10.1084/jem.20070818

Kainulainen, V., & Korhonen, T. K. (2014). Dancing to Another Tune—Adhesive Moonlighting Proteins in Bacteria. *Biology*, *3*(1), 178–204. https://doi.org/10.3390/biology3010178

Khan, I. K., Bhuiyan, M., & Kihara, D. (2017). DextMP: Deep dive into text for predicting moonlighting proteins. *Bioinformatics*, *33*(14), i83–i91. https://doi.org/10.1093/bioinformatics/btx231

Kinhikar, A. G., Vargas, D., Li, H., Mahaffey, S. B., Hinds, L., Belisle, J. T., & Laal, S. (2006). Mycobacterium tuberculosis malate synthase is a laminin-binding adhesin. *Molecular Microbiology*, *60*(4), 999–1013. https://doi.org/10.1111/j.1365-2958.2006.05151.x

Köseoğlu, V. K., & Agaisse, H. (2019). Evolutionary Perspectives on the Moonlighting Functions of Bacterial Factors That Support Actin-Based Motility. *MBio*, *10*(4), e01520-19. https://doi.org/10.1128/mBio.01520-19

Kunert, A., Losse, J., Gruszin, C., Hühn, M., Kaendler, K., Mikkat, S., Volke, D., Hoffmann, R., Jokiranta, T. S., Seeberger, H., Moellmann, U., Hellwage, J., & Zipfel, P. F. (2007). Immune evasion of the human pathogen Pseudomonas aeruginosa: Elongation factor Tuf is a factor H and plasminogen binding protein. *Journal of Immunology (Baltimore, Md.: 1950)*, *179*(5), 2979–2988. https://doi.org/10.4049/jimmunol.179.5.2979

Lebrun, I., Marques-Porto, R., Pereira, A. S., Pereira, A., & Perpetuo, E. A. (2009). Bacterial toxins: An overview on bacterial proteases and their action as virulence factors. *Mini Reviews in Medicinal Chemistry*, *9*(7), 820–828. https://doi.org/10.2174/138955709788452603

Leon-Sicairos, N., Reyes-Cortes, R., Guadrón-Llanos, A. M., Madueña-Molina, J., Leon-Sicairos, C., & Canizalez-Román, A. (2015). Strategies of Intracellular Pathogens for Obtaining Iron from the Environment. *BioMed Research International*, *2015*, e476534. https://doi.org/10.1155/2015/476534

Li, M., Gustchina, A., Cruz, R., Simões, M., Curto, P., Martinez, J., Faro, C., Simões, I., & Wlodawer, A. (2015). Structure of RC1339/APRc from Rickettsia conorii, a retropepsin-like aspartic protease. *Acta Crystallographica. Section D, Biological Crystallography*, *71*(Pt 10), 2109–2118. https://doi.org/10.1107/S1399004715013905

Liu, H., & Jeffery, C. J. (2020). Moonlighting Proteins in the Fuzzy Logic of Cellular Metabolism. *Molecules*, *25*(15), 3440. https://doi.org/10.3390/molecules25153440

Madasu, Y., Suarez, C., Kast, D. J., Kovar, D. R., & Dominguez, R. (2013). Rickettsia Sca2 has evolved formin-like activity through a different molecular mechanism. *Proceedings of the National Academy of Sciences*, *110*(29), E2677–E2686. https://doi.org/10.1073/pnas.1307235110

Mak, T. W., & Saunders, M. E. (2006). 22—Immunity to Pathogens. In T. W. Mak & M. E. Saunders (Eds.), *The Immune Response* (pp. 641–694). Academic Press. https://doi.org/10.1016/B978-012088451-3.50024-7

Mak, T. W., Saunders, M. E., & Jett, B. D. (Eds.). (2014). Chapter 3—Innate Immunity. In *Primer to the Immune Response (Second Edition)* (pp. 55–83). Academic Cell. https://doi.org/10.1016/B978-0-12-385245-8.00003-0

Maldonado, R. F., Sá-Correia, I., & Valvano, M. A. (2016). Lipopolysaccharide modification in Gram-negative bacteria during chronic infection. *FEMS Microbiology Reviews*, *40*(4), 480–493. https://doi.org/10.1093/femsre/fuw007

Marshall, N. C., Finlay, B. B., & Overall, C. M. (2017). Sharpening Host Defenses during Infection: Proteases Cut to the Chase. *Molecular & Cellular Proteomics : MCP*, *16*(4 Suppl 1), S161–S171. https://doi.org/10.1074/mcp.O116.066456

Matsuura, M. (2013). Structural Modifications of Bacterial Lipopolysaccharide that Facilitate Gram-Negative Bacteria Evasion of Host Innate Immunity. *Frontiers in Immunology*, *0*. https://doi.org/10.3389/fimmu.2013.00109

McLeod, M. P., Qin, X., Karpathy, S. E., Gioia, J., Highlander, S. K., Fox, G. E., McNeill, T. Z., Jiang, H., Muzny, D., Jacob, L. S., Hawes, A. C., Sodergren, E., Gill, R., Hume, J., Morgan, M., Fan, G., Amin, A. G., Gibbs, R. A., Hong, C., … Weinstock, G. M. (2004). Complete Genome Sequence of Rickettsia typhi and Comparison with Sequences of Other Rickettsiae. *Journal of Bacteriology*, *186*(17), 5842–5855. https://doi.org/10.1128/JB.186.17.5842-5855.2004

Meri, T., Blom, A. M., Hartmann, A., Lenk, D., Meri, S., & Zipfel, P. F. (2004). The Hyphal and Yeast Forms of Candida albicans Bind the Complement Regulator C4b-Binding Protein. *Infection and Immunity*, *72*(11), 6633–6641. https://doi.org/10.1128/IAI.72.11.6633-6641.2004

Merle, N. S., Noe, R., Halbwachs-Mecarelli, L., Fremeaux-Bacchi, V., & Roumenina, L. T. (2015). Complement System Part II: Role in Immunity. *Frontiers in Immunology*, *6*. https://doi.org/10.3389/fimmu.2015.00257

Milohanic, E., Pron, B., The European Listeria Genome Consortium, null, Berche, P., & Gaillard, J.-L. (2000). Identification of new loci involved in adhesion of Listeria monocytogenes to eukaryotic cells. European Listeria Genome Consortium. *Microbiology (Reading, England)*, *146 (Pt 3)*, 731–739. https://doi.org/10.1099/00221287-146-3-731

Pancholi, V., & Fischetti, V. A. (1992). A major surface protein on group A streptococci is a glyceraldehyde-3-phosphate-dehydrogenase with multiple binding activity. *The Journal of Experimental Medicine*, *176*(2), 415–426. https://doi.org/10.1084/jem.176.2.415

Parola, P., Paddock, C. D., Socolovschi, C., Labruna, M. B., Mediannikov, O., Kernif, T., Abdad, M. Y., Stenos, J., Bitam, I., Fournier, P.-E., & Raoult, D. (2013). Update on tick-borne rickettsioses around the world: A geographic approach. *Clinical Microbiology Reviews*, *26*(4), 657–702. https://doi.org/10.1128/CMR.00032-13

Parola, P., Socolovschi, C., Jeanjean, L., Bitam, I., Fournier, P.-E., Sotto, A., Labauge, P., & Raoult, D. (2008). Warmer Weather Linked to Tick Attack and Emergence of Severe Rickettsioses. *PLoS Neglected Tropical Diseases*, *2*(11), e338. https://doi.org/10.1371/journal.pntd.0000338

Pausa, M., Pellis, V., Cinco, M., Giulianini, P. G., Presani, G., Perticarari, S., Murgia, R., & Tedesco, F. (2003). Serum-resistant strains of Borrelia burgdorferi evade complement-mediated killing by expressing a CD59-like complement inhibitory molecule. *Journal of Immunology (Baltimore, Md.: 1950)*, *170*(6), 3214–3222. https://doi.org/10.4049/jimmunol.170.6.3214

Pleass, R. J., Areschoug, T., Lindahl, G., & Woof, J. M. (2001). Streptococcal IgA-binding proteins bind in the Calpha 2-Calpha 3 interdomain region and inhibit binding of IgA to human CD89. *The Journal of Biological Chemistry*, *276*(11), 8197–8204. https://doi.org/10.1074/jbc.M009396200

Pollack, S., Eisenstein, I., Mory, A., Paperna, T., Ofir, A., Baris, H., Weiss, K., Veszeli, N., Csuka, D., Shemer, R., Glaser, F., Prohászka, Z., & Magen, D. (2021). A Novel Homozygous In-Frame Deletion in Complement Factor 3 Underlies Early-Onset Autosomal Recessive Atypical Hemolytic Uremic Syndrome—Case Report. *Frontiers in Immunology*, *12*, 608604. https://doi.org/10.3389/fimmu.2021.608604

Ram, S., Cullinane, M., Blom, A. M., Gulati, S., McQuillen, D. P., Monks, B. G., O'Connell, C., Boden, R., Elkins, C., Pangburn, M. K., Dahlbäck, B., & Rice, P. A. (2001). Binding of C4b-binding protein to porin: A molecular mechanism of serum resistance of Neisseria gonorrhoeae. *The Journal of Experimental Medicine*, *193*(3), 281–295. https://doi.org/10.1084/jem.193.3.281

Raoult, D. (2015). 187—Introduction to Rickettsioses, Ehrlichioses, and Anaplasmosis. In J. E. Bennett, R. Dolin, & M. J. Blaser (Eds.), *Mandell, Douglas, and Bennett's Principles and Practice of Infectious Diseases (Eighth Edition)* (pp. 2194–2197). W.B. Saunders. https://doi.org/10.1016/B978-1-4557-4801-3.00187-9

Reddick, L. E., & Alto, N. M. (2014). Bacteria Fighting Back – How Pathogens Target and Subvert the Host Innate Immune System. *Molecular Cell*, *54*(2), 321–328. https://doi.org/10.1016/j.molcel.2014.03.010

Ribeiro, D. M., Briere, G., Bely, B., Spinelli, L., & Brun, C. (2019). MoonDB 2.0: An updated database of extreme multifunctional and moonlighting proteins. *Nucleic Acids Research*, *47*(D1), D398–D402. https://doi.org/10.1093/nar/gky1039

Riley, S., Patterson, J., & Martinez, J. (2012). The rickettsial OmpB β-peptide of Rickettsia conorii is sufficient to facilitate factor H-mediated serum resistance. *Infection and Immunity*, *80*(8). https://doi.org/10.1128/IAI.00349-12

Rogers, L. D., & Overall, C. M. (2013). Proteolytic post-translational modification of proteins: Proteomic tools and methodology. *Molecular & Cellular Proteomics: MCP*, *12*(12), 3532–3542. https://doi.org/10.1074/mcp.M113.031310

Rolain, J. M., Maurin, M., Vestris, G., & Raoult, D. (1998). In Vitro Susceptibilities of 27 Rickettsiae to 13 Antimicrobials. *Antimicrobial Agents and Chemotherapy*, *42*(7), 1537–1541.

Rosbjerg, A., Genster, N., Pilely, K., & Garred, P. (2017). Evasion Mechanisms Used by Pathogens to Escape the Lectin Complement Pathway. *Frontiers in Microbiology*, *0*. https://doi.org/10.3389/fmicb.2017.00868

Rovery, C., & Raoult, D. (2008). Mediterranean Spotted Fever. *Infectious Disease Clinics of North America*, *22*(3), 515–530. https://doi.org/10.1016/j.idc.2008.03.003

Sahni, A., Fang, R., Sahni, S. K., & Walker, D. H. (2019). Pathogenesis of Rickettsial Diseases: Pathogenic and Immune Mechanisms of an Endotheliotropic Infection. *Annual Review of Pathology: Mechanisms of Disease*, *14*(1), 127–152. https://doi.org/10.1146/annurev-pathmechdis-012418-012800

Schartz, N. D., & Tenner, A. J. (2020). The good, the bad, and the opportunities of the complement system in neurodegenerative disease. *Journal of Neuroinflammation*, *17*(1), 354. https://doi.org/10.1186/s12974-020-02024-8

Sharma, A. K., Dhasmana, N., Dubey, N., Kumar, N., Gangwal, A., Gupta, M., & Singh, Y. (2017). Bacterial Virulence Factors: Secreted for Survival. *Indian Journal of Microbiology*, *57*(1), 1–10. https://doi.org/10.1007/s12088-016-0625-1

Sharma, D., & Masison, D. C. (2009). Hsp70 Structure, Function, Regulation and Influence on Yeast Prions. *Protein and Peptide Letters*, *16*(6), 571–581.

Shirafkan, F., Gharaghani, S., Rahimian, K., Sajedi, R. H., & Zahiri, J. (2021). Moonlighting protein prediction using physico-chemical and evolutional properties via machine learning methods. *BMC Bioinformatics*, *22*(1), 261. https://doi.org/10.1186/s12859-021-04194-5

Sidorin, E. V., & Solov'eva, T. F. (2011). IgG-binding proteins of bacteria. *Biochemistry. Biokhimiia*, *76*(3), 295–308. https://doi.org/10.1134/s0006297911030023

Smith, M. C., Pensky, J., & Naff, G. B. (1982). Inhibition of zymosan-induced alternative complement pathway activation by concanavalin A. *Infection and Immunity*, *38*(3), 1279–1284.

Spernovasilis, N., Markaki, I., Papadakis, M., Mazonakis, N., & Ierodiakonou, D. (2021). Mediterranean Spotted Fever: Current Knowledge and Recent Advances. *Tropical Medicine and Infectious Disease*, *6*(4), 172. https://doi.org/10.3390/tropicalmed6040172

Thepparit, C., Bourchookarn, A., Petchampai, N., Barker, S. A., & Macaluso, K. R. (2010). Interaction of Rickettsia felis with histone H2B facilitates the infection of a tick cell line. *Microbiology (Reading, England)*, *156*(Pt 9), 2855–2863. https://doi.org/10.1099/mic.0.041400-0

Thomassin, J.-L., Brannon, J. R., Gibbs, B. F., Gruenheid, S., & Le Moual, H. (2012). OmpT Outer Membrane Proteases of Enterohemorrhagic and Enteropathogenic Escherichia coli Contribute Differently to the Degradation of Human LL-37. *Infection and Immunity*, *80*(2), 483–492. https://doi.org/10.1128/IAI.05674-11

Thu, M. J., Qiu, Y., Matsuno, K., Kajihara, M., Mori-Kajihara, A., Omori, R., Monma, N., Chiba, K., Seto, J., Gokuden, M., Andoh, M., Oosako, H., Katakura, K., Takada, A., Sugimoto, C., Isoda, N., & Nakao, R. (2019). Diversity of spotted fever group rickettsiae and their association with host ticks in Japan. *Scientific Reports*, *9*(1), 1500. https://doi.org/10.1038/s41598-018-37836-5

Torres, A. N., Chamorro-Veloso, N., Costa, P., Cádiz, L., Del Canto, F., Venegas, S. A., López Nitsche, M., Coloma-Rivero, R. F., Montero, D. A., & Vidal, R. M. (2020). Deciphering Additional Roles for the EF-Tu, l-Asparaginase II and OmpT Proteins of Shiga Toxin-Producing Escherichia coli. *Microorganisms*, *8*(8), 1184. https://doi.org/10.3390/microorganisms8081184

Tseng, Y., Wang, S.-W., Kim, K. S., Wang, Y.-H., Yao, Y., Chen, C.-C., Chiang, C.-W., Hsieh, P.-C., & Teng, C.-H. (2012). NlpI Facilitates Deposition of C4bp on Escherichia coli by Blocking Classical Complement-Mediated Killing, Which Results in High-Level Bacteremia. *Infection and Immunity*, *80*(10), 3669–3678. https://doi.org/10.1128/IAI.00320-12

Van Kirk, L. S., Hayes, S. F., & Heinzen, R. A. (2000). Ultrastructure of Rickettsia rickettsii Actin Tails and Localization of Cytoskeletal Proteins. *Infection and Immunity*, *68*(8), 4706–4713.

Vellaiswamy, M., Kowalczewska, M., Merhej, V., Nappez, C., Vincentelli, R., Renesto, P., & Raoult, D. (2011). Characterization of rickettsial adhesin Adr2 belonging to a new group of adhesins in α-proteobacteria. *Microbial Pathogenesis*, *50*(5), 233–242. https://doi.org/10.1016/j.micpath.2011.01.009

Vidarsson, G., Dekkers, G., & Rispens, T. (2014). IgG Subclasses and Allotypes: From Structure to Effector Functions. *Frontiers in Immunology*, *5*. https://www.frontiersin.org/articles/10.3389/fimmu.2014.00520

Walker, D. H., & Ismail, N. (2008). Emerging and re-emerging rickettsioses: Endothelial cell infection and early disease events. *Nature Reviews Microbiology*, *6*(5), 375–386. https://doi.org/10.1038/nrmicro1866

Wampler, J. L., Kim, K.-P., Jaradat, Z., & Bhunia, A. K. (2004). Heat shock protein 60 acts as a receptor for the Listeria adhesion protein in Caco-2 cells. *Infection and Immunity*, *72*(2), 931–936. https://doi.org/10.1128/IAI.72.2.931-936.2004

Wan, L., Guo, Y., Hui, C.-Y., Liu, X.-L., Zhang, W.-B., Cao, H., & Cao, H. (2014). The surface protease ompT serves as Escherichia coli K1 adhesin in binding to human brain micro vascular endothelial cells. *Pakistan Journal of Pharmaceutical Sciences*, *27*(3 Suppl), 617–624.

Wang, G., Xia, Y., Cui, J., Gu, Z., Song, Y., Chen, Y. Q., Chen, H., Zhang, H., & Chen, W. (2014). The Roles of Moonlighting Proteins in Bacteria. *Current Issues in Molecular Biology*, *16*, 15–22.

Wang, H., & Liu, M. (2021). Complement C4, Infections, and Autoimmune Diseases. *Frontiers in Immunology*, *12*, 694928. https://doi.org/10.3389/fimmu.2021.694928

Wu, T., Perrings, C., Kinzig, A., Collins, J. P., Minteer, B. A., & Daszak, P. (2017). Economic growth, urbanization, globalization, and the risks of emerging infectious diseases in China: A review. *Ambio*, *46*(1), 18–29. https://doi.org/10.1007/s13280-016-0809-2

Xolalpa, W., Vallecillo, A. J., Lara, M., Mendoza-Hernandez, G., Comini, M., Spallek, R., Singh, M., & Espitia, C. (2007). Identification of novel bacterial plasminogen-binding proteins in the human pathogen Mycobacterium tuberculosis. *Proteomics*, *7*(18), 3332–3341. https://doi.org/10.1002/pmic.200600876

Chapter VI- Supplementary Data

pET28a-APRc$_{110-231}$HisShort

110-EVGEIIIARNRDGHFYINAFVNNVKIKFMV**D**TGASDIALTKEDAQKLGFDLTKLKYTRTYLTANGENKAAPITLNSVVIGKEFKNIKGHVGLGDLDISLLGMSLLERFKGFRIDKDLLILNY HHHHHH

pET28a_APRc$_{110-231}$HisShort_D140N

110-EVGEIIIARNRDGHFYINAFVNNVKIKFMV**N**TGASDIALTKEDAQKLGFDLTKLKYTRTYLTANGENKAAPITLNSVVIGKEFKNIKGHVGLGDLDISLLGMSLLERFKGFRIDKDLLILNY HHHHHH

Figure S1: Schematic representation of the amino acid sequence of the constructs pET28a_ APRc110-231HisShort and pET28a_APRc110-231HisShort_D140N. These constructs present the coding sequence of the short soluble form of APRc, presenting the amino acids 110-231, fused with the C-terminal histidine tag (HHHHHH). The construct pET28a_APRc$_{110-231}$HisShort_D140N is the catalytic dead mutant of pET28a_ APRc$_{110-231}$HisShort, presenting a single mutation where the aspartate was replaced by an asparagine. These residues are highlighted in the sequences. Image adapted from (Barro, 2021).

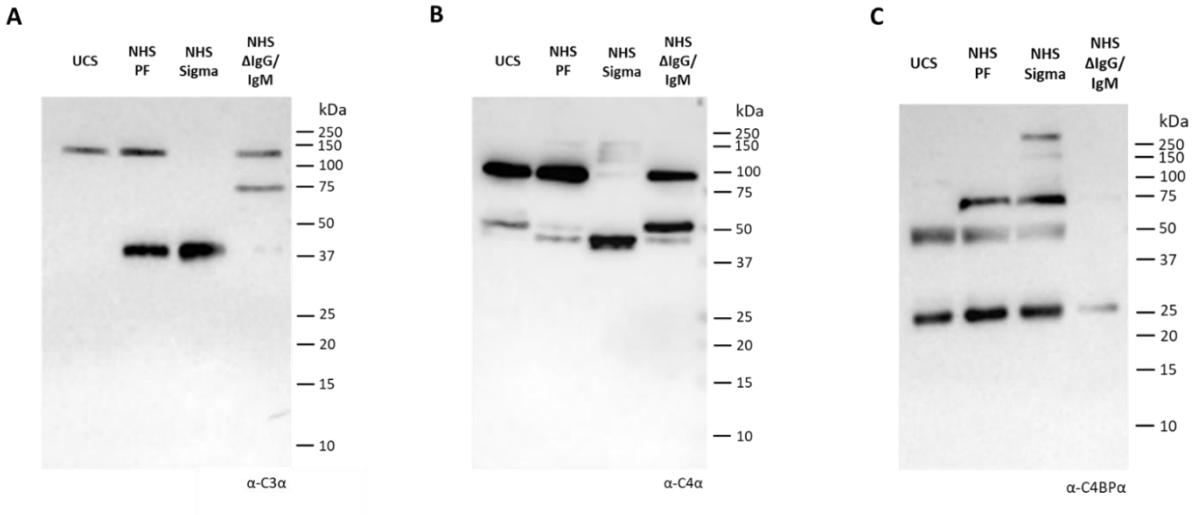

Figure S2: Protein profiles of the used serums in this study. Umbilical cord serum UCS, Normal Human serum Pel-Freez (NHS PF), NHS Sigma and NHS depleted in IgG and IgM (NHSΔIgG/IgM) were diluted 15x in PBS and denatured. Samples were assessed by Western Blot probed with (A) anti-C3α, (B) anti-c4α and (C) anti-C4BPα.

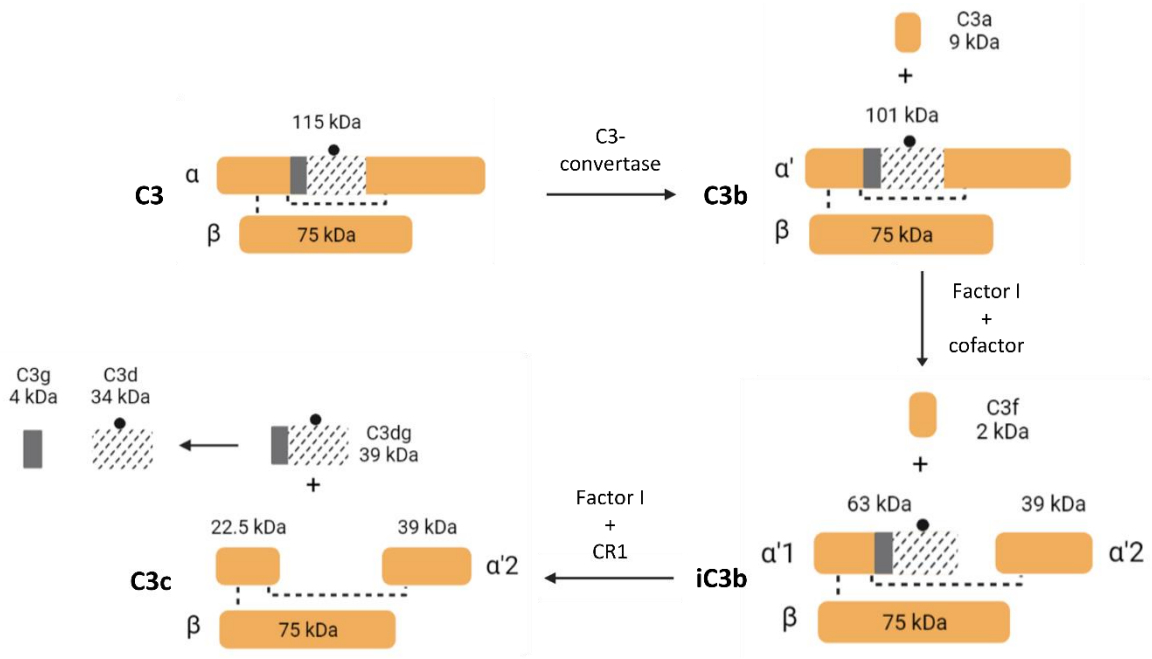

Figure S3: Schematic representation of complement protein C3 processing. The C3 protein comprises one α-chain (115 kDa) and one β-chain (75 kDa). C3 (190 kDa) is cleaved by the C3-convertase, resulting in the formation of anaphylatoxin C3a (9 kDa) and opsonin C3b. C3b is cleaved by the Factor I and cofactors, generating the fragments iC3b and C3f (2 kDa). The interaction of factor I and CR1 mediates the degradation of iC3b and originates C3c and C3dg (39 kDa). The latter fragment can be cleaved by tryptic enzymes, forming C3g (4 kDa) and C3d (34 kDa). The black dot represents the thioester bond. Dashed lines represent the disulfide bonds.

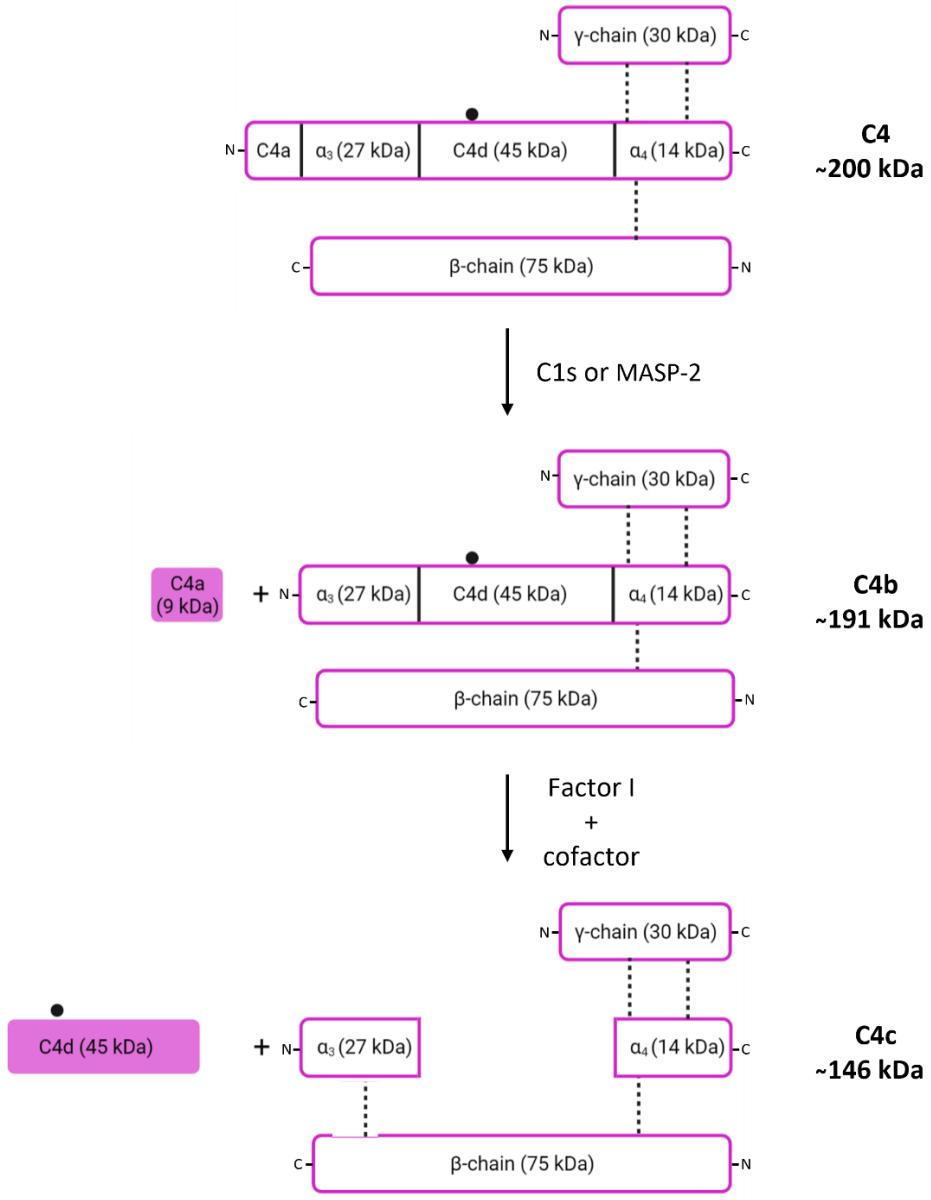

Figure S4: Schematic representation of complement protein C4 processing. The C4 protein comprises one γ-chain (30 kDa), one α-chain (95 kDa) and one β-chain (75 kDa). C4 (~200 kDa) is cleaved by the classical pathway serine protease C1s or lectin pathway MASP2, resulting in the formation of anaphylatoxin C4a (9 kDa) and opsonin C4b (~191 kDa). C4b is cleaved and inactivated by the Factor I and cofactors, generating the fragment C4d (45 kDa) and C4c (~146 kDa). The black dot represents the thioester bond. Dashed lines represent the disulfide bonds.

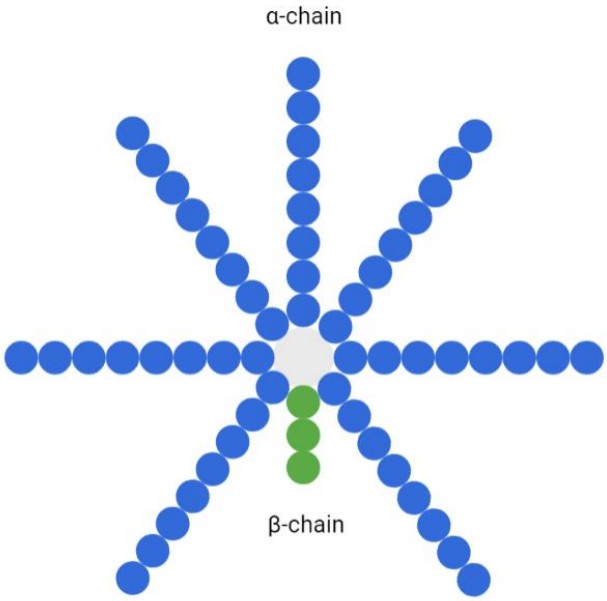

Figure S5: Schematic representation of the complement regulator C4BP. The most abundant C4BP isoform contains seven α-chains (blue) and one β-chain (green). Each α-chain (75 kDa) is composed by 8 complement control protein domains and the β-chain (45 kDa) is composed by 3. The grey circle represents the central core.